

# Structural Characterization of Antibody Binding to the Prion Protein

by

Mridula Swayampakula

A thesis submitted in partial fulfillment of the requirements for the degree of

Doctor of Philosophy

Department of Biochemistry  
University of Alberta

© Mridula Swayampakula, 2014

# Abstract

Transmissible Spongiform Encephalopathies (TSEs) are a class of fatal, infectious neurodegenerative disorders affecting the central nervous system. The critical event in the pathogenesis of TSEs is the autocatalytic conformational conversion of the cellular prion protein (PrP<sup>C</sup>) into an insoluble,  $\beta$ -sheet-rich, toxic isoform (PrP<sup>Sc</sup>). The native PrP<sup>C</sup> is a GPI anchored glycoprotein with a highly flexible amino-terminal domain and a globular, folded carboxyl-terminal domain with three  $\alpha$ -helices and two  $\beta$ -strands. Over the last decade, considerable efforts have been made into developing passive immunization strategies to combat prion diseases and to prevent the harmful conformational conversion of the native PrP<sup>C</sup>. Our collaborators in Zurich generated the POM monoclonal antibodies with epitopes throughout the recombinant mouse prion protein. The POM1 antibody binds to the globular domain and causes rapid neurotoxicity in cerebellar slices. The POM2 antibody binds to the octapeptide repeats (OR) in the amino-terminal domain and prevents the POM1 induced toxicity. The POM6 antibody is innocuous to the cerebellar slices and competes with the toxic POM1 antibody for binding to the globular domain of the prion protein. The research described in this dissertation examines the structural characterization of the two anti-PrP monoclonal antibodies - POM2 and POM6 in complex with their respective epitopes in the mouse prion protein. We report the crystal structure of a tandem OR peptide of PrP<sup>C</sup> bound to the POM2 Fab that was solved at a resolution of 2.3 Å. It is the first crystal structure that shows the molecular features of an entire OR peptide in its protein bound form. Our structure shows that POM2 Fab uses

only back bone and hydrophobic interactions to disrupt the  $\beta$ -turn like structure of the unbound octapeptide repeats resulting in their extended conformation. As many OR ligands have been found to show therapeutic potential by delaying the disease onset, the structural study presented in this dissertation makes important contributions to designing smaller and tighter binding OR ligands to improve the efficacy of their binding *in vivo*. We also report the crystal structure of the mouse PrP125-225 bound to the POM6 Fab that was solved at a resolution of 1.83 Å. The POM6 Fab was found to have epitopes on all the three  $\alpha$ -helices of the prion protein. An analysis of the changes in the intra- and inter domain salt bridges and hydrogen bonds in the POM6 bound PrP125-225 in comparison to the wild type PrP shows networks of interactions specifically in the  $\beta$ 2- $\alpha$ 2 loop that may potentially enhance the stability of the POM6 bound PrP. Hence, the POM6 Fab bound PrP molecule may potentially resist conversion to PrP<sup>Sc</sup>. A comparison of the toxicity inducing POM1 Fab bound PrP120-231 (PDB ID 4H88) with the innocuous POM6 bound PrP125-225 showed a lack of inter-domain stabilizing salt bridges and hydrogen bonds within the POM1 Fab bound PrP molecule. The comparative analysis between the two Fab- PrP complexes points to vulnerable regions within the prion protein that may influence its aggregation tendencies.

# Preface

The research presented in this thesis forms part of an international research collaboration between the labs of Drs. Michael James, Nat Kav at the University of Alberta, Canada and Dr. Adriano Aguzzi at the University Hospital of Zurich, Switzerland. Dr. Adriano Aguzzi's lab provided Drs. Michael James and Nat Kav with the hybridoma of POM1, POM2 and POM6. All the molecular biology and protein purification work presented in the Chapter 2 on the POM2 scFv engineering and purification were performed by myself. The crystallization, X-ray data collection and analysis presented in Chapter 3 and Chapter 4 were performed by myself with guidance from Dr. PK Baral. The literature analysis presented in the introductory Chapter 1, the data analysis in Chapter 3 and 4 and the concluding analysis in Chapter 5 are my original work.

Samples of the purified POM2 scFv that were prepared by myself (presented in Chapter 2) were used by the research group at Dr. Adriano Aguzzi's lab and the ensuing results have been included in a journal article published as: Sonati T, Reimann RR, Falsig J, Baral PK, O'Connor T, Hornemann S, Yaganoglu S, Li B, Herrmann US, Wieland B, Swayampakula M, Rahman MH, Das D, Kav N, Riek R, Liberski PP, James MN, Aguzzi A. *Nature*. 2013 Sep 5;501(7465):102-6. The toxicity of anti-prion antibodies is mediated by the flexible tail of the prion protein. My contribution was that I had provided the purified samples of POM2 scFv.

The Chapter 3 of this thesis has been published as Swayampakula M, Baral PK,

Aguzzi A, Kav NN, James MN. *Protein Science* 2013 Jul;22(7):893-903. The crystal structure of an octapeptide repeat of the prion protein in complex with a Fab fragment of the POM2 antibody. I crystallized the protein complex, Dr.PK Baral collected the data and assisted me in solving the structure. I was responsible for the data analysis and manuscript writing.

Chapter 4 of this thesis is part of a manuscript in preparation.

# Acknowledgements

I would like to express my sincere gratitude to my supervisor, Prof. Michael James for accepting me into his lab as his Ph.D. student to work on the prion project. It has been an honour to have had the opportunity of doing my Ph.D. under his tutelage. I could not have asked for a more encouraging and supportive supervisor. Dr. James' love for protein X-ray crystallography is awe-inspiring. Over the years, the lessons that I have learnt from him on the interpretation of protein structures and on efficient scientific writing will always be cherished by me.

I would like to extend my sincere gratitude to my co-supervisor, Prof. Nat Kav for considering me a suitable candidate to be a part of the prion project. Prof. Kav had recommended that I apply to Prof. Michael James' lab for an admission into the Department of Biochemistry's graduate program. I might not have been in this project if it weren't for Dr. Kav. I would also like to thank him for his supervision during the time that I had worked in his lab.

I would like to sincerely thank Dr. Pravas K Baral for being an amazing mentor and teaching me all the techniques in protein X-ray crystallography. All the knowledge that I have today from crystallizing a protein to collecting data to solving structures to refining them, to designing experiments, to planning and writing papers were taught to me by him. It has been an absolute pleasure working with him.

I would like to sincerely thank Dr. Shiv Verma for being a great mentor and teaching me all that I know today about molecular biology techniques from primer

designing to complex mutagenesis. I could not have done most of my work on scFv engineering if it weren't for his able mentorship.

I would like to sincerely thank Dr. Barbara Wieland for teaching me all the tricks of the trade in protein purification. I was able to improve the POM2 scFv yield in part due to her expert advice.

I would like to thank Drs. Haying Bie, Jiang Yin, Muhammad Rahman and Mr. Sheraz Khan for being very supportive colleagues and helping me with advice whenever I needed it. I would also like to give a special thanks to Dr. Yin for helping me pick and freeze my very small and delicate POM6-PrP crystals.

I would like to thank Dr. Gina Thede for introducing me to the sport of ultimate frisbee. I would also like to thank all my friends at the Edmonton Ultimate Players Association. For the past three years, ultimate frisbee has become a big part of my life. I have made so many friends through playing ultimate and it has been the perfect way to de-stress away from work.

Last but certainly not the least, I would like to thank my family especially my parents for being so very supportive of me when I had expressed an interest in doing a PhD in an unknown place and on a disease they had never even heard the name of. I could not have done this without their unwavering support. My mother, Dr. Marthi Nalini had always inspired me to take up the path of research. I would also like to thank my husband, Barath for being there for me and for introducing me to the joys of the typesetting software,  $\text{\LaTeX}$ .

I would like to acknowledge the technical support provided for my work by the Canadian Light Source and the Stanford Synchrotron Radiation Lightsource. I would also like to thank all my funding agencies such as the Alberta Prion Research Institute (APRI), PrioNet, the Alberta Livestock and Meat Agency Ltd. (ALMA) and PrioNet.

# Contents

<b>Abstract</b>	<b>ii</b>
<b>Preface</b>	<b>iv</b>
<b>Acknowledgements</b>	<b>vi</b>
<b>Contents</b>	<b>viii</b>
<b>List of Tables</b>	<b>x</b>
<b>List of Figures</b>	<b>xi</b>
<b>List of Abbreviations</b>	<b>xii</b>
<b>1 Transmissible Spongiform Encephalopathies</b>	<b>1</b>
1.1 Introduction . . . . .	1
1.2 Prions and the protein-only hypothesis . . . . .	7
1.3 Prion protein . . . . .	8
1.4 Anti-Prion therapy . . . . .	16
1.5 Research goals . . . . .	25
<b>Chapter 2:</b>	
<b>POM2 scFv engineering and purification . . . . .</b>	<b>26</b>
2.1 Introduction . . . . .	26
2.2 Materials and Methods . . . . .	27
2.3 Results . . . . .	39
2.4 Discussion . . . . .	42
2.5 Conclusions . . . . .	43
<b>Chapter 3:</b>	
<b>Crystal structure of POM2 Fab-Octapeptide Repeat . . . . .</b>	<b>44</b>
3.1 Introduction . . . . .	44
3.2 Materials and Methods . . . . .	47
3.3 Results . . . . .	50
3.4 Discussion . . . . .	55
3.5 Conclusions . . . . .	62



<b>Chapter 4:</b>		
	<b>Crystal structure of moPrP125-225-POM6 Fab . . . . .</b>	<b>64</b>
4.1	Introduction . . . . .	64
4.2	Materials and Methods . . . . .	65
4.3	Results . . . . .	68
4.4	Discussion . . . . .	79
4.5	Conclusions . . . . .	83
<b>Chapter 5:</b>		
	<b>Conclusions . . . . .</b>	<b>87</b>
5.1	Introduction . . . . .	87

# List of Tables

1.1	List of TSEs- their hosts, aetiology and year of the first reported case	3
1.2	Different TSEs- age of onset, disease duration and clinical symptoms	4
1.3	Popular nomenclatures for prion protein isoforms and their definitions	9
1.4	A list of published models of PrP27-30 . . . . .	15
2.1	A list of the primers used for cloning POM2 scFv and its variants . .	33
3.1	Data-collection and refinement statistics of OR2-POM2. . . . .	49
3.2	Summary of interactions between OR2 peptide and POM2 Fab . . . .	57
4.1	Data-collection and refinement statistics of POM6-PrP125-225 . . . .	70
4.2	Summary of interactions of PrP125-225 with POM6 Fab . . . . .	75

# List of Figures

1.1	Animals affected with TSEs . . . . .	2
1.2	Neuropathologic symptoms characteristic of TSEs . . . . .	2
1.3	3-D structure of the recombinant mouse prion protein . . . . .	11
1.4	Amino acid sequence alignment of 8 mammalian prion proteins . . . . .	12
1.5	A schematic representation of the native Prion protein . . . . .	13
1.6	Progression of prion infection based on the route of entry . . . . .	18
1.7	Anti-Prion therapeutic strategies . . . . .	20
1.8	POM monoclonal antibodies and their epitopes . . . . .	24
2.1	An IgG molecule and its functional fragments . . . . .	28
2.2	A schematic representation of the overlap-extension PCR . . . . .	32
2.3	POM2 scFv cloned into pET30b vector . . . . .	37
2.4	POM2 scFv cloned into pET22b+ vector . . . . .	38
2.5	POM2 scFv with 218 linker cloned into pET22b+ vector . . . . .	41
2.6	An SDS-PAGE gel showing purification of $V_L$ G99C and $V_H$ G44C chains . . . . .	41
3.1	Published NMR structures of the OR domain . . . . .	46
3.2	The asymmetric unit of the POM2 Fab-OR2 peptide complex . . . . .	51
3.3	The CDR loops of the POM2 Fab molecule . . . . .	53
3.4	$2 F_o  -  F_c $ difference electron density map of the OR2 peptides . . . . .	56
3.5	Intermolecular contacts between the OR2 and POM2 Fab . . . . .	58
3.6	LIGPLOTs of the OR2 peptide with POM2 Fab . . . . .	59
3.7	The hydrophobic binding pockets in POM2 Fab-OR2 complex . . . . .	60
3.8	An electrostatic potential based surface representation of the POM2 Fab and the OR2 peptide . . . . .	61
4.1	Crystallization of POM6-PrP . . . . .	69
4.2	The crystal structure of POM6-PrP . . . . .	71
4.3	An electrostatic potential based surface representation of the POM6 Fab and PrP125-225 . . . . .	76
4.4	LIGPLOTs of the hydrophobic contacts between POM6 and PrP . . . . .	77
4.5	Crystal contacts in POM6-PrP . . . . .	78
4.6	The affected salt-bridges in POM6-PrP . . . . .	81
4.7	Alignment of POM6 and POM1 Fab bound PrP molecules . . . . .	85
4.8	Structural difference between POM6-PrP & POM1-PrP . . . . .	86

# List of Abbreviations

2xYT	2xYeast Tryptone media
APBS	Adaptive Poisson-Boltzmann Solver
APC	Antigen Presenting Cells
BASE	Bovine Amyloidotic Spongiform Encephalopathy
BBB	Blood brain barrier
bp	Base pairs
BSEs	Bovine Spongiform Encephalopathies
Buffer U	8M urea, 100mM NaH <sub>2</sub> PO <sub>4</sub> , 10mM Tris, 5mM Imidazole pH 8.0
CD	Circular Dichroism
CDRs	Complementarity determining regions
CJD	Creutzfeldt-Jakob disease
CNS	Central Nervous System
COCS	Cerebellar Organotypic Slice Culture
CWD	Chronic Wasting Disease
dsFv	Disulfide linked variable fragments
EDTA	Ethylene diaminetetraacetic acid
FDC	Follicular dendritic cell
FFI	Fatal Familial Insomnia
FSE	Feline Spongiform Encephalopathy
FTIR	Fourier Transform Infrared spectroscopy
GPI	Glycophosphatidylinositol

GSS	Gerstmann-Straussler-Scheinker syndrome
IB	Inclusion bodies
IgG	Immunoglobulin G
IPTG	Isopropyl $\beta$ -D-1-thiogalactopyranoside
LB	Luria Bertani
LDL	Low density lipoprotein
MBM	Meat and bone meal
MDS	Molecular Dynamic Simulations
Ni-NTA	Nickel- Nitrilotriacetic acid
NMR	Nuclear Magnetic Resonance
OR	Octapeptide repeat (of the prion protein)
PCR	Polymerase chain reaction
PMCA	Protein Misfolding Cyclic Amplification
POPG	1-palmitoyl-2-oleoylphosphatidylglycerol
PPS	Pentosan Polysulfate
r.p.m.	rate per minute
RMSD	Root mean square deviation
ROS	Reactive oxygen species
scFv	single chain variable fragment
sCJD	sporadic CJD
SDS-PAGE	Sodium dodecyl sulphate - polyacrylamide gel electrophoresis
SEZ	Spongiform Encephalopathy of Zoo animals
sFI	Sporadic Fatal Insomnia
SLOs	Secondary lymphoid organs
STI1	Stress inducible protein1
TLS	Translation/Libration/Screw
TME	Transmissible mink encephalopathy

TN Buffer      50mM Tris and 200mM NaCl pH 8  
TSEs            Transmissible Spongiform Encephalopathies  
vCJD            variant CJD

# Chapter 1

## Transmissible Spongiform Encephalopathies

### 1.1 Introduction

Transmissible Spongiform Encephalopathies (TSEs) are a class of progressive, infectious and fatal neurodegenerative disorders of humans and other animals such as sheep, cattle and cervids (Figure 1.1). TSEs are typically characterized by long incubation periods and an absence of immune and inflammatory responses. Upon the manifestation of the primary clinical symptoms of cognitive and motor dysfunction such as dementia and ataxia<sup>44</sup>, these diseases rapidly progress to death. On the basis of their aetiology, TSEs can be categorized into three subtypes: sporadic, acquired and hereditary/familial. Table 1.1 lists various TSEs - their hosts and aetiology and Table 1.2 lists the clinical symptoms manifested by them.

TSEs show considerable differences in their neuropathologies, incubation times and clinical symptoms. For instance, incubation times range from 4-6 years in the case of Bovine Spongiform Encephalopathy (BSE)<sup>59</sup> to up to 40 years in the case of Kuru<sup>44</sup>. Nonetheless, common to all the TSEs, there is a classical triad of neuropathologic changes that are considered to be the hallmarks of their post-mortem diagnosis (Figure 1.2)<sup>6,77,116</sup>: (i) microscopic spongiform vacuolation in the grey matter neuropil; (ii) astrocytosis in gray matter and (iii) loss of neurons due to the darkening and shrinking of neuronal cell bodies. In some human TSEs such as variant Creutzfeldt-Jakob disease (vCJD) and Gerstmann-Straussler-Scheinker syndrome (GSS), classical amyloid plaques are also found. However, these plaques are absent in BSE and in most cases of scrapie<sup>116</sup>.

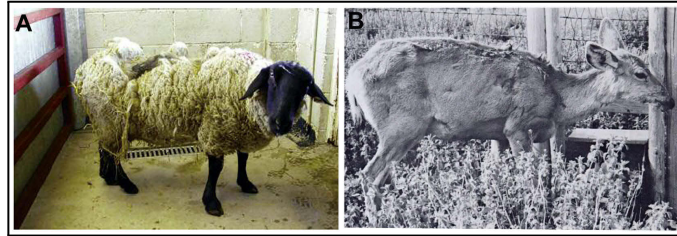


Figure 1.1: Animals affected with TSEs (A) A sheep affected with scrapie showing a characteristic symptom of compulsive scraping off of its fleeces against surfaces<sup>115</sup> and (B) a deer suffering from the Chronic Wasting disease with a characteristic symptom of severe weight loss<sup>204</sup>

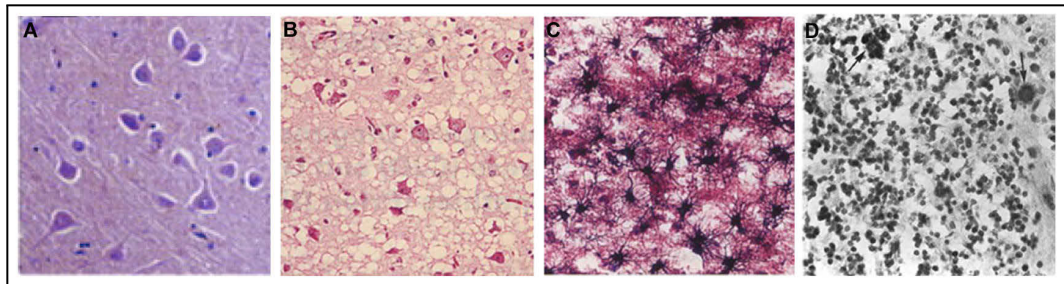


Figure 1.2: Classic triad of neuropathologic symptoms characteristic of TSEs (A) Healthy brain slice<sup>31</sup>, (B) spongiform vacuolation within the neuropil that distort the cortical cytoarchitecture<sup>32</sup> in Haematoxylin and Eosin stain, (C) astrocytosis with increased numbers of enlarged astrocytes in the cerebral cortex<sup>32</sup> (Cajal impregnation) (D) dark and shrinking neuronal cell bodies with a few cerebellar amyloid plaques (indicated by black arrows) stained with glial fibrillary acid protein immunocytochemistry (GFAP)<sup>110</sup>.



Table 1.1: List of TSEs - their hosts, aetiology and year of the first reported case<sup>9,10,59,113,200</sup>

Disease	Host	Aetiology	First reported
Kuru	Humans	Acquired- Ingestion through cannibalistic rituals	1957
CJD	Humans	Sporadic, Familial or iatrogenic	1920
vCJD	Humans	Acquired- Ingestion of BSE contaminated food (codon 129 M/M genotype)	1996
mock sCJD	Humans	Acquired- Blood transfusion from vCJD donor (codon 129 M/V genotype)	2004
FFI	Humans	Familial	
sFI	Humans	No mutation in PRNP gene (codon 129 M/M genotype)	1999
GSS	Humans	Familial	1936
Scrapie	Sheep, goat	Acquired and possibly familial	1732
Nor98	Sheep, goat	unknown	1998
BSE	Cattle	Acquired- Ingestion of BSE contaminated food	1986
BASE	Cattle	unknown	2004
CWD	Mule deer, white-tailed deer, elk	Acquired and possibly familial	1967
FSE	Zoological and domestic felids	Acquired- Ingestion of BSE contaminated food	1990
SEZ	Zoological ungulates and bovids	Acquired- Ingestion of BSE contaminated food	
TME	Mink	Acquired- Ingestion of Scrapie and/or BSE contaminated food	1964

Familial- PRNP germline mutation; Nor 98 also known as atypical scrapie  
 CJD- Creutzfeldt-Jakob disease; vCJD- variant CJD; sCJD- sporadic CJD;  
 FFI- Fatal familial insomnia; sFI- sporadic fatal insomnia; GSS- Gerstmann-  
 Straussler-Scheinker syndrome; BSE- Bovine spongiform encephalopathy;  
 BASE- Bovine amyloidotic spongiform encephalopathy; CWD- Chronic wasting  
 disease; FSE- Feline spongiform encephalopathy; SEZ - Spongiform encephalopathy  
 of zoo animals; TME- Transmissible mink encephalopathy.

Table 1.2: A list of TSEs -Age of onset, disease duration and clinical symptoms<sup>5,25,44,122,140</sup>

. See the bottom of the table for definitions of the abbreviations.

Disease	Onset age	Duration	Clinical features
Kuru	5-35 yrs	6-9 months	cerebellar ataxia, tremor, late onset dementia
CJD	50-75 yrs	2-8 months	dementia with confusion, memory loss and bizarre behaviour, cerebellar ataxia, visual signs, myoclonus, pyramidal and extra pyramidal
vCJD	~28 yrs	13-14 months	behavioural changes, anxiety, depression and withdrawal, cerebellar ataxia and myoclonus. Later signs include memory disturbances to severe cognitive impairment and akinetic mutism
FFI	40-50 yrs	12-16 months	insidious or subacute onset of insomnia, autonomic dysfunction- elevated blood pressure, excessive lacrimation, sexual and urinary tract dysfunction, a change in basal body temperature, appendicular ataxia
GSS	35-55 yrs	2-10 years	ataxia, dementia, dysarthria, nystagmus, spasticity and visual disturbances
BSE	4-5 yrs	2-6 months	behavioural changes, lack of coordination, difficulty in walking or standing up, decreased milk production and weight loss
CWD	2-7 yrs	≤ 12 months	weight loss, excessive salivation, trouble swallowing, difficulty in judging distance, changes in behaviour, polyuria
Scrapie	2-5 yrs	1-2 months	weight loss, salivation, pruritus, incoordination of hind limbs and altered behaviour such as observed nervousness, depression, excitability or aggressiveness

### 1.1.1 Economic impact

Over the last 30 years, TSEs have evolved from being relatively unknown, deadly diseases to ones with major agricultural, political and economic impact. The shift in the influence of TSEs on mankind was triggered in the late 1970s, when the United Kingdom cattle industry changed the process of rendering animal carcasses to provide meat and bone meal (MBM) as protein supplements to the herbivorous sheep, cattle and other livestock<sup>123</sup>. The ingestion of the contaminated MBMs led to the first case of Bovine Spongiform Encephalopathy (BSE) being reported in 1986. It turned into an epidemic by 1993 when almost 1,000 new cases of BSE per week were being reported resulting in the slaughtering of millions of cattle<sup>60</sup>. The ban on specified offal as well as the practice of feeding ruminants other ruminants successfully resulted in reducing BSE occurrence in the UK to only 3 cases reported in 2013<sup>143</sup>. However, BSE has spread to other parts of Europe and isolated cases have been reported in Japan, Canada, Israel and Russia.

The BSE epidemic in the UK created a major food and economic crisis that was heightened by the revelation that BSE could be transmitted to humans by ingestion of contaminated meat resulting in variant CJD - the human form of BSE<sup>7,44</sup>. As of 2014, there have been 177 cases of vCJD reported<sup>164</sup> that could be directly connected to the BSE epidemic in the UK. Moreover, as the incubation times vary considerably from individual to individual, there is no clear way to predict accurately the number of vCJD cases that could be seen in the future.

The incident increased awareness about the potential dangers of exposure of humans to animal TSEs. In the United States, the increasing prevalence of Chronic Wasting Disease (CWD) in cervids has raised serious concerns about the transmission of CWD to humans through ingestion of contaminated venison. Additionally, we know that iatrogenic CJD (iCJD) can be transmitted by corneal and dura mater transplants, blood transfusion and pituitary hormone treatments<sup>9</sup> which have led to the formulation of new, stringent donor criteria worldwide. The use of contaminated surgical instruments and electroencephalography electrodes can also spread iCJD. In the last 20 years, 4 new TSEs have been identified along with a dramatic rise in Scrapie among the European sheep flocks as well as a rise in CWD cases in wild and captive populations of deer and elk in the Rocky Mountain and mid-western areas of US and Canada<sup>200</sup>. These alarming facts demand an urgency in understanding the mechanism of pathogenesis of the TSEs and in developing early diagnostic and pharmacological interventions to them.

### 1.1.2 Historical background

The first case of Scrapie was reported in Europe in the Spanish merino sheep in 1732<sup>115</sup>. The exportation of these sheep was thought to spread scrapie to the other sheep flocks in Europe. In the late 1930s, seminal experiments by Cuille and Chelle demonstrated the transmissible nature of scrapie<sup>89,90</sup>. It was then considered as a viral, infectious disease caused by a filterable agent resistant to formalin, high temperatures as well as ionizing radiation<sup>115</sup>. In 1963, after a lull in scrapie research during World War II, the discovery of transmissibility of scrapie from sheep to mice<sup>132</sup> sparked a range of lab based virological research on scrapie that resulted in the emergence of many hypotheses to describe the nature of the infectious agent<sup>115</sup>. However, there was never substantial proof for these hypotheses.

In a different part of the world Dr.D.Carleton Gajdusek, a virologist and paediatrician arrived in the Highlands of Papua New Guinea in 1957 to investigate a strange encephalitis-like terminal disease called Kuru afflicting the island's Stone Age Fore natives predominantly, the women and the children. He found Kuru to be the first chronic, human degenerative disease caused by a 'slow, unconventional virus' with very long incubation periods and a progressive pathology leading to death. Over the course of the next 20 years, Gajdusek found that Kuru resulted from the ritualistic cannibalism practised by the tribes people as a rite of mourning where the conjunctival, nasal, skin and highly infectious brain tissues were mostly shared amongst the women and children (nobelprize.org)<sup>115</sup>.

In 1959, William Hadlow, an employee at the US Department of Agriculture studying the pathology of scrapie pointed out the striking similarity between the neurohistology of scrapie and Kuru<sup>78</sup>. This prompted Gajdusek to test the transmissibility of Kuru to chimpanzees proving the broadly similar, infectious characteristics of Kuru and scrapie<sup>36</sup>. In 1976, Gajdusek was awarded the Nobel Prize for his seminal discovery of the infectious nature of Kuru that resulted in the cessation of the practice of cannibalism by the Highlanders in Papua New Guinea and the eventual near-eradication of Kuru (only 3 cases in 2003)<sup>115</sup>.

By the 1960s, a new class of infectious neurodegenerative diseases had started to emerge that shared similar neuropathology to Scrapie and Kuru and afflicted a wide range of animals from sheep, goats, minks to humans. In 1968, Creutzfeldt-Jakob disease- a rare, fatal human neurodegenerative disorder was also identified as belonging to this class. These diseases were later collectively called the Transmissible Spongiform Encephalopathies.

## 1.2 Prions and the protein-only hypothesis

In 1972, after the death of one of his patients from CJD, Dr. Stanley B. Prusiner set out to discover the identity of the infectious agent causing TSEs. After a systematic examination of the infectious agent purified from scrapie infected murine spleen extracts, Prusiner published a paradigm shifting paper in 1982 that suggested that the infectious agent predominantly consisted of a protein that was essential for its infectivity<sup>158</sup>. Prusiner named the infectious agent ‘prions’, short for *Proteinaceous infectious particle* and found that most nucleic acid - inactivating protocols failed to suppress their infectivity<sup>158</sup>. Prusiner’s theory was heretical at the time of its proposal as it went against the entire theoretical foundations of molecular biology that were based on the assumption that the spread of all infections were based on mutations in the genetic material.

About two decades before Prusiner published his findings, mathematician JS Griffith, in a visionary article<sup>73</sup> used a combination of thermodynamic equations with respect to dimer formations and free energy driving forces to propose a theory on the plausibility for a physiological protein or a set of proteins to self-replicate without the involvement of nucleic acids leading to the transmission of scrapie. Despite being unfamiliar with the biochemistry of protein oligomers and diseases of protein aggregation, Griffith had the foresight to propose that the infectious agent could be “a protein or a set of proteins which the animal is genetically equipped to make, but which it either does not normally make or does not make in that form. It may be passed between animals but be actually a different protein in different species<sup>73</sup>. ”

Stanley Prusiner became the torchbearer for the above ‘protein-only’ theory and over the next three decades, the work predominantly led by Prusiner’s research group made significant contributions to accumulating proof in favour of this theory. Prusiner was awarded the Nobel Prize in the year 1997 for his contributions to the field of Prion research ([www.nobelprize.org](http://www.nobelprize.org)).

A 27-30 kDa, proteinase K resistant protein core (termed PrP27-30; PrP short for Prion protein) was isolated from prions in the scrapie-infected brain extracts<sup>28</sup>. The purification of PrP27-30 enabled the identification of the amino acid sequence of its first 15 N-terminal residues<sup>159</sup>. Using a synthetic cDNA probe corresponding to the amino acid sequence, Chesebro et al found that the probe hybridized to an mRNA sequence present both in the scrapie infected as well as normal brains<sup>45</sup>. This endeavour brought to light the fact that the protein present in PrP27-30 was in fact, host-encoded<sup>138</sup> and did not belong to a foreign organism like a virus. By 1986, the

cDNA encoding the entire open reading frame of PrP was isolated from mice and its gene was named, *Prnp*<sup>117</sup>. It quickly became clear that PrP existed both as a normal cellular protein (designated *PrP<sup>C</sup>*, C-cellular) and as a pathological isoform (designated *PrP<sup>Sc</sup>*, Sc-scrapie) found in prions<sup>138</sup>. It was a finding that agreed very well with Griffith's proposed theory. There are many nomenclatures used for the different isoforms of the prion protein. Table 1.3 lists and explains many of these nomenclatures.

Experiments showed that prion infectivity and *PrP<sup>Sc</sup>* co-purified and the infectivity was directly proportional to the *PrP<sup>Sc</sup>* titre<sup>65</sup>. Additionally, protein denaturing agents as well as anti-PrP antibodies raised against PrP27-30 successfully reduced scrapie infectivity further cementing the theory of the proteinaceous nature of the infectious agent<sup>65</sup>. Another landmark experiment involved the use of *Prnp* knockout mice and showed that the lack the cellular *PrP<sup>C</sup>* made the mice resistant to TSEs<sup>33</sup>.

## 1.3 Prion protein

### 1.3.1 Structure of *PrP<sup>C</sup>*

The native, mature mouse *PrP<sup>C</sup>* (residues, 23-231) is a 209 amino acids long, un-, mono- or di-glycosylated, GPI-anchored protein<sup>184</sup>. In 1993, low resolution structural studies of the prion protein by Fourier Transform Infrared spectroscopy (FTIR) and Circular Dichroism (CD) showed that *PrP<sup>C</sup>* contains 42%  $\alpha$ -helix and only 3%  $\beta$ -sheet content whereas the infectious *PrP<sup>Sc</sup>* contains 30%  $\alpha$ -helix and a surprising 43%  $\beta$  sheet content<sup>144</sup>. In 1997, the Nuclear Magnetic Resonance (NMR) structure of the full length mouse PrP(23-231) was published<sup>167</sup> and in 2001, the crystal structure of human PrP(90-231) was solved at 2Å resolution<sup>102</sup>. This was soon followed by the structures of many other mammalian PrPs being solved<sup>118</sup> primarily using NMR spectroscopy. The structures revealed that the carboxy-terminal domain of PrP from residues 124-231 (numbered according to the mouse PrP sequence) is highly structured with three  $\alpha$ -helices (named  $\alpha 1$ ,  $\alpha 2$  and  $\alpha 3$ ), two short  $\beta$ -strands ( $\beta 1$ ,  $\beta 2$ ) and a disulfide bond connecting helices  $\alpha 2$  and  $\alpha 3$  (Figure:1.3A)<sup>167</sup>. The amino acid sequence of the prion protein is highly conserved across mammals<sup>207</sup> as shown in Figure 1.4. Not surprisingly, the global structures of the different mammalian PrPs (residues 124- 231) were found to be very similar as well (Figure 1.3B). However, it is very likely that the differences in the local features within the three dimensional structures of the different mammalian *PrP<sup>C</sup>*s dictate their susceptibility to TSEs<sup>118</sup>.

Table 1.3: Popular nomenclatures for prion protein isoforms and their definitions

Isoform	Significance
Prion	The infectious agent causing TSEs. It contains PrP <sup>Sc</sup> but might or might not contain other macromolecules
PrP	Total prion protein present without alluding to any one particular isoform
PrP <sup>C</sup>	Native,cellular protein present in healthy individuals. It is soluble, protease sensitive and has predominantly $\alpha$ -helical content
PrP <sup>Sc</sup>	TSE-associated prion protein present in individuals affected by TSE. This form is insoluble, protease resistant and has a large content of $\beta$ -sheet present
PrP27-30	The protein core that remains resistant after proteinase K treatment of PrP <sup>Sc</sup>
PrP <sup>sen</sup>	PrP isoform that is sensitive to Proteinase K. Usually refers to recombinant protein.
PrP <sup>res</sup>	A $\beta$ -sheet rich prion protein which may or may not be identical to PrP <sup>Sc</sup> . Usually refers to the protease resistant protein generated <i>in vitro</i> .

Interestingly, the amino-terminal domain comprising of almost half of the PrP from residues 23-123 was found to be highly flexible in solution<sup>167</sup> and its structure could never be determined. A unique feature of the amino terminal domain of PrP<sup>C</sup> is the presence of four consecutive repeats of an eight-amino acid sequence -PHGGG/SWGQ (residues 59-90) known as the ‘octapeptide repeat (OR) domain’. The OR domain also contains a non-canonical octapeptide repeat, PQGGTWGQ in mice (a nonapeptide in other species) present from residues 51-58. The OR domain is one of the most evolutionarily conserved domains of PrP<sup>C</sup> across most mammals (Figure 1.4). Although, the amino-terminal part of PrP from residues 32-90 is not strictly required for prion infectivity<sup>57</sup>, studies in both animal models and cell cultures have shown that the addition or deletion of ORs can influence susceptibility to TSEs<sup>58,153</sup>. Insertional mutations of two or more ORs in the amino-terminal domain have been known to lead to familial cases of CJD and Yam et al showed that the OR domain undergoes structural transition upon PrP<sup>Sc</sup> formation suggesting a possible role in pathogenesis<sup>208</sup>. The N-terminal domain modulates prion aggregation kinetics as well as properties of the aggregates including their size<sup>62</sup>. These studies demonstrate that the amino-terminal part of PrP<sup>C</sup>, specifically the OR domain could potentially play an important role in the pathogenesis of TSEs. However, detailed structural characteristics of the amino-terminal domain still remain unclear.

The structure of recombinant PrP is very similar to the structure of native PrP<sup>C</sup><sup>83</sup>. Hence, the structural studies performed on the recombinant PrP and their fragments are relevant and provide valuable information towards the structural characterization of the native PrP<sup>C</sup>. Figure 1.5 shows a schematic representation of the native PrP<sup>C</sup>.

### 1.3.2 Physiological role of PrP<sup>C</sup>

PrP<sup>C</sup> has been found to be expressed in brain, circulating leukocytes, heart, skeletal muscle, lung, lymphoreticular system, testis and ovary<sup>213</sup>. There are many conflicting reports on the physiological functions of PrP<sup>C</sup> in the literature. One of the reasons for this is that studies on the first *Prnp* knockout mice did not show any significant anatomical, behavioural or learning abnormalities<sup>34</sup>. Studies have shown that PrP<sup>C</sup> contributes to myelin maintenance in peripheral nerves<sup>29</sup> and affects haematopoietic stem cell self-renewal under stressful conditions. PrP<sup>C</sup> is also involved in T cell development and interactions with dendritic cells (DCs) to inhibit their phagocytosis in macrophages<sup>213</sup>. PrP also has a role in the pluripotency and differentiation of embryonic stem cells and in intestinal barrier function<sup>9</sup>. Due to the copper binding



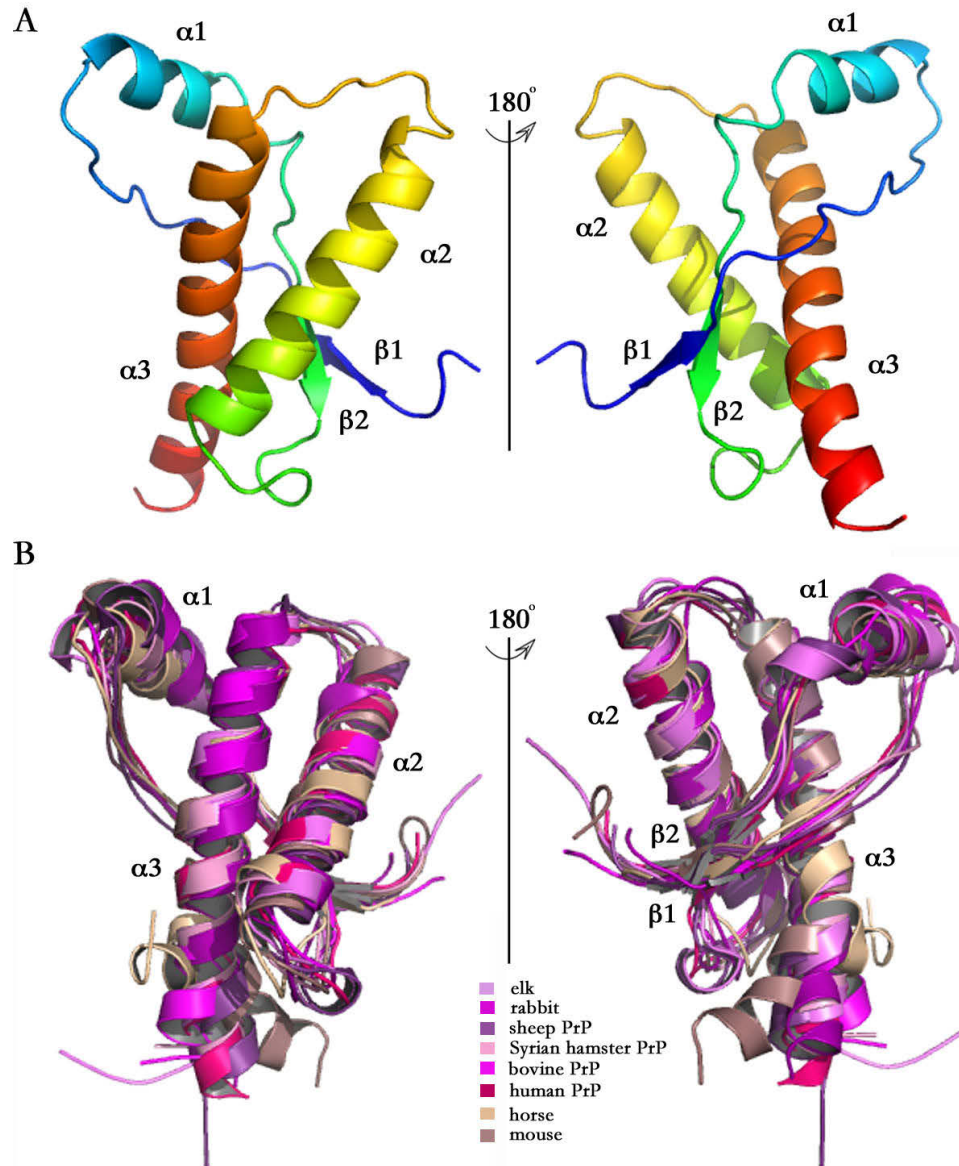


Figure 1.3: Three-dimensional structure of the globular domain of recombinant prion protein. (A) A cartoon representation of the NMR structure of the mouse prion protein, residues 124-231 (PDB ID 1AG2). The spectral colour scheme was chosen with the amino-terminal domain coloured blue progressing to red at the carboxy-terminal domain. The globular domain of the prion protein contains three  $\alpha$ -helices at residues 144-154, 173-194, and 200-226 and a short anti-parallel  $\beta$ -sheet comprising of the residues 128-131 and 161-164. (B) An alignment of the 8 different mammalian prion proteins - elk (PDB ID 1XYW), rabbit (PDB ID 2FJ3), sheep (PDB ID 1UW3), syrian hamster (PDB ID 1B10), cow (PDB ID 1DWZ), human (PDB ID 1QLX), horse (PDB ID 2KU4) and mouse (PDB ID 1AG2). Rabbits and horses are less likely to be prone to TSEs whereas the rest of the 6 mammals are more susceptible to TSEs. This figure depicts the high degree of conservation in the global structures of the mammalian prion proteins irrespective of their susceptibility to TSEs.

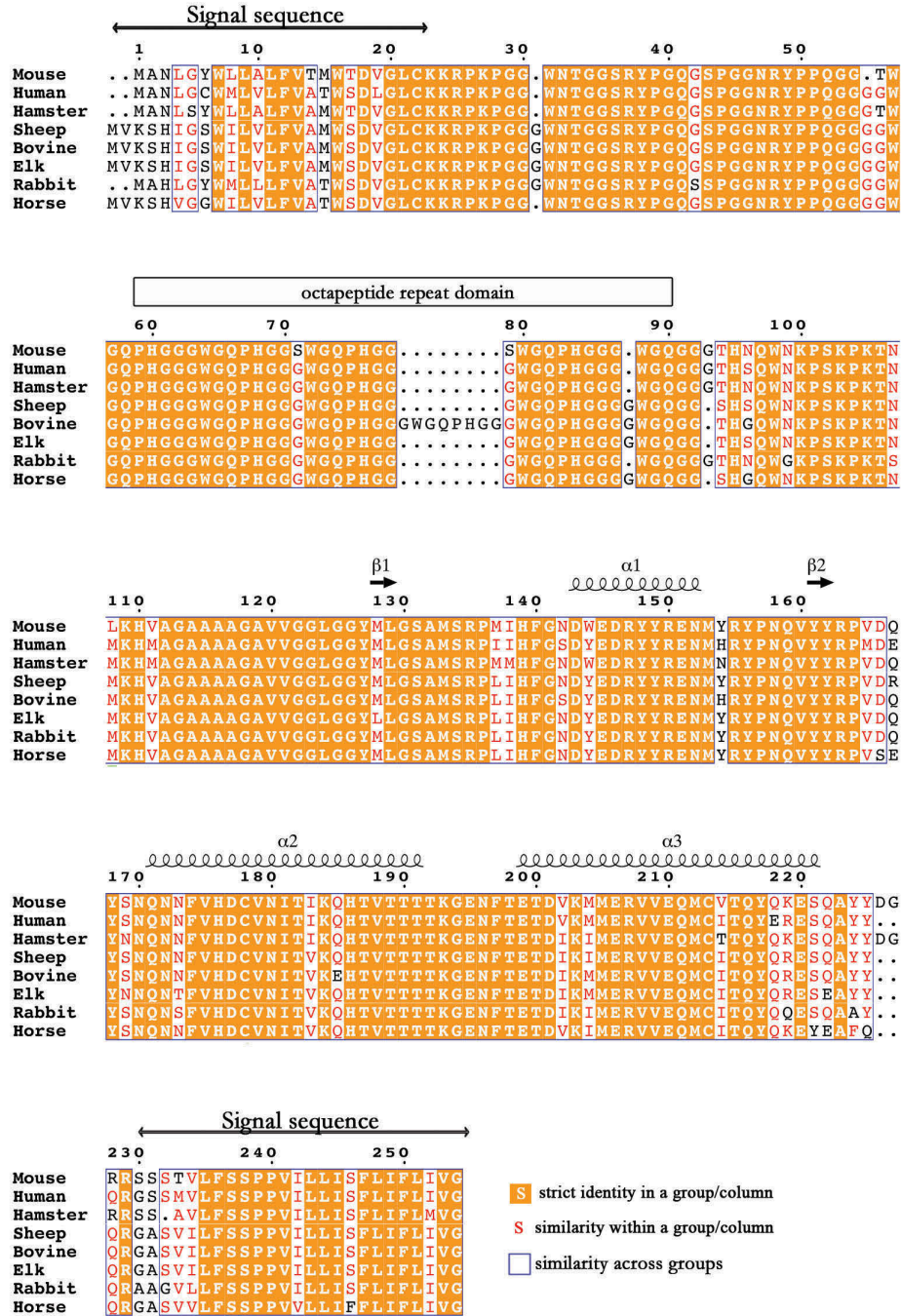


Figure 1.4: Amino acid sequence alignment of 8 mammalian prion proteins: mouse (mPrP), human (huPrP), syrian hamster (shPrP), sheep (ovPrP), bovine (boPrP), elk (ePrP), rabbit (rPrP) and horse (eqPrP) PrP. The sequence alignment was carried out using ClustalW2<sup>(111)</sup>. The numbers on the upper line indicate the residue numbering of mouse PrP. Residues 1-22 correspond to the amino terminal signal peptide and 232-254 correspond to the carboxy-terminal GPI anchor-addition signal peptide. The secondary structural elements are indicated on the top of the sequences with the  $\alpha$  helices shown as spirals and the  $\beta$  sheets as block arrows. The highly conserved region of the octapeptide repeats (residues 59-90) is also specifically labelled. Most of the mammals have 4 ORs whereas cows have 5 ORs. ESript 3.0<sup>169</sup> was used to generate the above figure.

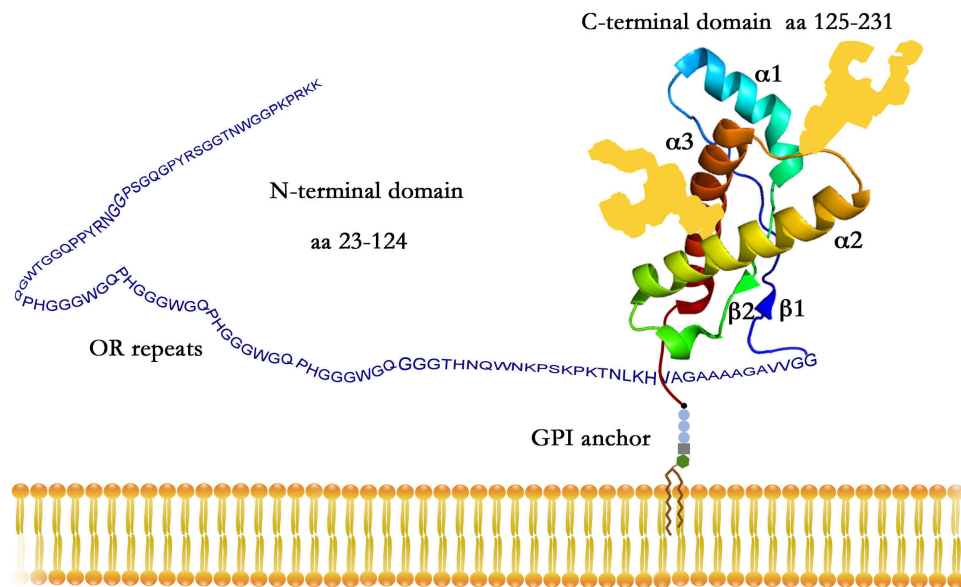


Figure 1.5: A schematic representation of the native Prion protein. The native, mature mouse  $PrP^C$  (residues, 23-231) is a GPI-anchored glycoprotein<sup>184</sup> with a structured carboxy terminal domain and an unstructured amino-terminal domain. The figure shows a schematic representation of the native full-length  $PrP^C$  attached to the bi-lipid layer of a cell *in vivo*<sup>166</sup>. Due to the absence of a defined structure for the amino terminal half of the protein from residues 23-124, the domain has been represented with the sequence of the amino acids that make it up. The globular structure of the C-terminal domain PrP from residues 124-231 has been represented using the NMR structure of mouse PrP (PDB ID 1AG2) and is coloured in the spectral scheme that starts with blue at the amino-terminus domain and progresses to red at the carboxy-terminus domain.  $PrP^C$  is N-glycosylated at residues Asn-180 and Asn-196 and can exist in un-, mono- or di- glycosylated forms<sup>79</sup>. The glycans (colored yellow) and the GPI anchor site are also shown in the figure.

ability of PrP<sup>C</sup><sup>30</sup>, it was proposed that PrP<sup>C</sup> may play a role in buffering Cu<sup>+2</sup> levels in the synapse to protect synapses from the reactive oxygen species (ROS) generated by Fenton reactions<sup>108</sup>. It must be noted that none of these functions have been unambiguously proved.

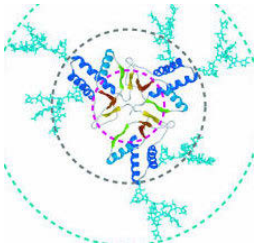
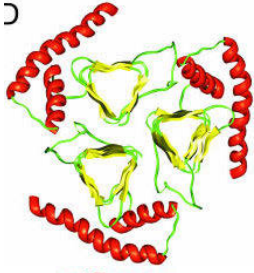
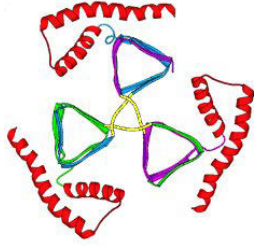

### 1.3.3 Structural models of PrP<sup>Sc</sup>

Chemical differences between the PrP<sup>C</sup> and PrP<sup>Sc</sup> isoforms such as amino acid composition or a post-translational chemical modification could not be detected<sup>183</sup>. However, structural and biochemical studies by Meyer et al., reported that PrP<sup>C</sup> is monomeric, protease sensitive and soluble in non-denaturing detergents whereas PrP<sup>Sc</sup> is oligomeric with a protease resistant core and insoluble in detergents<sup>126</sup>. Using negative-stain electron microscopy, PrP<sup>Sc</sup> was observed for the first time as fibrils that were named ‘scrapie associated fibrils’<sup>125</sup> or ‘prion rods’<sup>160</sup>. The three-dimensional structures of PrP<sup>Sc</sup> and PrP27-30 have always been difficult to determine using X-ray crystallography and NMR due to their heterogeneity and aggregation tendencies. Instead, scientists have adopted molecular modelling methods to predict their structures. However, due to the lack of sufficient experimental data to restrain and test the models generated, the literature is filled with different models of PrP<sup>Sc</sup> that do not agree with one and another<sup>163</sup>. See Table 1.4 for some of the existing models of PrP27-30 and their drawbacks. PrP<sup>C</sup> to PrP<sup>Sc</sup> conversion is the central event in TSE however, the structure of PrP<sup>Sc</sup> continues to be a major unanswered question.

### 1.3.4 Replication of PrP<sup>C</sup> to PrP<sup>Sc</sup>

The crux of the ‘protein-only’ hypothesis is that PrP<sup>Sc</sup> directly interacts with the normal, host encoded isoform, PrP<sup>C</sup> and acts as a scaffold to induce the conversion of PrP<sup>C</sup> to PrP<sup>Sc</sup> without the presence of nucleic acids<sup>66,73,158</sup>. In 1994, this phenomenon was demonstrated in the cell free environment by inducing the conversion of PrP<sup>C</sup> to PrP<sup>res</sup> on the addition of specific amounts of PrP<sup>Sc</sup> that was purified from scrapie-infected brain tissue<sup>103</sup>. Hence, the central event in the TSEs is the auto-catalytic conformational conversion of cellular, monomeric, protease-sensitive PrP<sup>C</sup> into a toxic, infectious, protease resistant, oligomeric PrP<sup>Sc</sup>. The cyclical nature of this conversion was further confirmed by a novel *in vitro* conversion system called PMCA (short for protein misfolding cyclic amplification) that was designed for transforming large quantities of PrP<sup>sen</sup> with minute amounts of PrP<sup>res</sup>. It was unambiguously demonstrated that the newly produced PrP<sup>res</sup> was capable of prop-

Table 1.4: A summary of the various molecular models of PrP27-30<sup>163</sup>

Year	Model basis	Structure	Drawback	Figure
2004	Simulation of the conversion of recPrP to PrP <sup>Sc</sup> at acidic pH	spiral model with 3 $\alpha$ -helices and 4 $\beta$ -strands	$\beta$ -strand orientation disagrees with fiber diffraction, predicts $\alpha$ -helices	
2004	higher resolution 2D electron crystallography	Trimeric unit cells, left handed parallel $\beta$ -helical fold	predicts the presence of $\alpha$ -helices	
2005	MD simulations to refine $\beta$ -helical fold	3 fold domain swap in the trimeric unit cell	predicts the presence of $\alpha$ -helices	
2007	site-directed spin labeling and EPR spectroscopy	parallel, in-register $\beta$ -sheet structure	disagrees with the fiber diffraction data	

agating the misfolded protein<sup>172</sup>. Irrefutable evidence in favour of the ‘protein-only’ theory came in 2004 when Legname et al. showed that the inoculation of fibrils formed from recombinant Prp 89-230 to transgenic mice resulted in the development of neurologic dysfunction in mice<sup>114</sup>. Furthermore, in 2010 Wang et al showed that Prions generated from recombinant PrP in the presence of polyanions such as POPG (1-palmitoyl-2-oleoylphosphatidylglycerol) and RNA were infectious to mice when injected intracerebrally<sup>197</sup>. Later studies showed that RNA was not essential for the infectivity<sup>198</sup>.

There are many theories that predict the mechanism of conversion of PrP<sup>C</sup> to PrP<sup>Sc</sup> with the most popular one being the seeded polymerization theory<sup>38,40,46</sup>. This theory proposes that the two isoforms of prion protein - PrP<sup>C</sup> and monomeric PrP<sup>Sc</sup> (or PrP<sup>Sc</sup>-like molecule) are in reversible thermodynamic equilibrium. An amyloid can be formed only if several monomeric PrP<sup>Sc</sup> molecules are recruited to form a highly ordered nucleus resembling a crystal-like seed. It is the formation of such an ordered nucleus ranging in size from small oligomers of PrP<sup>Sc</sup> to large amyloid plaques, that is crucial for amyloid formation. The fragmentation of these seeds would increase the number of nuclei which could in turn recruit more PrP<sup>Sc</sup> to accelerate the replication of PrP<sup>C</sup><sup>8,10</sup>. This theory is supported by several studies performed on the amyloid fibril forming abilities of small synthetic peptide fragments of the PrP<sup>46,61,67</sup>.

## 1.4 Anti-Prion therapy

### 1.4.1 Invasion of Prions from periphery to neurons

In most cases of acquired TSEs, the infectious agent replicates within the extracerebral (peripheral) tissues before invading the brain<sup>9</sup>. In the case of TSEs caused by oral consumption of contaminated meat, prions withstand exposure to the harsh environment of the digestive tract consisting of gastric acid and digestive enzymes to get absorbed through the digestive tract wall and enter the host lymphoreticular system<sup>99</sup>. Due to the lack of immunogenicity of PrP<sup>Sc</sup>, these absorbed prions escape inspection by the host immune system and multiply in the Follicular dendritic cell (FDC) membranes in the lymphoid follicles of secondary lymphoid organs (SLOs) such as Peyer’s patch, spleen, tonsils and lymph nodes<sup>9</sup>. Peripheral prion replication is seen in Scrapie, CWD and vCJD which are also termed lymphotropic TSEs but is absent in human sporadic or genetic TSEs<sup>9</sup>.

In the lymphotropic TSEs, after the initial peripheral accumulation within SLOs,



prions invade the central nervous system (CNS) through the sympathetic autonomic nervous system via retrograde axonal transport<sup>22</sup>. As SLOs are sympathetically innervated, they facilitate prion neuroinvasion<sup>68,156</sup>. It has been suggested that upon neuroinvasion, the Milk fat globule epidermal growth factor 8 (Mfge8) mediates large-scale microglial activation and proliferation that enhances clearance of apoptotic neuronal cell bodies caused by PrP<sup>Sc</sup> deposition<sup>81,107</sup>. The characteristic spongiform vacuolation and neuronal loss occur when the PrP<sup>Sc</sup> replication far exceeds prion clearance by microglia. However, the exact mechanism of neurodegeneration remains unclear. In the case of neurotropic TSEs, the peripheral prion replicative phase is completely bypassed to progress towards prion neuroinvasion<sup>130</sup>. Figure 1.6 shows a schematic representation of the different stages of prion replication based on the route of prion entry.

### 1.4.2 Therapeutic strategies

Limited understanding of prion neurotoxicity and the complexities involved in drug delivery to the CNS are two of the major challenges faced while designing prophylactic or therapeutic interventions towards TSEs. A majority of the anti-prion therapeutic efforts are based on attempts to inhibit the conformational conversion of PrP<sup>C</sup> to PrP<sup>Sc</sup>. Prevention of prion accumulation in SLOs in the asymptomatic lymphoreticular phase is another novel approach being studied in order to attempt to prevent or delay prion neuroinvasion<sup>10</sup>. Below is a summary of the different approaches and targets that are being studied in the field of Prion therapeutics<sup>10,106,145</sup>. Validation of some of these approaches has only been done using *in vitro* methods while that of others has progressed to testing in cell cultures, animal models and even human clinical trials.

1. Inhibition of the PrP<sup>C</sup> to PrP<sup>Sc</sup> conversion or the formation of higher order aggregates by
  - (a) blocking the domains within PrP<sup>C</sup> that are known to be ‘initiators’ of prion conversion process using compounds or antibodies (active and passive immunity)<sup>11,17</sup> (Figure 1.7A).
  - (b) interfering with PrP expression by *Prnp* mRNA knockdown using antisense oligonucleotides<sup>135</sup> to reduce the availability of PrP<sup>C</sup> for prion conversion (Figure 1.7B). This gene therapy has resulted in delaying the onset of the disease in mice.

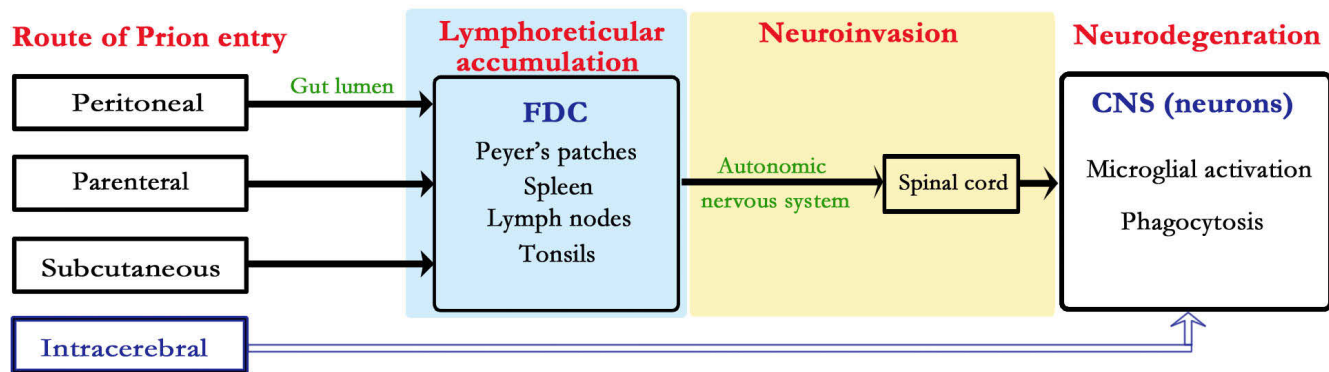


Figure 1.6: **Progression of prion infection based on the route of entry:** Peripheral exposure to prions occurs when the routes of prion entry are peritoneal, parenteral and subcutaneous. After the peripheral exposure, prions accumulate and replicate in the follicular dendritic cells (FDCs) of the secondary lymphatic organs (SLOs) like Peyer's patches, spleen, lymph nodes and tonsils. Prion neuroinvasion starts from the SLOs via the autonomic nervous system and progresses towards the mid-thoracic spinal cord and then gradually spreads to the brain<sup>177</sup>. Upon neuroinvasion, enhancement of microglial activation by Mfge8 enhances the clearance of apoptotic neurons<sup>81,107</sup>. However, the clinical symptoms start manifesting once the prion replication rate exceeds the clearance rate by microglia. In the case of intracerebral prion entry, prions bypass the lymphatic reticular system and directly enter the central nervous system.



- (c) lentiviral vector mediated RNA silencing of PrP<sup>C</sup> which has also resulted in delaying the onset of prion infection in mice<sup>150</sup>
  - (d) sequestering all the available PrP<sup>Sc</sup> molecules with pharmacological compounds to prevent the use of PrP<sup>Sc</sup> as a template for prion conversion<sup>10</sup> (Figure 1.7C)
  - (e) stabilizing prion fibrils using chemical compounds or antibodies to prevent further nucleation and higher order aggregation (Figure 1.7C)
2. Alteration of cell surface localization of PrP<sup>C</sup><sup>24,41</sup>
  3. Inactivation of the PrP<sup>Sc</sup> isoform using compounds like  $\beta$ -sheet breaker peptides and intercalating compounds such as congo red<sup>11</sup>
  4. Acceleration of bio-clearance of PrP<sup>Sc</sup> using compounds<sup>157</sup> or PrP<sup>Sc</sup>-specific antibodies<sup>10</sup>.
  5. Elimination/ inactivation of functional FDCs to block lymphoid prion accumulation and replication sites<sup>10</sup>
  6. Targeting the lymphotoxin  $\beta$  receptor pathway by LT $\beta$ -R-Ig fusion protein to block FDC maturation and prevent scrapie neuroinvasion<sup>119</sup>.
  7. Lentiviral vector-mediated RNA silencing of an important prion binding protein<sup>192</sup>- the Laminin receptor (LRP/LR) which prolonged the preclinical phase of scrapie infected mice<sup>151</sup>.

None of the above approaches have been successful in completely reversing the progress of the disease in animal models or humans. Moreover, most of these approaches display major limitations in terms of toxic effects and/or pharmacokinetics. Small molecules compounds such as Pentosan polysulfate, quinacrine, Amphotericin B showed sufficient promise to progress to the stage of human clinical trials but failed to reverse the clinical manifestations in any of the patients<sup>145</sup>. All the patients in the trials eventually succumbed to the disease.

### 1.4.3 Passive Immunization

The last decade has seen increased research efforts in developing active and passive immunity against TSEs. The promising translation of drug trials from murine models to humans in the case of Alzheimer's disease<sup>50</sup> has added impetus to increasing the

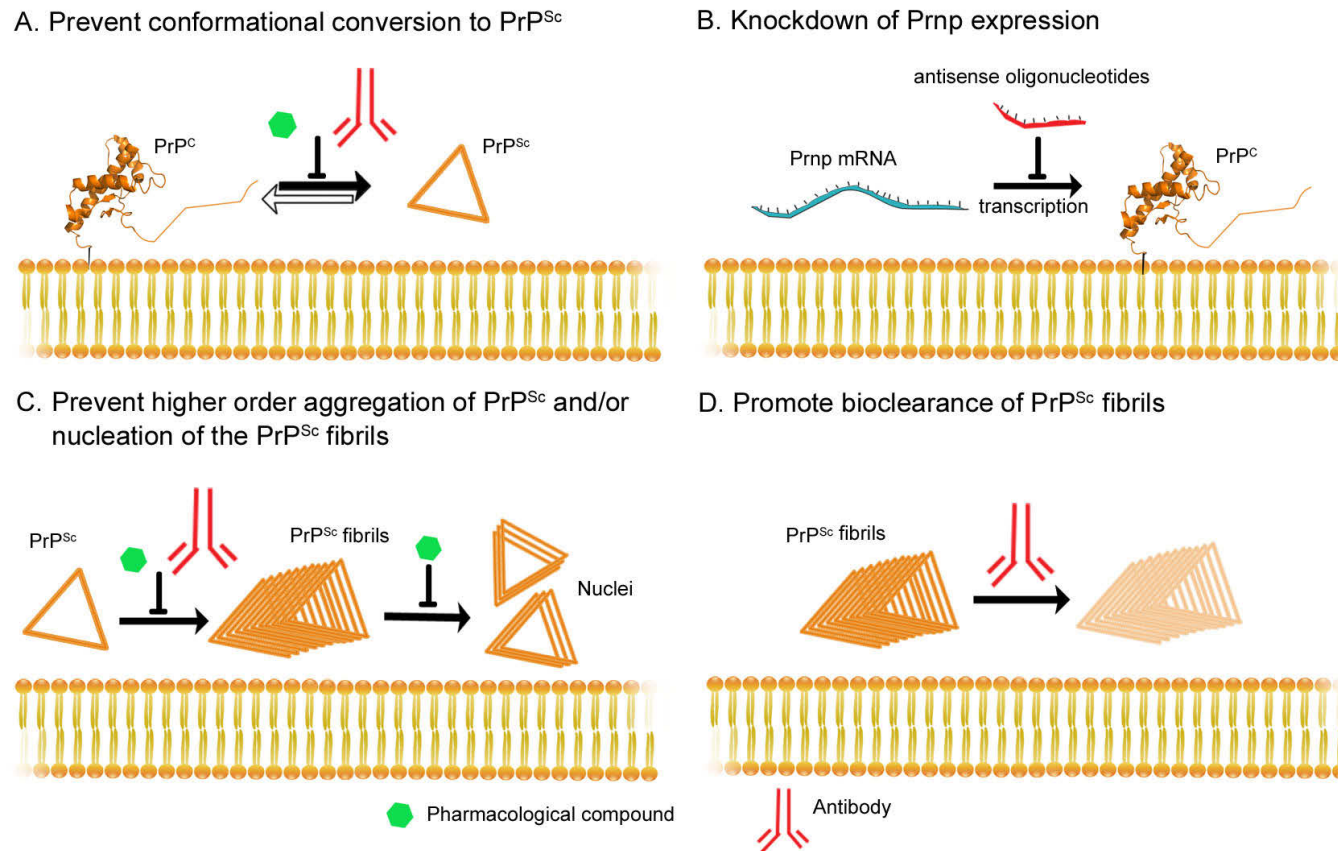


Figure 1.7: Potential anti-Prion therapeutic strategies (A) Pharmacological compounds or antibodies can bind to and stabilize PrP<sup>C</sup> to prevent its conformational conversion to PrP<sup>Sc</sup>. (B) Knockdown or RNA silencing of the Prnp mRNA to reduce the availability of PrP<sup>C</sup>. (C) Pharmacological compounds or antibodies can bind to PrP<sup>Sc</sup> to prevent the formation of higher order aggregates such as PrP<sup>Sc</sup> fibrils. Compounds could also be used to stabilize PrP<sup>Sc</sup> fibrils to prevent the formation of more nuclei. (D) Antibodies binding to PrP<sup>Sc</sup> fibrils can promote their bioclearance.

efforts to developing prion immunotherapy. PrP<sup>Sc</sup> is not immunogenic and does not induce a humoral immune response in the host. It is likely that resistance of PrP<sup>Sc</sup> to proteolytic degradation impairs the presentation of PrP<sup>Sc</sup> fragments to T-cells by phagocytic antigen presenting cells (APC), such as dendritic cells (DCs), macrophages, and microglia leading to the absence of a host immune response<sup>182</sup>. Currently, this lack of immune response creates the biggest challenge to developing active immunization for TSEs. There have been a few studies that showed success in eliciting host immune responses using synthetic PrP peptides<sup>9,171</sup> but most of them resulted in only delaying the onset of the disease but failed to arrest the progression of the disease. It should also be noted that there is a danger that active immunization strategies used for human TSEs can lead to severe autoimmune disorders such as meningoencephalitis<sup>171</sup>. Hence, most researchers prefer the passive immunization approach towards TSEs .

Passive immunity is developed in a host by transferring large amounts of ready made anti-PrP antibodies. There are a vast number of monoclonal antibodies that have been raised against the various fragments (such as PrP peptides, recombinant full-length PrP) and isoforms (PrP<sup>C</sup> and PrP<sup>Sc</sup>)<sup>80,120,154,171,173</sup> of the prion protein that have become critical to characterizing the various domains of PrP and their role in the pathophysiology of TSEs. Although, monoclonal antibody technology has been primarily used to facilitate the structural as well as the functional studies of proteins via their immunogenic regions, when the antibodies show therapeutic effects in cell cultures and/or mice models, they become good candidates for developing passive immunotherapy. There have been several *in vitro*, *ex vivo* and *in vivo* experiments that have shown that anti-PrP monoclonal antibodies (mAb) that bind to specific regions of PrP<sup>C</sup> - octapeptide repeat domain 59-90, residues 90-110, the helices  $\alpha$ 1,  $\alpha$ 2,  $\alpha$ 3, prevent prion conversion<sup>9,72,134,145,171</sup>. During the past decade, intense efforts have been undertaken to develop passive immunotherapy to combat prion diseases.

Two seminal experiments conducted in animal models of prion disease showed the potential of passive immunotherapy to combat peripheral prion infection. In 2001, Heppner et al demonstrated that transgenic mice expressing the  $\mu$  chain of the 6H4 anti-PrP monoclonal antibody (epitope residues 144-152 moPrp)<sup>80</sup> were protected from peripheral prion inoculation and showed an inhibition in PrP<sup>Sc</sup> accumulation in spleen. And in 2003, White et al performed a true passive immunization experiment by long term intraperitoneal administration of either mAbs ICSM 35 (epitope, aa91-110) or ICSM18 (epitope, aa146-159) in FVB/N wild type mice and showed an inhibition in PrP<sup>Sc</sup> accumulation in spleen<sup>201</sup>. Similarly, in 2009 Sadowski et al

showed that the passive immunization of CD-1 mice with mAb 6D11( epitope residues 97-100 moPrP) suppressed peripheral prion accumulation in spleen and prolonged the survival time of mice<sup>173</sup>. The scFv D18 antibody fragment (epitope aa132-156) delivered using recombinant adeno-associated virus mediated vector was also found to delay the onset of the disease in peripherally challenged mice<sup>55</sup>. In all the cases, however, mice succumbed to the disease in the case of cerebral prion challenge or when the mAb or scFv administration was started in the late stages of prion infection after the appearance of the first clinical signs.

In the above cases, despite all the treatments failing to reverse the symptoms, they have been successful in significantly prolonging the survival times in mice. These effects are promising enough to warrant deeper studies into the mechanism of the actions of the antibodies, their efficacy, pharmacokinetics and efficient delivery into the CNS. It is highly likely that the lack of efficacy in the case of intracerebral prion challenge is due to the poor blood-brain-barrier (BBB) penetration of antibodies. However, a recent study<sup>141</sup> showed that the peripheral administration of mAb 31C6 (epitopes 143- 149 moPrP) in mice reduced the levels of PrP<sup>Sc</sup> in the brain and prolonged its survival showing promising potential for the peripheral route of antibody administration<sup>141</sup>. One of the future challenges is to make the anti-PrP mAbs, their Fab fragments or recombinant mini-antibodies such as scFv more BBB-permeable in order to improve their efficacy against intracerebral prion infection.

#### 1.4.4 POM monoclonal antibodies

Our collaborators Aguzzi et al, generated a panel of monoclonal antibodies in *Prnp* knockout mice to obtain novel specificities toward recombinant full length mouse PrP<sup>154</sup>. These antibodies named POM1 through POM19 include several antibodies that recognize regions in the carboxy-terminal domain of PrP such as POM1, POM6, POM7 and POM19 while antibodies such as POM2 and POM12 recognize residues in the flexible amino-terminal domain of PrP<sup>154</sup>. The antibodies that are of interest to us are POM1, POM2 and POM6.

The crystal structure of POM1 Fab with PrP 120-231 (PDB ID 4H88)<sup>180</sup> confirmed that POM1 has a discontinuous epitope in PrP comprising of the domains -  $\beta$ 1- $\alpha$ 1 loop,  $\alpha$ 1 and  $\alpha$ 3 helices<sup>18,154</sup> (Figure 1.8A). In order to characterize anti-PrP antibodies functionally under conditions that closely mimic intracerebral prion infection *in vivo*, the cerebellar organotypic slice culture (COCS) assay was used which allows for prion amplification and titration in cultured slices of the cerebellum<sup>53,54</sup>.

Sonati et al discovered that the exposure of POM1 Fab and scFv to COCS and mice led to rapid and severe neurotoxicity<sup>180</sup>. Interestingly, the neurotoxicity was very similar to that seen in prion infections as it was accompanied by calpain activation and was antagonized by calpain inhibitors. However, the crystal structure of POM1 Fab-PrP120-231 complex revealed no changes in the structure of the globular domain of PrP suggesting that the neurotoxicity could potentially be due to changes in the amino-terminal domain of PrP.

The potential functional effects of the amino-terminal domain of PrP upon POM1 binding was studied using the POM2 antibody. Epitope mapping studies showed that POM2 has an epitope in the OR domain<sup>154</sup> and up to two POM2 molecules can bind to one PrP molecule at any time (Figure 1.8B). POM2 can bind to any one of the 4 ORs and binds to both the mouse and human PrP<sup>C</sup> molecules. Sonati et al showed that POM1 induced neurotoxicity in COCS and mice was inhibited by both POM2 Fab and POM2 scFv<sup>180</sup>. Moreover, the inhibition of POM1 toxicity was also seen upon deleting the OR domain<sup>180</sup>. The blocking of the OR domain with ligands such as POM2 Fab or scFv may have a great potential for therapy. The important implication of this study is that such N-terminal-mediated toxicity could potentially play a crucial role in the pathogenesis of familial TSEs in humans like the familial CJD that occurs due to the presence of extra octapeptide repeats in their *Prnp* gene.

The main conclusion of the study<sup>180</sup> was that the binding of some PrP-specific antibodies to the globular domain of PrP<sup>C</sup> results in severe toxicity that is mediated by the flexible amino-terminal domain<sup>180</sup>. A third antibody - POM6 binds to the globular, carboxy-terminal domain of PrP. POM6 competes with POM1 for PrP binding and has an epitope in the  $\alpha$ 1 helix (Figure 1.8B). Interestingly, upon determining the functional effect of POM6 Fab on COCS slices, Sonati et al showed that POM6 Fab, unlike POM1 is completely innocuous to the cerebellar slices showing a complete lack of neurotoxicity<sup>180</sup>. A comparative structural analysis of POM6 and POM1 Fab binding to the Prion protein could reveal the underlying cause of POM1 induced neurotoxicity.

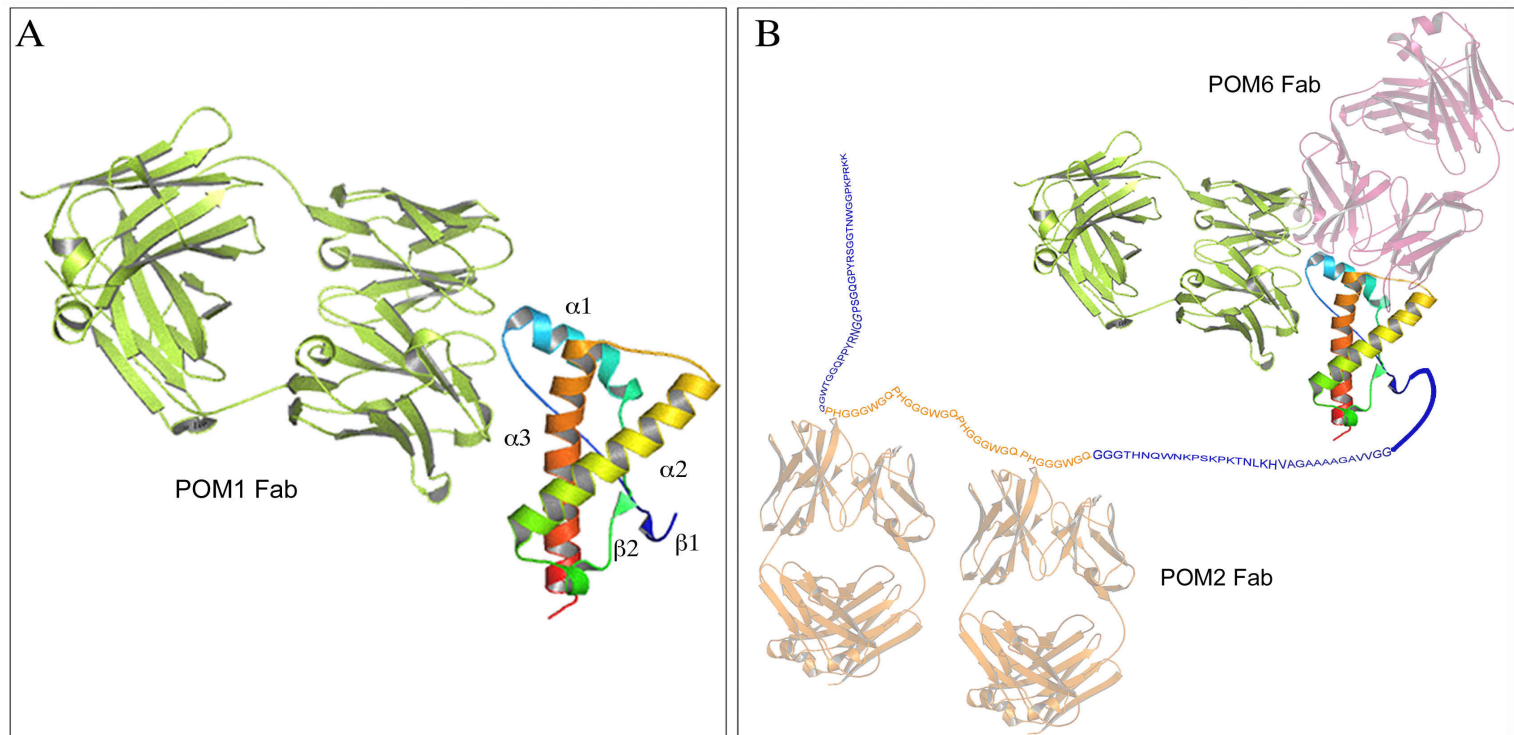


Figure 1.8: POM monoclonal antibodies - POM1, POM2, POM6 and their epitopes. (A) The crystal structure of the complex of POM1 Fab - PrP120-231 (PDB ID 4H88). The POM1 Fab interacts with the  $\beta 1$ - $\alpha 1$  loop and  $\alpha 1$  and  $\alpha 3$  helices (residues 138-147; 204/208/212)<sup>18,154</sup>. POM1 Fab molecule is shown in green whereas PrP120-231 is coloured in the spectral scheme with the amino terminus coloured blue to the carboxy-terminus coloured red. (B) A representation of the predicted binding sites of POM2 Fab and POM 6 Fab in complex with the full length Prion protein based on previous epitope binding studies<sup>154</sup>. PrP23-231 is represented as seen previously in Figure 1.5. Two molecules representing POM2 Fab (coloured in orange) are shown in their predicted binding site in the octapeptide repeat domain (aa 59-90) of mouse PrP23-231<sup>154</sup>. Polymenidou et al showed that POM6 binds to  $\alpha 1$  helix and competes with POM1 for binding. A molecule representing POM6 Fab (coloured in warm pink) is shown in its predicted binding site. Note that the molecules of POM2 Fab and POM6 Fab are schematic representations only and are shown with 50% transparency with respect to POM1 Fab molecule. POM1 Fab shown (coloured in green) is part of a crystal structure (PDB ID 4H88).

## 1.5 Research goals

We have access to three very interesting anti-PrP antibodies - POM1, POM2 and POM6<sup>154</sup>. Extensive structural and functional characterization of the POM1 antibody has already been published<sup>17,19,180</sup> and shows that the POM1 antibody causes neurotoxicity similar to that seen in prion infections and is mediated by the amino terminal domain of PrP. While the POM1 antibody is toxic to cerebellar slices, POM2 and POM6 antibodies are innocuous. More interestingly, the POM2 antibody inhibits the toxicity of POM1. The structural characterization of the POM2 antibody would not only aid in the development of better inhibitors of neurotoxicity but also might aid in determining the role of the ORs in the amino terminal domain mediated neurotoxicity. POM6 and POM1 antibodies have neighbouring epitopes on PrP and compete with each other for binding<sup>154</sup>. Despite this, they show opposite functional effects in COCS assays. A comparative structural characterization of the modes of binding of the POM1 and POM6 antibodies with the prion protein could determine the domains within the PrP molecule that trigger the cascade of events that lead to the amino terminal domain mediated toxicity.

My overall research goal is to use the technique of X-ray crystallography and to structurally characterize the mode of binding of two anti-PrP antibodies - POM2 and POM 6 to the prion protein. The study of POM2 would facilitate the development of a more robust, tightly bound inhibitor of neurotoxicity that could potentially be a candidate for prion therapeutics. The study of POM6 would enable the determination of the neurotoxicity-causing motifs within the prion protein. The three specific research goals of my project are :

1. Engineer, express and produce large quantities of a POM2 minibody such as the single chain variable fragment (scFv).
2. Structurally to characterize the binding of the prion protein with POM2 antibody fragments (scFv or Fab) in high resolution using X-ray crystallography.
3. Structurally to characterize the binding of the prion protein with POM6 antibody fragments (Fab) in high resolution using X-ray crystallography.

# Chapter 2

## POM2 scFv engineering and purification

### 2.1 Introduction

A typical immunoglobulin G (IgG) molecule is a Y shaped glycoprotein comprised of four polypeptide chains - two identical large chains (heavy, H) and two identical small chains (light, L) (Fig 2.1A). The H and L chains are connected to one another by inter-chain disulfide bonds. Based on the sequence variability across the antibodies of the same class, the H and L chains are sub-divided into constant ( $C_H$ ,  $C_L$ ) and variable ( $V_H$ ,  $V_L$ ) domains. Each of the  $V_H$  and  $V_L$  domains contain three loops with hypervariable sequences that are separated by four conserved framework regions. These hypervariable loops are known as the Complementarity Determining Regions (CDRs); they dictate the specificity of an IgG to its antigen<sup>97</sup>. The arms of the Y-shaped IgG molecule are joined by flexible stretches of polypeptide chains that make up the hinge region (Fig 2.1A)<sup>121</sup>. These hinges create an inherent intrinsic segmental flexibility within an IgG<sup>86</sup> that facilitates the binding of a single IgG molecule to epitopes from either two different antigens or two repeating epitopes from a single antigen<sup>170</sup>. Unfortunately, from a structural biology point of view, this segmental flexibility often interferes with the crystallization of IgG molecules by impeding the formation of a regular, repeating crystal lattice<sup>86</sup> (Fig 2.1B). The fragmentation of the IgG molecules to obtain smaller, well-ordered but functional domains has been a proven way to circumvent their non-crystallizability<sup>47</sup>. Hence, we undertook the task of crystallizing functional fragments of POM2 IgG namely, variants of the single chain variable fragment such as scFv, dsFv or the Fab fragments (Fig 2.1 B, C & D).



An scFv molecule is one of the smallest functional units of an IgG molecule. It is made up of the  $V_H$  and  $V_L$  chains tethered together by a flexible peptide linker (Fig 2.1C)<sup>27</sup>. Due to its divalency, an IgG molecule has a higher avidity than its corresponding scFv. However, an scFv molecule has the advantage of being easily expressed in large quantities using most bacterial expression systems. An scFv can also be easily re-engineered to improve its antigen affinity or to alter its specificity by mimicking somatic hypermutation<sup>71</sup> seen during an immune response<sup>128</sup>. There are a number of crystal structures of scFvs bound to their respective antigens in the literature<sup>82,137,210,211</sup>. ScFvs have several clinical advantages over IgG or Fab molecules including reduced immunogenicity and better tumor penetration<sup>12</sup>. A variety of scFvs are now being designed for research, diagnostic, and therapeutic purposes to overcome the drawbacks associated with conventional antibodies<sup>136</sup>.

A recent study by our collaborators showed that POM2 scFv successfully inhibits POM1 generated toxicity in mice cerebellar slices<sup>180</sup> highlighting the potential for POM2 scFv to be developed as a therapeutic solution for prion diseases. Hence, our first objective was to conduct a crystallographic study of POM2 scFv in complex with its binding partner- the full length Prion protein or its fragments, most specifically the octapeptide repeat domain (residues 58-89). We intend to discover the effects of POM2 scFv binding on the structure of the prion protein that could potentially shed light on its mechanism of inhibition of POM1 toxicity.

## 2.2 Materials and Methods

### 2.2.1 Expression and purification of scFv POM2 from inclusion bodies

The scFvPOM2 gene was constructed previously<sup>154</sup> using phage display methods and sub-cloned into a pET-30a vector between the NdeI and XhoI endonuclease restriction sites (New England Biolabs). The expression and purification protocol has been described previously<sup>154</sup>. This plasmid was transformed into chemically competent Rosetta(DE3)pLysS cells (Promega) by the heat-shock method and plated onto Agar-Luria Bertani (LB) media with 50 $\mu$ g/ml Kanamycin and 34 $\mu$ g/ml Chloramphenicol. A fresh, single colony of transformed cells was inoculated in LB media with Kanamycin and Chloramphenicol and grown overnight at 37 °C with constant shaking at 250 r.p.m. The overnight culture was further propagated (1:1,000) in fresh media until the optical density at 600nm ( $OD_{600}$ ) reached  $\sim$  0.5-0.6 and was then

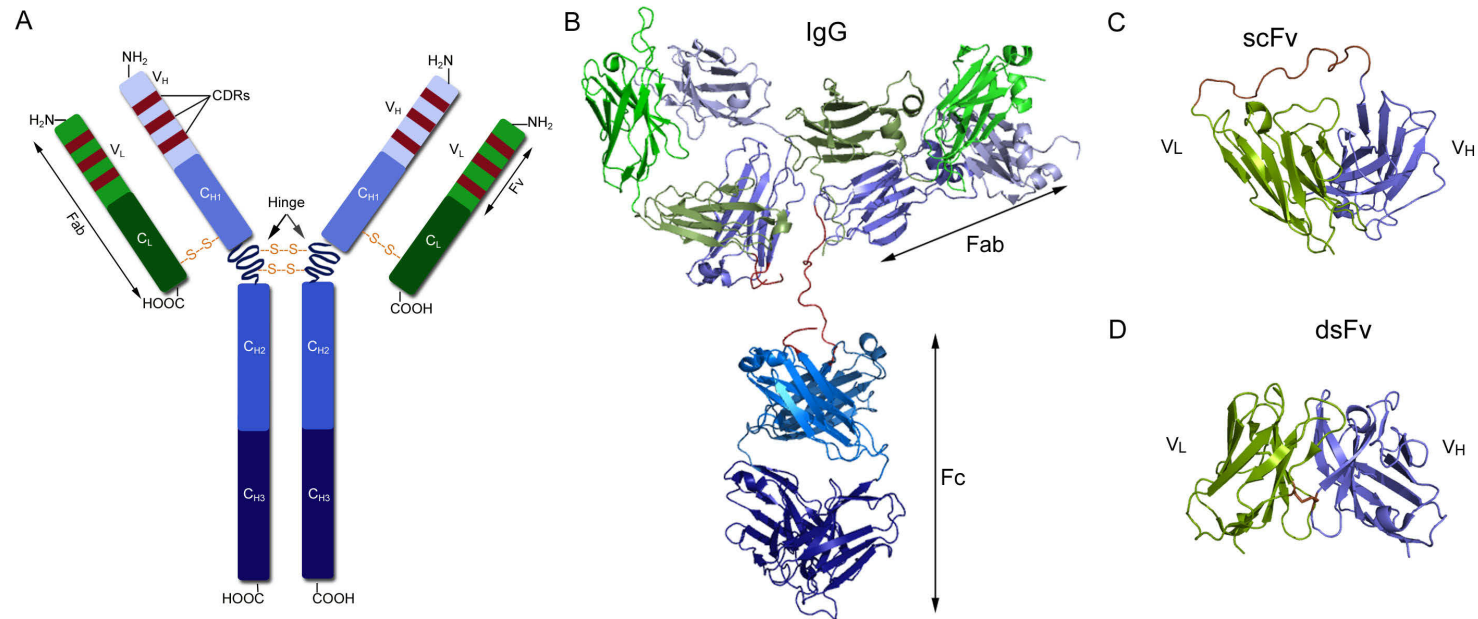


Figure 2.1: IgG molecule and its functional fragments (A) A schematic representation of an IgG molecule with a typical Y-shaped structure. The heavy chain of the IgG contains a constant domain (all shades of dark blue) that can be further subdivided into three constant domains -  $C_{H1}$ ,  $C_{H2}$ ,  $C_{H3}$ . The variable domain of the heavy chain ( $V_H$ , light blue) depicts the three hypervariable regions or CDRs (brown). The constant domain of the light chain ( $C_L$ ) is colored in dark green whereas the variable domain ( $V_L$ ) is coloured in light green and also depicts the three CDRs. The flexible hinge region connects the  $C_{H1}$  domain to the  $C_{H2}$  domain. (B) A crystal structure of an IgG molecule submitted in the protein data bank (PDB ID 1HZH). A Fab molecule is made up of the  $V_L$ ,  $C_L$ ,  $V_H$  and  $C_H$  domains (C) An scFv molecule is made up of the  $V_L$  and  $V_H$  domains tethered together by a peptide linker (PDB ID 1X9Q) whereas (D) a dsFv molecule comprises of a  $V_L$  and  $V_H$  domain linked together by a disulfide bond (PDB ID 1I8K).

induced with Isopropyl  $\beta$ -D-1-thiogalactopyranoside (IPTG) to a final concentration of 1mM. The induction was allowed to continue for 4 hours at 37 °C and 250 r.p.m . The cells were harvested and resuspended in 10ml of 1x PBS pH 7.0 for every 1 gm of the cell pellet. The pellet was processed in a cell disruptor at 20 kpsi and centrifuged at  $15,000 \times g$  for 30 min at 4°C to collect the inclusion bodies (IB). The IB were incubated with 10% sodium deoxycholate for 30min at room temperature after which the detergent was washed away with at least three washes of the TN buffer (50mM Tris, 200mM NaCl pH 8.0). The IB was solubilized in Buffer U (8M urea, 100mM  $\text{NaH}_2\text{PO}_4$ , 10mM Tris, 5mM Imidazole pH 8.0). The clarified soluble protein extract was loaded onto a Ni-NTA (Qiagen) column and the unbound protein and impurities were washed off with 3 column volumes of buffer U containing 50mM Imidazole. The scFv was eluted with Buffer U containing 200mM Imidazole. The purity of the eluates was checked using Sodium dodecyl sulphate -polyacrylamide gel electrophoresis (SDS-PAGE).

We used two different strategies to refold POM2 scFv to its functional state. The first strategy was the 'refolding by dilution' strategy<sup>101</sup> which involved the renaturation of scFv before allowing disulfide formation. The initial renaturation was carried out in buffers such as sodium phosphate, HEPES and Tris-HCl with pHs ranging from pH 6.0 to 8.0 in the presence of 0.5mM  $\beta$ -mercaptoethanol. However, all of these buffer conditions resulted in copious amounts of protein precipitation leaving only trace amounts of soluble POM2 scFv. Our second strategy for scFv refolding was the 'redox refolding' strategy<sup>101</sup> that involved the simultaneous renaturation and disulfide bond formation within the scFv. We used a wide range of buffers to renature the protein concomitantly with reduced glutathione/ oxidized glutathione redox coupling system.

### **2.2.2 Expression and purification of POM2 scFv from periplasm**

The scFv POM2 gene was sub-cloned into the pET-22b(+) vector between EcoRI and XhoI endonuclease restriction sites (New England Biolabs). The details of the construct are shown in figure 2.4. The resulting plasmid was transformed into chemically competent Rosetta (DE3) pLysS cells by heat-shock and plated onto Agar-LB media with 100 $\mu\text{g}/\text{ml}$  Ampicillin and 34 $\mu\text{g}/\text{ml}$  Chloramphenicol. The expression and purification protocol was previously described<sup>180</sup>. A fresh, single colony of transformed Rosetta cells was inoculated in 2xYT media with 100 $\mu\text{g}/\text{ml}$  ampicillin and 34 $\mu\text{g}/\text{ml}$  chloramphenicol (2xYT-AC media) and grown overnight at 37 °C with con-

stant shaking at 250 r.p.m. The overnight culture was further propagated (1:1,000) in fresh 2xYT-AC media until the  $OD_{600} \sim 0.4 - 0.5$ . The culture was then cooled down to 25°C in a cold water bath and induced with IPTG to a final concentration of 0.5mM. The induction was allowed to continue overnight at 25°C and 250 r.p.m. The cells were collected and resuspended in 50 ml of freshly prepared, pre-chilled periplasmic extraction buffer (200mM Tris-HCl, 20% (w/v) sucrose, 1mM EDTA pH 8.0) for every 1L of the original culture volume and incubated on ice for 1h with occasional stirring. The suspension was spun down at  $15,000 \times g$  for 30min at 4°C. The supernatant was collected as the soluble protein extract. The extract was thoroughly dialysed against 50mM Tris-HCl, 100mM NaCl, pH 7.0 at 4°C to eliminate the sucrose and further clarified by centrifugation at  $15,000 \times g$  for 30 min at 4°C. The clarified soluble protein extract was loaded onto a Ni-NTA agarose column equilibrated with 50mM Tris-HCl 100mM NaCl pH 7.0. The unbound protein and impurities were washed off with 50mM Tris, 100mM NaCl, 50mM imidazole pH 7.0 and the elution was performed with 50mM Tris, 100mM NaCl 500mM Imidazole pH 7.0. The purity of the protein sample was checked by running the samples on a 12% gel by SDS-PAGE. Pure scFv POM2 samples were dialysed against 50mM Tris, 100mM NaCl, 50mM Imidazole pH 7.0 and concentrated to 3mg/ml.

### 2.2.3 Gene assembly with linker modification

An overlap-extension PCR was used to construct the POM2-218 gene. The 218 linker is an 18 amino acid linker with the amino acid sequence - GSTSGSGKPGS-GEGSTKG<sup>142,148,149</sup>. The 218 linker connects the carboxyl terminus of the  $V_L$  domain to the amino terminus of the  $V_H$  domain of POM2. The POM2-218 gene was constructed in two steps. In the first step, the  $V_L$  and  $V_H$  genes were amplified separately by PCR from the POM2 scFv gene. In the second step, an overlap-extension PCR<sup>84</sup> was used to combine the  $V_L$  and  $V_H$  genes via the 218 linker to form the POM2-218 gene. The two PCR steps are explained in detail below and a schematic representation is shown in Figure 2.2. Table 2.1 has a comprehensive list of all the primers used for the cloning of POM2 -218 scFv.

In the first step, the  $V_L$  gene was amplified using the P2VL<sub>a</sub> sense and P2-218b antisense primers whereas the  $V_H$  gene was amplified using the P2-218c sense and P2VH<sub>b</sub> antisense primers (Figure 2.2). The PCR reaction mixture (50  $\mu$ l) contained 10 ng plasmid DNA, 0.1 mM dNTP, 0.5 mM of each primer, 0.5 unit of Taq polymerase (New England Biolabs, Pickering, ON, Canada), and standard Taq polymerase

buffer. The PCR was carried out in a Perkin-Elmer thermal cycler with an initial denaturation at 94°C for 5 min; 30 cycles of 94°C for 30sec, 60°C for 30sec, and 72°C for 1 min; and a final extension at 72°C for 10 min. The  $V_L$  and  $V_H$  fragments were purified on a 1% agarose gel and extracted from the gel slice using QIAquick Gel Extraction Kit (QIAGEN, Mississauga, ON, Canada).

P2-218b and P2-218c primers were designed to have long overhangs comprised respectively, of the two halves of the 218 linker with a 6bp overlapping, complementary segment (Figure 2.2). In the second stage PCR, this complementarity was used to splice the  $V_L$ ,  $V_H$  PCR products from the first reaction and used as a template to amplify the entire POM2-218 fragment. The PCR reaction mixture consisted of the P2VLa sense and P2VHb antisense primers and 10ng each of purified  $V_L$  and  $V_H$  PCR products as the template. The rest of the PCR mix composition and running conditions were the same as used in the first step. The  $V_L$ -218- $V_H$  product was gel-purified for restriction endonuclease digestion at 37 °C for 2h with EcoRI and XhoI restriction enzymes (Figure 2.5B). The same conditions were also used to digest the pET22b+ vector with EcoRI and XhoI. The digested products were gel purified and ligated using the T4 DNA ligase kit (Roche Applied sciences, Laval, QB, Canada) to obtain the final POM2-218 scFv gene in the pET22b+ vector. Competent *Escherichia coli* DH5 $\alpha$  cells (Invitrogen, Burlington, ON, Canada) were transformed with the ligation product and plated on Agar -LB medium with Ampicillin (100  $\mu$ g/ml). A colony PCR was performed for the randomly picked colonies with the P2VLa sense, P2VHb antisense primers to identify clones with the desired construct. Plasmids were extracted from the positive clones using the QIAprep Spin Miniprep kit (Qiagen) and their sequences were verified. POM2-218 scFv was expressed and purified from the periplasm as described previously in section 2.2.2.

#### 2.2.4 Construction of $V_L$ and $V_H$ genes

The  $V_L$  and  $V_H$  chains were amplified by PCR separately from the POM2 scFv gene and incorporated into the pET22b+ vector. The  $V_L$  gene was amplified using the nc-P2VLa sense and P2VLb-Thr antisense primers whereas the  $V_H$  gene was amplified using the nc-P2VHa sense and P2VHb-Thr antisense primers. Table 2.1 has a comprehensive list of all the primers used for the cloning of  $V_L$  and  $V_H$  chains . Due to the absence of a His tag cleavage site in the pET22b+ vector, both the P2VLb-Thr and P2VHb-Thr antisense primers were designed to include a thrombin cleavage site at the 5' end of the gene. The PCR reaction mixture (50  $\mu$ l) contained 10 ng plasmid

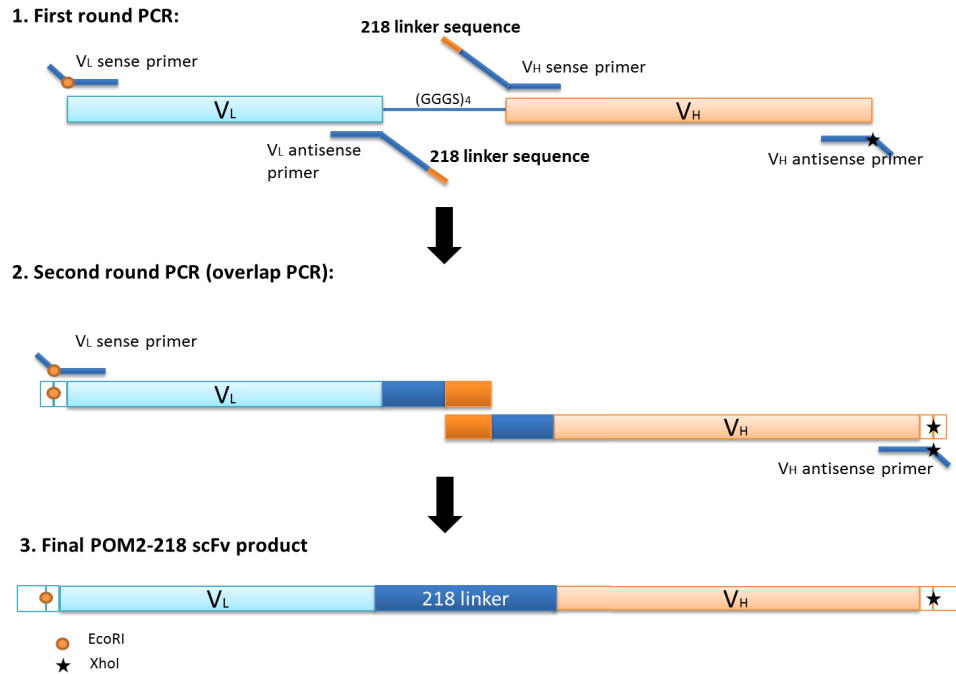


Figure 2.2: A schematic representation of the overlap- extension PCR utilized for linker modifications in scFv . The figure depicts the linker modification from  $(G_3S)_4$  to linker 218. In the first round of PCR, POM2 scFv was used as a template to amplify  $V_L$  and  $V_H$  chains, separately. In this step, the  $V_L$  antisense and  $V_H$  sense primers are designed to contain portions of the new linker in their overhang. A 6bp complementary sequence (shown in orange) is also introduced into these two primers thereby providing the region of overlap that is used to splice the two chains together. In the second round of PCR,  $V_L$  sense and  $V_H$  antisense primers are used along with the two products from step1 as template. This results in the incorporation of the new linker into the final PCR product.

Table 2.1: A list of the primers used for cloning POM2 scFv and its variants

Primer name	sequence
P2VL <sub>a</sub> sense	5'-CGACATCGAATTCGGATATTGTGATGACACAGTCTCAC-3'
P2-218b antisense	5'-ACCAGGCTTACCAGAACCAGAAGTAGAACCACGTTTGATTTC-3'
P2-218c sense	5'-CCTGGTTCTGGTGAGGGTTCTACTAAGGGTGAGGTAAAGCTT-3'
P2VH <sub>b</sub> antisense	5'-TGGTAAACTCGAGCGAGGAGACGGTGACTGAGG-3'
nc-P2VL <sub>a</sub> sense	5'-CGACATGCCATGGATATTGTGATGACACAGTCTCACAAA-3'
P2VL <sub>b</sub> -Thr antisense	5'-TAAAATCCTCGAGACTACCGCGTGGCACCAGCAGCTTGGTACCTCCACC-3'
nc-P2VH <sub>a</sub> sense	5'-CGACATGCCATGGAGGTAAAGCTTCAGGAGTCTGGA -3'
P2VH <sub>b</sub> -Thr antisense	5'-TAAAATCCTCGAGACTACCGCGTGGCACCAGGACTGAGGTTCCCTTGACC- 3'
dsP2VH <sub>m</sub> 44f sense	5'-CAGAGGCCTGGACAGTGCCTTGAGTGGATTG-3'
dsP2VH <sub>m</sub> 44r antisense	5'- CAATCCACTCAAGGCACTGTCCAGGCCTCTG-3'
P2VLg99g-f sense	5'-CTATCCGACGTTTCGGTGGCGGTACCAAGCTGCTGG-3'
P2VLg99g-r antisense	5'-CCAGCAGCTTGGTACCGCCACCGAACGTCGGATAG-3'
P2VLg99c-f sense	5'-CTATCCGACGTTTCGGTTCGGTACCAAGCTGCTGG-3'
P2VLg99c-r antisense	5'-CCAGCAGCTTGGTACCGCAACCGAACGTCGGATAG-3'
Tev-mVl-rev antisense	5'-CGCGGCCGCGCCTTCATTGAGATAGAATTGACCCAGCTTGGTACC-3'
Tev-mVh-for sense	5'-GCCGCGGGCGGCGAAAATCTCTATTTCCAAGGTGAGGTAAAGCTT-3'
PrP125-221for	5'-AATATAGGATCCCTTGGTGGCTACATGCTG-3'
PrP125-225rev	5'-AAGGTACGAATTCTTAGTAATAGGCCTGGGACT-3'

DNA, 0.1 mM dNTP, 0.5 mM of each primer, 0.5 unit of Taq polymerase, and standard Taq polymerase buffer. The PCR was carried out with an initial denaturation at 94°C for 3 min followed by 30 cycles of 94°C for 45sec, 60°C for 30sec, and 72°C for 30sec; and a final extension at 72°C for 7 min. The  $V_L$  and  $V_H$  fragments were purified on a 1% agarose gel and extracted from the gel slice and set up for restriction endonuclease digestion at 37°C for 2h with NcoI and XhoI restriction enzymes. The same conditions were also used to digest the pET22b+ vector with NcoI and XhoI. The digested products were gel purified and ligated to obtain the  $V_L$  and  $V_H$  genes respectively, in the pET22b+ vector with a C-terminal His-tag cleavage site. Competent DH5 $\alpha$  cells were transformed with the ligated products and plated on Agar - LB medium with Ampicillin (100  $\mu$ g/ml). A colony PCR was performed for the randomly picked colonies to identify clones with the desired construct. Plasmids were extracted from the positive clones and their sequences were verified. As plasmids produced from most *E. coli* strains are methylated, we used the above purified, methylated plasmids of  $V_L$  and  $V_H$  as templates during the site directed mutagenesis of  $V_L$  and  $V_H$  genes as shown in section 2.2.5.

### 2.2.5 Site directed mutagenesis of $V_L$ and $V_H$ genes

To design the POM2 dsFv, we studied a model of POM2 scFv (unpublished, modelled by Dr.PK Baral) to determine the residues in the  $V_L$  and the  $V_H$  chains that should be mutated to Cys in order to form a disulfide bridge connecting the two chains. Our first criterion was to introduce the Cys residues in the conserved framework part of the scFv so that it did not interfere with the CDR-antigen interactions. Our second criterion was to ensure that the distance between the  $V_L$  and  $V_H$  domains was close enough to promote the formation of an inter-domain disulfide bridge. After identifying several sites, we constructed the POM2 dsFv models and refined the models by energy minimization to determine the best mutation sites. We determined that the mutation of the residues Gly99 in  $V_L$  and Gly44 in  $V_H$  chains to Cys gave the best energy minimized model of POM2 dsFv . Table 2.1 has a comprehensive list of all the primers used for the cloning of  $V_L$ G99C and  $V_H$ G44C.

The  $V_L$ G99C chain mutant was made using the PCR-based QuikChange mutagenesis procedure<sup>146</sup> and methylated  $V_L$  plasmid was used as the template DNA for this procedure (section2.2.4). The light chain mutation was completed in two stages. In the first stage, the codon GGA coding for Gly99 was mutated to GGC (which also codes for Gly); in the second stage, the codon GGC was mutated to codon TGC cod-



ing for Cys. The two stage mutagenesis protocol had to be adopted as a simultaneous mutagenesis of two base pairs (from GGA to TGC) was unsuccessful. An initial PCR reaction was carried out with the P2VLg99g-f sense and the P2VLg99g-r antisense primers, separately. Each PCR mix (50 $\mu$ l) contained 125pmol of a primer, 10nmol of dNTP, 2.5U of Pfu polymerase in Pfu buffer and 50ng of the template DNA ( $V_L$ ). A short PCR cycle was run with each of the two PCR mixes. The cycle was: initial denaturation at 95°C for 30 s; 4 cycles at 95°C for 30s, 55°C for 1minute, 68°C for 7 min. After the run was complete, 25 $\mu$ l of each of the two PCR products was mixed and the same PCR reaction was continued for another 20 cycles. Upon completion of the second PCR run, 1 $\mu$ l of DpnI was added directly to the reaction mixture at 37°C for 1 hour to cleave the template DNA. To ensure complete digestion, another 1 $\mu$ l of DpnI restriction enzyme was added and the digestion was allowed to proceed for 4-6 hours. Electromax<sup>TM</sup> DH10B<sup>TM</sup> cells (Invitrogen, Burlington, ON, Canada) were transformed with the PCR product by electroporation and plated on Agar-LB medium with Ampicillin (100  $\mu$ g/ml). Plasmids were extracted from colonies and their sequences were verified. This plasmid with the single mutation from GGA to GGC codon was used as a template for the second reaction that mutates GGC (Gly) to TGC (Cys). The primers used for the second stage are P2VLg99c-f sense and P2VLg99c-r antisense. The procedure for the second mutagenesis was the same as that used in the first stage.

In contrast, the process of mutating the  $V_H$  chain to  $V_H$ G44C was straightforward. It involved a one step process of mutating the GGC codon to TGC. The primers used for this step were dsP2VHm44f sense and dsP2VHm44r antisense. The protocol followed was the same as that used in the first stage of  $V_L$  mutation. The purified  $V_H$ G44C plasmid was verified by sequencing.

### 2.2.6 Gene assembly of POM2 sc-dsFv

An overlap-extension PCR was used to construct the POM2 sc-dsFv as previously described in section 2.2.3. The linker used is a 20 amino acid linker with the amino acid sequence - GQFYLNAGAAAGGENLYFQG. This linker connects the carboxyl terminus of  $V_L$ G99C to the amino terminus of  $V_H$ G44C and contains a TEV cleavage site. The POM2 sc-dsFv gene was constructed in two steps. In the first step, the  $V_L$ G99C and  $V_H$ G44C genes were amplified separately by PCR from their respective plasmids. In the second step, an overlap-extension PCR<sup>84</sup> was used to splice the  $V_L$ G99C and  $V_H$ G44C genes via the linker to form the POM2 sc-dsFv gene. The

two PCR steps are explained in detail below. Table 2.1 has a comprehensive list of all the primers used for the cloning of POM2 sc-dsFv.

In the first step, the  $V_L$ G99C gene was amplified using the P2VL<sub>a</sub> sense and Tev-mVl-rev antisense primers whereas the  $V_H$ G44C gene was amplified using the Tev-mVh-for sense and P2VHb-Thr antisense primers. The PCR reaction mixture (50  $\mu$ l) contained 10 ng plasmid DNA, 0.1 mM dNTP, 0.5 mM of each primer, 0.5 unit of Taq polymerase, and standard Taq polymerase buffer. The PCR was carried with an initial denaturation at 94°C for 5 min; 30 cycles of 94°C for 30sec, 60°C for 30sec, and 72°C for 1 min; and a final extension at 72°C for 10 min. The  $V_L$ G99C and  $V_H$ G44C fragments were purified on a 1% agarose gel and extracted from the gel slice. The Tev-mVl-rev and Tev-mVh-for primers were designed to have long overhangs comprised respectively, of the two halves of the linker with a 6bp overlapping, complementary segment. Since these two primers had particularly long overhangs, T4DNA Ligase was used to ligate the two PCR products-  $V_L$ G99C and  $V_H$ G44C at the overlapping 6bp complementary region in the overhangs. (10ng of the two PCR products from the first PCR were taken in one tube, boiled for 15 minutes and immediately placed on ice. After 5 min, T4 DNA ligase was added to help ligate PCR products and the reaction was allowed to continue for 30 min at room temperature).

In the second stage PCR, we used the above ligated product as the template. The PCR reaction mixture consisted of the P2VL<sub>a</sub> sense and P2VHb-Thr antisense primers. The rest of the PCR mix composition and running conditions were the same as that used in the first step. The  $V_L$ G99C-linker- $V_H$ G44C product was gel-purified for restriction endonuclease digestion at 37°C for 2h with NcoI and XhoI restriction enzymes. The same conditions were also used to digest the pET22b+ vector with NcoI and XhoI. The digested products were gel purified and ligated using the T4 DNA ligase kit to obtain the final POM2 sc-dsFv gene in the pET22b+ vector. DH5 $\alpha$  cells were transformed with the ligation product and plated on Agar-LB medium with Ampicillin (100  $\mu$ g/ml). A colony PCR was performed for randomly picked colonies with the P2VL<sub>a</sub> sense, P2VHb antisense primers to identify clones with the desired construct. Plasmids were extracted from the positive clones and their sequences were verified.

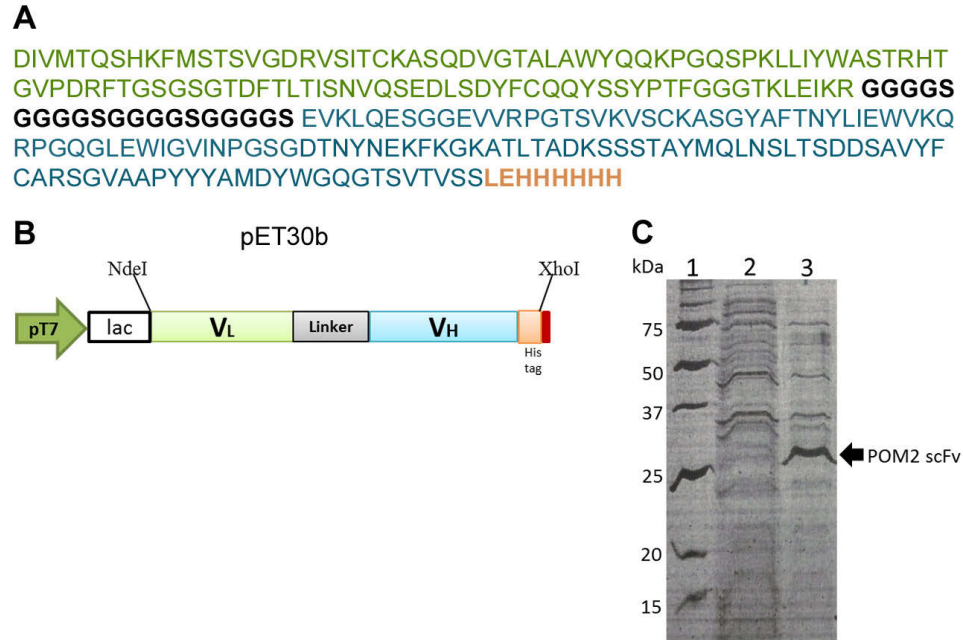


Figure 2.3: Details of POM2 scFv cloned into pET30b vector (A) The sequence of POM2 scFv. The  $V_L$  chain is coloured in green and the  $V_H$  is coloured in blue. The linker is shown in black and the His-tag is shown in orange (B) A schematic vector map of pET30b with POM2 scFv. The stop codon is shown in red. (C) An SDS-PAGE gel showing the induction of POM2 scFv (Lane3) with lane 2 showing the un-induced control.  $5\mu\text{l}$  of each sample was loaded in each lane.

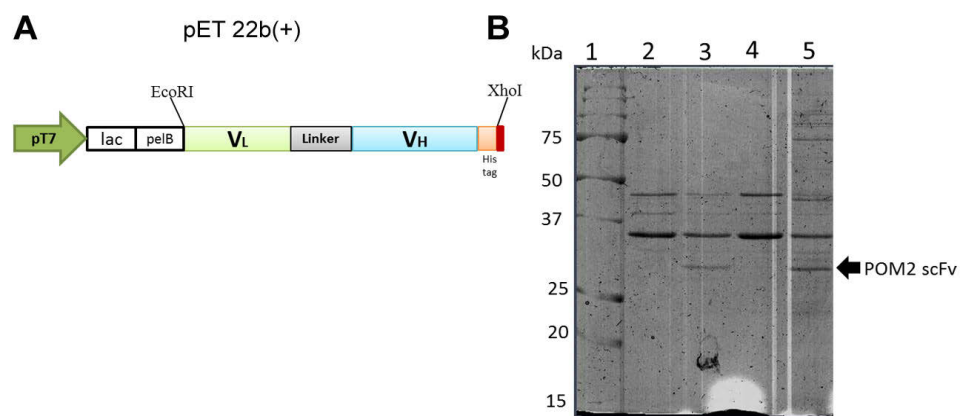


Figure 2.4: Details of POM2 scFv cloned into pET22b+ vector (A) A schematic vector map of pET22b+ with the same colour scheme as described in Fig 2.3. (C) An SDS-PAGE gel showing the periplasmic induction of POM2 scFv - Lane2 and 4 show un-induced controls at 4 hours and overnight induction, respectively; Lanes 3 and 5 show POM2 scFv induction at 4 hours and overnight, respectively. 20 $\mu$ l of each sample was loaded in each lane.

## 2.3 Results

### 2.3.1 POM2 scFv expression in inclusion bodies

The POM2 scFv gene was sub-cloned into the pET30b vector with a C-terminal His-tag (Figure 2.3B). We induced the expression of POM2 scFv in large quantities in inclusion bodies in the reduced environment of the cytoplasm of *E. coli* (Figure 2.3C). The purification of POM2 scFv was carried out successfully in its denatured state by affinity chromatography. We used two different strategies to refold POM2 scFv to its functional state - (i) the 'refolding by dilution' strategy<sup>101</sup> and (ii) the 'redox refolding' strategy<sup>101</sup>. Both the approaches led to copious amounts of precipitation of the scFv. Glycerol was also used in the different buffer conditions to attempt to reduce protein aggregation as described previously<sup>191</sup>. However, we did not see any improvement in the yield of the soluble scFv.

### 2.3.2 POM2 scFv expression in periplasmic space

As the purification of large quantities of POM2 scFv was unsuccessful with the pET30a vector, we used the pET22b+ vector (Novagen) to promote the secretion of soluble POM2 scFv into the periplasmic space of *E. coli* (Figure 2.4B). As expected, the periplasmic expression of POM2 scFv was much less compared to its expression in the inclusion bodies (Figure 2.4C). The purification of POM2 scFv was done in its natively folded form at pH 7.0 by affinity chromatography. Upon elution of the pure, properly folded POM2 scFv from the Ni-IMAC column, we dialysed the protein in 10mM Tris pH 7 to remove all traces of salt. POM2 scFv remained completely soluble in this buffer. However, on concentrating the protein in centrifugation filters (AMICON) after dialysis, we found that most of the POM2 scFv precipitated in the filter and could not be concentrated to beyond 0.6 mg/ml. We used 50mM Gln and 50mM Arg in the buffer conditions to improve the solubility of the scFv and prevent its aggregation as described previously<sup>69</sup>. This approach improved the concentration of the scFv marginally but it was not sufficient to set up crystallization trials. However, the low concentrated POM2 scFv that was obtained was sent in large quantities to Zurich to be used in performing experiments on mice cerebellar slices to determine its effect on POM1 toxicity.

### 2.3.3 Linker modified POM2 scFv

In order to improve the solubility of POM2 scFv, the (GGGS)<sub>3</sub> linker was modified to a more hydrophilic linker with the sequence, GSTSGSGKPGSGEGSTKG (Figure 2.5A). The presence of threonine, lysine and glutamic acid residues increases the hydrophilicity of the new linker and hence, the solubility of the protein whereas the presence of the proline residue gives structural rigidity to the linker to improve the chances of crystallizing the protein. The periplasmic expression levels of POM2-218 scFv were comparable to those of the POM2 scFv (Figure 2.5C). The pure POM2-218 scFv obtained by affinity chromatography was concentrated in a centrifugation filter in the buffer 10mM Tris, 50mM Arg and 50mM Gln pH 7.0 to a final concentration of 7.6mg/ml, as measured by Bicinchoninic acid assay (BCA)<sup>178</sup>. This sample was immediately used to set up crystal trials. However, we did not see any promising crystal hits with this sample.

### 2.3.4 Disulfide linked POM2 Fvs

The POM2 dsFv was designed so that the  $V_L$  and the  $V_H$  domains were joined by a disulfide bridge instead of by a peptide linker<sup>162</sup>. One Cys mutation each was introduced in  $V_L$  (G99C) and  $V_H$  (G44C) chains. If the  $V_L$ G99C and  $V_H$ G44C chains could be expressed and purified separately, then the two chains could be mixed in equimolar ratios followed by air-oxidation to form the heterodimers of POM2 ds-Fvs. While the expression of the  $V_H$ G44C domain in the inclusion bodies was very high, that of the  $V_L$ G99C domain was very poor (Figure 2.6). Therefore, creating a homogenous solution of POM2 dsFv for crystallization purposes was highly unlikely.

### 2.3.5 Disulfide linked POM2 Fvs with a linker

In order to enable uniform levels of expression of the  $V_L$ G99C and  $V_H$ G44C and aid in the formation of heterodimers, we used a linker with a TEV cleavage site to tether the two chains together. This would enable uniform levels of expression of the two domains and simplify the formation of the heterodimers of the dsFv. As the linker has a TEV cleavage site designed in it, it would allow us to cleave the linker to eliminate its high flexibility and increase the chances of crystallizing POM2 sc-dsFv. Although, we found that the expression of POM2 sc-dsFv was good (figure not shown), concentrating it resulted in excessive precipitation making it unsuitable for crystallization purposes.

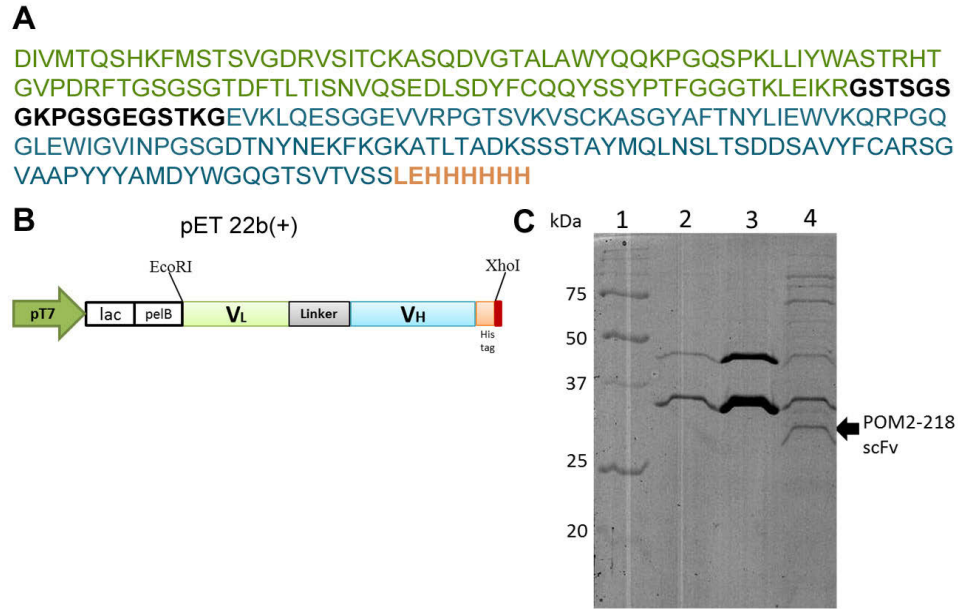


Figure 2.5: Details of POM2 scFv with 218 linker cloned into pET22b+ vector (A) The sequence of POM2-218 scFv with the same colour scheme as described in Fig 2.3 (B) A schematic vector map of pET22b+ with POM2-218 (C) An SDS-PAGE gel showing the induction of POM2-218 scFv (Lane4) with lanes 2 and 3 showing the un-induced control. 20 $\mu$ l of each sample was loaded in each lane.

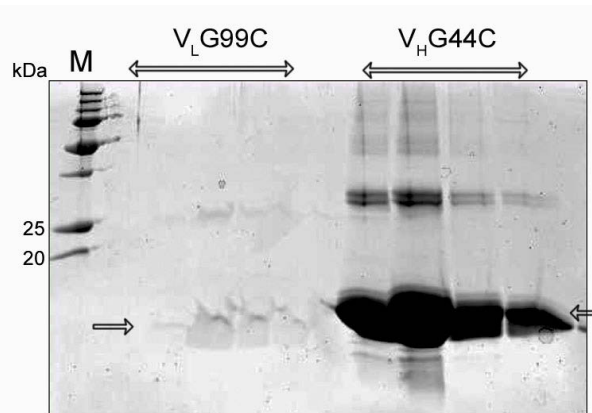


Figure 2.6: SDS-PAGE gels showing the various elutes from Ni-IMAC purification of the protein extracted from the inclusion bodies of  $V_L$ G99C chain and  $V_H$ G44C chain of POM2. As is clearly evident from the gels, the expression of the  $V_L$ G99C chain is unusually low compared to that of the  $V_H$ G44C chain. The arrows indicate the bands of the proteins of interest. 20 $\mu$ l of each sample was loaded in each lane.

## 2.4 Discussion

There are two ways to approach the large scale bacterial expression of recombinant scFv in *E. coli*. In the first approach, the scFv is overexpressed in the reduced environment of the cytoplasm in inclusion bodies but involved laborious and time consuming *in vitro* protein refolding procedures. In the second approach, a leader sequence was fused to the amino terminus of the scFv to enable its secretion into the oxidized environment of the periplasm of *E. coli*. While the oxidized environment ensures the correct folding of the periplasmic scFv, the protein yields are very low compared to that from the inclusion bodies<sup>100</sup>. In the case of POM2 scFv we initially attempted to express the protein as inclusion bodies in order to obtain large quantities of POM2 scFv to set up crystallization trials. However, after our failed attempts to refold the denatured POM2 scFv, we argued that our time and efforts could be better spent on the periplasmic expression of POM2 scFv in large culture volumes to obtain a completely folded protein that could be used for crystallization trials.

As periplasmic space contains an oxidizing environment that is rich with chaperones that enable the correct disulfide bond formations within the scFv<sup>94</sup>, we were able to obtain completely folded and soluble POM2 scFv from bacterial periplasmic expression. However, we found that the POM2 scFv was not soluble at higher concentrations and hence could not be successfully used for setting up crystal trials. Previous studies have shown that the sequence as well as length of the peptide linker in an scFv contribute significantly to its solubility and aggregation tendencies<sup>190,203</sup>. The minimum criteria for a good peptide linker is to link the  $V_H$  and  $V_L$  domains without interfering with the intra-domain folding or the inter-domain contacts. The  $(G_4S)_3$  linker is an archetypal, 15 residue peptide linker present in POM2 scFv<sup>88</sup>. It was one of the first linkers designed for scFvs and is still very widely used. This linker is highly flexible due to the presence of Gly residues and yet exhibits reasonable solubility due to the presence of the Ser residues<sup>63,64</sup>. However, due to the limited solubility of POM2 scFv, we modified the  $(G_4S)_3$  linker to increase its length<sup>203</sup> and to incorporate more charged residues. We substituted the peptide linker  $(G_4S)_3$  with the linker ‘218’ comprising of GSTSGSGKPGSGEGSTKG. Linker 218 has been previously shown to improve the antigen affinity and reduce the aggregation in scFvs<sup>203</sup> and is now widely used in the scFv literature<sup>142,148,149</sup>. The linker modification successfully improved the solubility of POM2-218 scFv and it remained stable in solution at concentrations that were reasonably sufficient to set up crystal trials. However, there were no successful hits observed in any of the crystal screens.



It is likely that the failure of POM2-218 scFv to crystallize was due to segmental flexibility created by the unstructured 218 linker. In order to minimize the overall flexibility within POM2-218, we designed a modified scFv where the  $V_H$  and the  $V_L$  domains were joined by a disulfide bridge instead of by a peptide linker. Studies have previously shown that the disulfide linked Fvs show more structural stability and less aggregation tendencies than scFvs due to the elimination of the long, flexible peptide linker<sup>205</sup>. Although we had very good expression of the  $V_H$ G44C chain, the  $V_L$ G99C chain had extremely poor expression (Figure 2.6). Hence, we were unable to complete the construction of POM2 dsFv.

In order to overcome the differences in the expression levels of the light and heavy chains, we designed a construct that linked the two chains of POM2 by disulfide linkage as well as by a peptide linker. This construct is called sc-dsFv and is a good solution to overcome both the instability of the scFvs as well as the expression issues with dsFvs. Unfortunately, we observed heavy precipitation of the POM2 sc-dsFv at higher concentrations and hence, could not successfully use it for co-crystallizing the octapeptide region of the Prion protein.

## 2.5 Conclusions

Our overall objective is to deduce the structural changes occurring in the prion protein upon POM2 antibody binding. Single chain variable fragments are very interesting systems to work with due to their small size and therapeutic potential. Hence, our first objective was to study the structure of POM2 scFv and its mode of binding to the octapeptide repeats of the prion protein. However, as we were unable to crystallize POM2 scFv or its numerous modified versions, we concluded that the most prudent way to achieve our overall objective of studying the mechanism of binding of POM2 antibody was to crystallize a more stable, crystallizable Fab fragment of POM2 IgG with the prion protein. We were however, successful in sending large quantities of POM2 scFv to our collaborators in Zurich to test the effects of POM2 scFv in COCS assay (Refer 1.4.4). The results from these assays have now been published by Sonati et al<sup>180</sup>.

# Chapter 3

## Crystal structure of POM2 Fab with an Octapeptide Repeat of the mouse PrP<sup>C</sup>

### 3.1 Introduction

A major component of the N-terminal domain is the four tandem repeats of a glycine-rich octapeptide (PHGGG/SWGQ) known as the octapeptide repeat (OR) domain spanning residues 59-89. The OR domain also includes residues 51-58 that are made up of a non-canonical octapeptide (PQGGTWGQ) in mice and a nonapeptide in other species. The OR domain is one of the most conserved domains of the Prion protein. The presence of one to nine additional copies of the OR is associated with familial forms of CJD<sup>37,152</sup> or GSS<sup>194</sup> and the number of repeats determine the histology of the host cerebellum<sup>195</sup>. A lack of the OR domain in PrP<sup>C</sup> has also shown to slow the progress of the disease in mice<sup>58</sup>. These studies indicate the possibility of a complex, modulatory role for the OR domain in the progression of Prion diseases. Several studies on potential biological binding partners of the OR domain showed that along with its flanking residues, it binds to a variety of ligands such as copper, zinc, sulfated aminoglycans, hemin, nucleic acids, stress inducible protein1 (STI1), the laminin receptor and the LDL receptor<sup>39</sup>.

Metal ligand binding has been one of most extensively studied structural properties of the OR domain. Many scientific groups have dedicated a better part of the last decade attempting to determine the structure of the OR domain both in it's metal bound and it's metal unbound forms<sup>15,35,42,129,186,193,209</sup>. Millhauser et al.,

presented the first and so far the only crystal structure of a minimal binding fragment (HG<sub>3</sub>GW) of a single OR of PrP in complex with copper<sup>35</sup>. NMR studies on isolated peptide fragments of the OR domain suggest a  $\beta$ -turn like conformation<sup>209</sup> (Figure 3.1A). In 2010, the solution NMR structure of the N-terminal domain fragment, PrP(23-106) in complex with Pentosan Polysulfate (PPS) was reported; it showed a unique mode of binding of the OR domain involving a series of loops and  $\beta$ -like turns exposing tryptophan side chains that are poised to interact with PPS through possible  $\pi - \pi$  stacking interactions<sup>188</sup> (Figure 3.1B).

Due to the absence of a well-defined tertiary structure, it has not been possible to study the native, unbound OR domain using the classical high resolution technique of X-ray crystallography. However, when bound to specific ligands, the OR domain has been found to attain a certain level of order that would allow X-ray crystallographic studies<sup>35,186</sup>. There have been several reports of antibodies with epitopes in the OR domain showing promising therapeutic efficacy by extending the survival of peripherally prion infected mice<sup>134,147,174</sup>. These reports would clearly benefit from structural studies investigating the nature of the interactions of the OR domain with its various ligands at high resolution in order to enable the possibility of designing smaller and more tightly binding ligands.

Polymenidou et al., developed a unique panel of 19 monoclonal antibodies in *PrP<sup>0/0</sup>*-knockout mice, named POM1 through POM19; these antibodies have epitopes spanning the entire sequence of the mature prion protein<sup>154</sup>. Of these antibodies, the POM2 antibody recognizes an epitope in the OR domain. Sonati et al showed that the POM2 antibody inhibits the toxicity induced by the POM1 antibody indicating a potential therapeutic role for the POM2 antibody in prion diseases<sup>180</sup>. As the crystallization of IgG molecules is a challenging process due to the presence of glycosylation sites, we chose to use the Fab fragments of POM2 IgG for our crystallization studies. In this thesis, we show the crystal and molecular structures of the tandem octapeptide repeats (OR2) of PrP<sup>C</sup> in complex with the POM2 Fab. The structure shows an extended conformation of one of the octapeptide repeats revealing how the POM2 Fab binding disrupts the reported  $\beta$ -turn conformation of the ORs<sup>188,209</sup>.

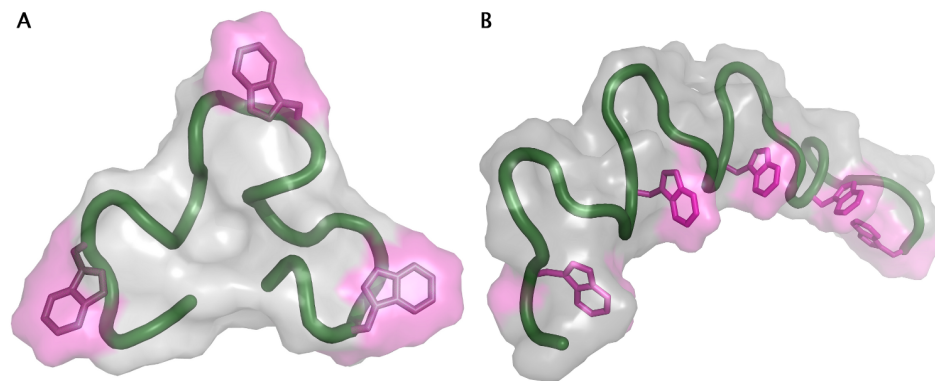


Figure 3.1: The surface and cartoon representation of the two reported NMR structures of the OR domain of *PrP<sup>C</sup>* with only the tryptophan residues highlighted in magenta. (A) The unbound OR domain is predicted to have a  $\beta$ -turn conformation<sup>209</sup> (PDB ID 10EI) (B) The NMR structure of OR domain bound to PPS is also predicted to have a series of  $\beta$ -turn conformations<sup>188</sup> (PDB ID 2KKG)

## 3.2 Materials and Methods

### 3.2.1 Preparation of POM2 Fab and the OR2 peptide

The POM2 IgG hybridoma cell line was generated as described previously<sup>154</sup> and cultured in the Roswell Park Memorial Institute (RPMI) media 1640 (GIBCO) supplemented with 5% Fetal Bovine Serum (FBS). The IgG-rich hybridoma culture supernatant was purified by affinity chromatography using a Protein G sepharose (PIERCE) column. Pure POM2 IgG was eluted from the column with 0.1M Glycine pH 2.8. Papain (SIGMA) 0.25%(w/v) was used to digest POM2 IgG into Fab fragments as previously described<sup>14</sup>. The digestion was allowed to take place for 5 hours in a water bath at 37 °C in freshly prepared 50 mM Tris, 150 mM NaCl pH 8.0, 20 mM EDTA, 20 mM Cysteine. The digestion was stopped by adding 30 mM Iodoacetamide. The POM2 Fab molecules were separated from their cleaved  $F_c$  fragments and undigested POM2 IgG molecules using a Protein A sepharose (PIERCE) column followed by further purification on a Hiload 16/60 Sephadex 75 (Amersham Biosciences) gel filtration column in 50 mM Tris, 25 mM NaCl pH 7.0 buffer. The pure POM2 Fab obtained was concentrated to 20mg/ml using centrifugal filter units (Millipore).

The peptide OR2 with the sequence PHGGSWGQPHGGSWGQ was synthesized by and purchased from the Institute for Biomolecular Design at the University of Alberta, Canada. There were no protective groups added to either end of the peptide.

### 3.2.2 Crystallization

POM2 Fab was mixed with a 2-fold molar excess of the OR2 peptide and incubated at room temperature for 30min. The resulting solution was concentrated to 20 mg/ml with 30kDa cut-off centrifugal filter units to remove any unbound OR2 peptide. Pure POM2 Fab-OR2 peptide complex was stored in 50 mM Tris, 25 mM NaCl, 1mM  $\text{NaN}_3$  pH 7.0 buffer at 4°C. Commercial crystal screening solutions from the Crystal screen and the Index screen (Hampton Research) were used to explore a variety of crystallization conditions by the sitting drop vapour diffusion method in 96-well Intelli-Plates (Hampton Research) set up using a crystallization robot (Hydra 96 Plus One, Robbins Scientific). A crystallization hit was obtained with 0.2M  $\text{CaCl}_2 \cdot 2\text{H}_2\text{O}$ , 0.1M HEPES pH-7.5, 28% PEG1000 as the reservoir solution at room temperature. The sitting drop was prepared by mixing 1 $\mu$ l of the protein solution with 1 $\mu$ l of the reservoir solution. Diffraction quality crystals were obtained after 14 days. The crystals were flash-cooled in liquid  $\text{N}_2$  after adding 20% glycerol as cryoprotectant.

### 3.2.3 Data collection and structure determination

A full data set was collected to 2.3 Å resolution at the beamline 9-2 in the Stanford Synchrotron Radiation Lightsource (SSRL)<sup>179</sup> from one crystal. The data had an overall completeness of 99.80%. The AUTOXDS script developed at SSRL was used for data processing, scaling and integration<sup>70,93</sup>. The data collection statistics are presented in Table 3.1. The crystals were indexed in the orthorhombic space group  $P2_122_1$  with two 1:1 POM2 Fab-OR2 peptide complexes in the asymmetric unit. The structure of Fab POM2-OR2 was solved by molecular replacement using the program PHASER<sup>124</sup> in the CCP4 suite<sup>206</sup> with the POM1 Fab<sup>19</sup> protein as the search model (PDB ID 4DGI) .

### 3.2.4 Structure refinement

The PHENIX suite was used to perform crystallographic refinement<sup>3</sup> on the molecular model of the POM2 Fab-OR2 peptide complex. 5% of the reflections from the data collected were randomly selected and set aside to calculate the  $R_{free}$  factor for monitoring the progress of refinement. In the initial rounds of refinement, Translation/Libration/Screw (TLS) and the individual Atomic Displacement Parameter (ADP) refinements along with the NCS restraints were applied to the model. The electron density of the OR2 peptide was clearly visible in the  $|F_o| - |F_c|$  difference map calculated after the first round of refinement. In the final rounds of refinement, coordinates' refinement was performed by applying stereochemical restraints on the molecular model. The positions of water molecules were initially identified using PHENIX and their positions were subsequently confirmed by manually checking for positive peaks in both the  $2|F_o| - |F_c|$  and the  $|F_o| - |F_c|$  electron density maps. Water molecules with B-factors greater than 60 Å<sup>2</sup> were removed. The program, COOT was used for manual model building<sup>52</sup>. Structure validation was performed with the program MOLPROBITY<sup>43</sup>. Potential hydrogen bonds and van der Waals contacts were analyzed using the program LIGPLOT<sup>196</sup>. PyMOL<sup>175</sup> was used to calculate the RMSDs and to create all the figures. The coordinates and the structure factors for the model have been deposited in the PDB with accession ID of 4J8R.

Table 3.1: Data-collection and refinement statistics of OR2-POM2.

Wavelength(Å )	0.979	
Matthew's co-efficient (Å <sup>3</sup> /Da)	2.57	two molecules in the asymmetric unit
Space group	P2 <sub>1</sub> 22 <sub>1</sub>	
Unit-cell parameters a (Å)		
a, b, c	65.41, 71.57, 207.59	
Resolution range (Å) <sup>a</sup>	39.6-2.3 (2.31-2.30)	
Total no. of reflections	319,135 (51,348)	
Unique reflections	44,080 (6956)	
$R_{meas}$ (%) <sup>b</sup>	16.1(186.5)	
Average I/ $\sigma$ (I)	10.82(1.16)	
$CC_{1/2}$ (%) <sup>c</sup>	99.7 (35.0)	
no.of pairs of reflections <sup>d</sup>	44047 (6924)	
Completeness(%)	99.8 (99.4)	
Multiplicity	7.24 (7.38)	
<b>Refinement</b>		
$R_{work}$ (%) <sup>e</sup>	24.7	
$R_{free}$ (%) <sup>e</sup>	25.7	
Number of refined atoms		
Total	6791	
Protein	6626	
Water	165	
<i>Mean B-factor</i> (Å <sup>2</sup> )		
Overall	56.2	
Solvent	54.0	
	<b>Mol1</b>	<b>Mol2</b>
POM2 Fab-OR2	55.8	56.3
OR2	73.8	63.5
<i>Ramachandran plot</i>		
Favored(%)	97.23	
Allowed(%)	1.85	
Disallowed(%)	0.92	
r.m.s.d. bonds (Å)	0.03	
r.m.s.d. angles (°)	1.9	
PDB ID	4J8R	

<sup>a</sup> Values in the parentheses are for the highest resolution shell.

<sup>b</sup>  $R_{meas} = \frac{\sum_{hkl} \sqrt{\frac{n}{n-1}} \sum_{j=1}^n |I_{hkl,j} - \langle I_{hkl} \rangle|}{\sum_{hkl} \sum_j I_{hkl,j}}$  is the redundancy independent indicator of data quality.

<sup>c</sup>  $CC_{1/2}$  = percentage of correlation between intensities from random half-datasets.

<sup>d</sup> The pairs of reflections are used in calculating  $CC_{1/2}$ .

<sup>e</sup>  $R_{work}$  and  $R_{free} = \frac{\sum_{hkl} ||F_{obs}| - |F_{calc}||}{\sum_{hkl} |F_{obs}|}$  for reflections in the working and test (5% of the data) sets, respectively.

## 3.3 Results

### 3.3.1 Overall structure of the OR2-POM2 Fab complex

The complex of the POM2 Fab bound to the OR2 peptide was successfully co-crystallized in the space group  $P2_122_1$ . The asymmetric unit is composed of two molecules of the POM2 Fab-OR2 complex - Mol1 and Mol2 (Figure 3.2). As suggested previously<sup>96</sup>, the high resolution cut-off of 2.3 Å was determined based upon the  $CC_{1/2}$  factor of the diffraction data instead of being based upon the average  $I/\sigma(I)$ . The final model was refined to a crystallographic  $R_{work}$  factor of 24.7% and  $R_{free}$  of 25.8% with 876 protein residues and 165 water molecules. The difference electron density map ( $|F_o| - |F_c|$ ) clearly shows an OR2 peptide bound to each of the POM2 Fab molecules in the asymmetric unit. A MOLPROBITY validation report shows that only 8 residues (0.92%) are in the disallowed region of the Ramachandran plot. All the residues of the POM2 Fab are numbered according to the standard Kabat and Wu numbering system<sup>1,92</sup>; this numbering system describes the precise delineation of the CDRs of both light and heavy chains of antibodies in general. Throughout this chapter, the residue numbers of the OR2 peptide, POM2 Fab light and heavy chains will be preceded by the letters P, L and H respectively.

### 3.3.2 Structure of the bound POM2 Fab

The global folding of the POM2 Fab molecule is characteristic of that of an immunoglobulin molecule. Each Fab molecule contains a light chain (L) and a heavy chain (H) bound to each other by two disulphide bonds. Each of the L and H chains contain a constant and variable domain and the variable domains in turn, contain three Complementarity Determining Regions (CDR) - loops L1, L2, L3 in the L chain and loops H1, H2 and H3 in the H chain (see Figure 3.3A); in POM2 Fab all the 6 CDRs have well-defined electron densities in the  $2|F_o| - |F_c|$  map. The elbow angle of POM2 Fab which is an indicator of the relative disposition of its variable domain with respect to its constant domain was calculated to be 161.6° for Mol1 and 166.3° for Mol2 and is within the expected range for IgGs (<http://proteinmodel.org/AS2TS/RBOW/index.html>). However, as the difference in elbow angles of the two Fab molecules in the asymmetric unit is considerable, we calculated the root-mean-square-deviations (RMSD) of the variable and constant domains of the two Fab molecules separately using PyMOL<sup>175</sup>; the RMSD values are 0.31Å<sup>2</sup> (228 C<sub>α</sub> pairs) and 0.42Å<sup>2</sup> (201 C<sub>α</sub> pairs) for the variable and constant do-



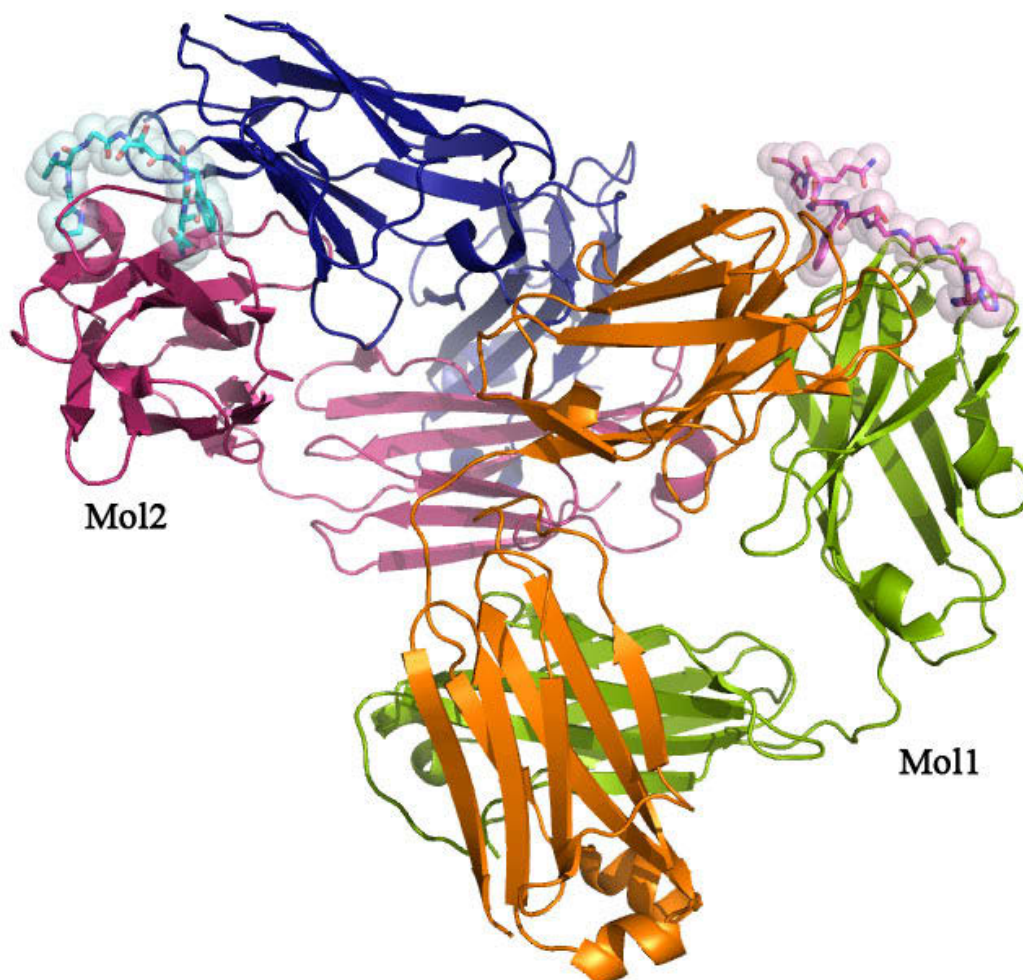


Figure 3.2: The asymmetric unit of the POM2 Fab-OR2 peptide complex crystal structure in the  $P2_122_1$  space group. The Fab molecules are shown in a cartoon representation and the bound OR2 peptides have been displayed as sticks inside transparent spheres. In Mol1, the light chain, heavy chain and the OR2 peptide are shown in orange, green and magenta, respectively. In Mol2, the light chain, heavy chain and the OR2 peptide are shown in blue, pink and cyan, respectively.

mains, respectively. Thus, the structures of the two POM2 Fab molecules in the asymmetric unit are quite similar.

Out of the 18 standard canonical conformations described for the CDR loops, POM2 Fab CDR loops L1, L2, L3, H1 and H2 fall into canonical classes  $\kappa 1,1,1,1$  and 3 respectively<sup>13</sup>. The POM2 Fab CDR H3 loop (Figure 3.3B) exhibits a commonly observed  $\beta$ -bulged torso at Asp H101 stabilized by an Arg H94-Asp H101 salt bridge and a hydrogen bond between the backbone carbonyl oxygen of Met (H100E) and the N $\epsilon$ 1 of a highly conserved Trp H103<sup>131,165,185</sup>. Interestingly, of all six CDRs of the POM2 Fab, only the CDR H3 loop makes hydrogen bonded interactions with the OR2 peptide while the CDRs in the light chain make interactions with the OR2 peptide via van der Waal's and aromatic contact interactions.

The POM2 Fab CDR H3 loop has the AAAPTYYYAM sequence ; it contains two adjacent Tyr residues flanked by small, hydrophobic residues that function to keep the loop conformationally flexible in order to facilitate antigen recognition. Several previous studies have shown that the large, polar, aromatic Tyr residues play dominant roles in antigen-antibody contacts<sup>104,127,161</sup>. In the POM2 Fab, residue Tyr H100B forms a hydrogen bond with Asp H58 of the CDR H2 loop and critical interactions with the OR2 peptide whereas Tyr H100C forms an important hydrogen bond with the backbone carbonyl oxygen of Ala H97 that keeps the CDR H3 loop conformationally stable (Figure 3.3B).

### 3.3.3 The structure of the OR2 peptide

The 16 residue OR2 peptide is bound to the POM2 Fab in a cleft spanning the interface between the variable domains of the L and H chains of the POM2 Fab. In the  $2|F_o| - |F_c|$  electron density map, the OR2 peptide in Mol1 could be traced up to Pro P9 (Figure 3.4A) whereas in Mol2, the peptide could only be traced up to Gln P8 (Figure 3.4B). Neither of the OR2 peptide chains show sufficient electron density to unambiguously model the second octapeptide repeat of OR2. The OR2 peptide is bound to the POM2 Fab in an extended conformation with a distance of 16.19 Å and 14.13 Å between the Pro P1 to Gln P8 residues in Mol1 and Mol2, respectively. The shape complementarity scores calculated by the Sc program<sup>112</sup> of the CCP4 suite for the POM2 Fab H chain and OR2 peptide surfaces are 0.72 and 0.75 for Mol1 and Mol2, respectively whereas the Sc scores for the L chain of POM2 Fab and the OR2 peptide are 0.52, 0.71 for Mol1 and Mol2, respectively. A score of 1 indicates perfect shape complementarity and 0 indicates uncorrelated topography. Except in the case

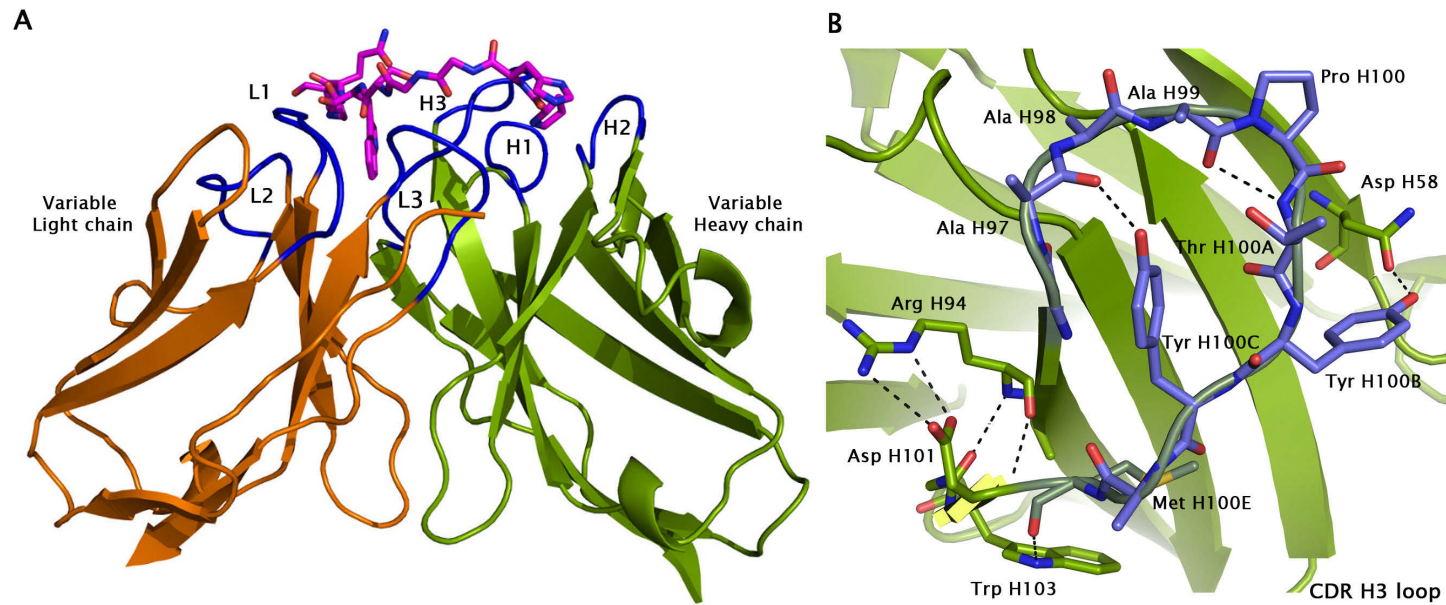


Figure 3.3: The CDR loops of the POM2 Fab molecule. (A) The light (orange) and heavy (green) variable domains of Mol1 with the CDR loops highlighted in blue. The bound OR2 peptide is displayed as sticks in magenta. (B) The intramolecular contacts within the CDR H3 loop and its neighbouring residues in Mol1. Only the residues in the CDR H3 loop are colored in blue while its neighbouring residues are colored in green.

of the L chain of Mol1, the Sc scores indicate good surface complementarity between the POM2 Fab molecule and the OR2 peptide.

The overall RMSD between the  $C_\alpha$  atoms of the OR2 peptide in Mol1 and Mol2 is 1.28 Å<sup>2</sup> ( for 8  $C_\alpha$  atom pairs). The percentage buried surface areas of the OR2 peptide upon binding to the POM2 Fab are 46.5% (575 Å<sup>2</sup>) and 59.8% (653.2 Å<sup>2</sup>) for Mol1 and Mol2, respectively<sup>85</sup>. The overall average B-factors of the OR2 peptide chains are 73.8 Å<sup>2</sup> and 63.5 Å<sup>2</sup> in Mol1 and Mol2, respectively. The residues of the OR2 peptide that are critical to the complex formation with POM2 Fab have been determined by the nature and number of contacts formed by each peptide residue with the Fab molecule (Figure 3.5A and B). A summary of the significant hydrogen bonding interactions (between 2.7-4.0 Å) of the two chains of OR2 peptides with their respective POM2 Fab molecules is presented in Table 3.2. In Mol1 and Mol2, the side chain of Pro P1 dips into a binding pocket formed by the three CDR loops of the H chain of the POM2 Fab. The amide nitrogen of the Pro P1 residue forms a hydrogen bond with a water molecule situated in this pocket which in turn forms a hydrogen bond with the Glu H35 residue of the CDR H1 of the POM2 Fab . The Pro P1 amide also forms a hydrogen bond with the backbone carbonyl oxygen of the Thr H100A residue. Pro P1 is further anchored in to this pocket by a hydrogen bond between the backbone amide of His P2 to the carbonyl oxygen of Pro H100. Also seen in both Mol1 and Mol2 are the backbone hydrogen bonding interactions between the amide of Tyr H100B to the carbonyl oxygen of Gly P3 and the amide of Ser P5 to the backbone carbonyl oxygen of Tyr H100B that contribute to anchoring the peptide to the CDR H3 loop of POM2 Fab. The residue Gly P4 does not contribute to any hydrogen bonding interactions with the POM2 Fab. The side chain of Ser P5 also participates in hydrogen bonding interactions with the side chain Oγ1 of Thr H100A.

There are also some differences observed in the hydrogen bonding of the OR2 peptides in Mol1 and Mol2 . In Mol2, Trp P6 is better positioned than in Mol1 in the binding cleft of the POM2 Fab, thereby facilitating the hydrogen bonding from Nε1 in Trp P6 to the backbone carbonyl oxygen of Ala H100D. In addition, the side chain of Gln P8 Oε1 in Mol2 forms a hydrogen bond with backbone amide of Ala H97.

An analysis of the hydrophobic interactions between the Fab molecule and the OR2 peptide using LIGPLOT<sup>196</sup> reveals that there are 31 and 33 hydrophobic contacts in Mol1 and Mol2, respectively between the OR2 peptide and POM2 Fab (Figure 3.6). In both of the peptide chains in the asymmetric unit, the two residues Pro P1 and Trp P6 make the greatest contributions to the formation of the peptide-antibody complex. Pro P1 makes 41.9% and 45.4% of the hydrophobic contacts in Mol1 and

Mol2, respectively and interacts with the residues Val H50, Asn H58, Pro H100 and Tyr H100B (Figure 3.7A) whereas Trp P6 makes 51.6% and 45.4% of the hydrophobic contacts in Mol1 and Mol2, respectively and is well placed in a hydrophobic binding pocket to make T-shaped (or edge-on) geometry favoured<sup>87</sup> aromatic interactions with Tyr H100C, Tyr L90 and Trp L48 residues (Figure 3.7B). In Mol1, Trp P6 contributes more towards the hydrophobic binding whereas in Mol2, both Pro P1 and Trp P6 make equal contributions. In addition, an analysis of the electrostatic potential surface map of the POM2 Fab-OR2 complex indicates partial electrostatic surface complementarity (Figure 3.8A and B). The electrostatic potential was calculated using the programs PDB2PQR<sup>49</sup> and APBS<sup>16</sup>. The first four residues of the OR2 peptide form a basic patch that is complementary to an acidic patch on the POM2 Fab binding cleft.

### 3.4 Discussion

As the OR domain of PrP<sup>C</sup> is intrinsically disordered in the native solution, the popular approach to study its structural characteristics has been to truncate the OR domain to variants of its fundamental binding unit<sup>15</sup> and then stabilize them by ligand binding. We have adopted a similar approach and have successfully crystallized a tandem octapeptide repeat of PrP<sup>C</sup> in complex with the POM2 Fab molecule. The crystal structure of the POM2 Fab-OR2 peptide shows for the first time an extended conformation adopted by a single octapeptide repeat of PrP<sup>C</sup> when in complex with a binding partner. The structure shows that the monoclonal antibody fragment, POM2 Fab has a continuous epitope in the OR domain comprising residues PHGGSW, thus confirming previous epitope mapping experiments<sup>154</sup>. The OR2 peptide binds to the POM2 Fab by embedding the Pro P1 residue in a hydrophobic binding pocket followed by firm anchoring of the HGGS residues to the CDR H3 loop by backbone hydrogen bonding interactions. In addition, there is good surface complementarity as well as ample hydrophobic and aromatic interactions between the POM2 Fab and the OR2 peptide surfaces. As expected, the aromatic residues Tyr H100B and Tyr H100C in the CDR H3 loop of POM2 Fab play critical roles in the OR binding<sup>56,161</sup>.

Considerable advances have been made in the field of Prion disease therapeutics as OR domain-binding polyanionic ligands such as Heparin/Heparan sulphate<sup>199</sup>, Pentosan polysulfate<sup>48,95</sup> (PPS) have been reported as potential anti-prion compounds based on numerous *ex vivo* and *in vivo* experiments. PPS specifically has shown remarkable results in prolonging the incubation periods for PrP<sup>Sc</sup> formation when

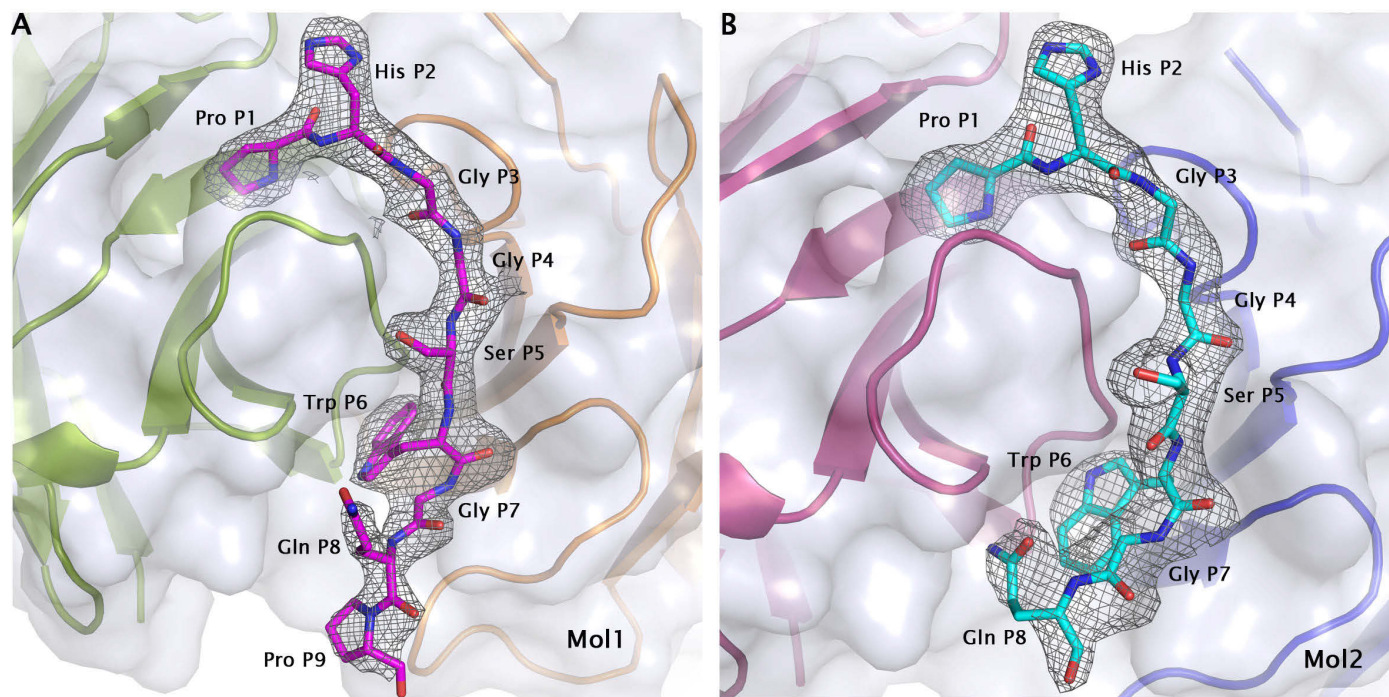


Figure 3.4: The final  $2|F_o| - |F_c|$  difference electron density map contoured at  $1 \sigma$  for the OR2 peptides at  $2.3 \text{ \AA}$  resolution represented as chicken wire in (A) Mol1 and (B) Mol2. The OR2 peptides are shown as sticks and the POM2 Fab molecules are displayed in a cartoon fashion along with a surface representation of the binding cleft. The color scheme is similar to the one used in Figure 3.2.

OR2	HOH	POM2 Fab	Distance(Å)	
			Mol1	Mol2
Pro P1 N	HOH 196		3.89	
	HOH 196	Glu H35 $\delta$ 2	2.87	
Pro P1 N	HOH 6			3.59
	HOH 6	Glu H35 $\delta$ 2		3.11
Pro P1 N		Thr H100A O	2.89	2.74
His P2 N $\epsilon$ 1		Pro H100 O	2.85	2.69
Gly P3 O		Tyr H100B N	2.76	2.75
Ser P5 N		Tyr H100B O	3.49	3.27
Ser P5 O $\gamma$		Tyr H100A O $\gamma$ 1	3.21	3.81
Trp P6 N $\epsilon$ 1		Ala H100D O		2.88
Gln P8 O $\epsilon$ 1		Ala H97 N		3.44

Table 3.2: Summary of interactions between OR2 peptide and POM2 Fab



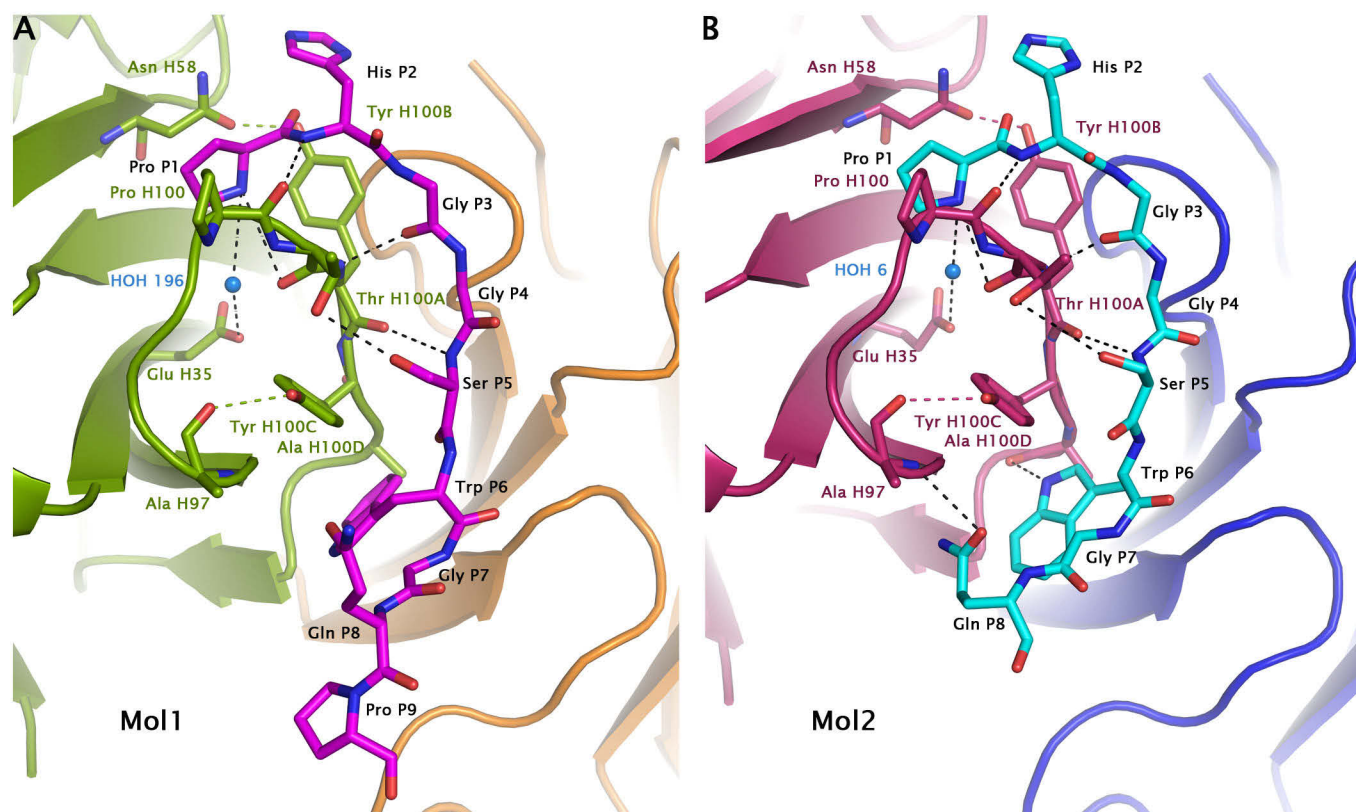


Figure 3.5: The intermolecular contacts between the OR2 peptide and the POM2 Fab molecule in (A) Mol1 and (B) Mol2. The colour scheme is similar to the one used in Figure 3.2. The water molecule is displayed as a sphere (light blue). The intermolecular hydrogen binding between the residues of OR2 peptide and residues of the POM2 Fab molecule are shown as black dashes. Intramolecular hydrogen bonds between the residues in the POM2 Fab molecule are shown as green and pink dashes in (A) and (B), respectively.



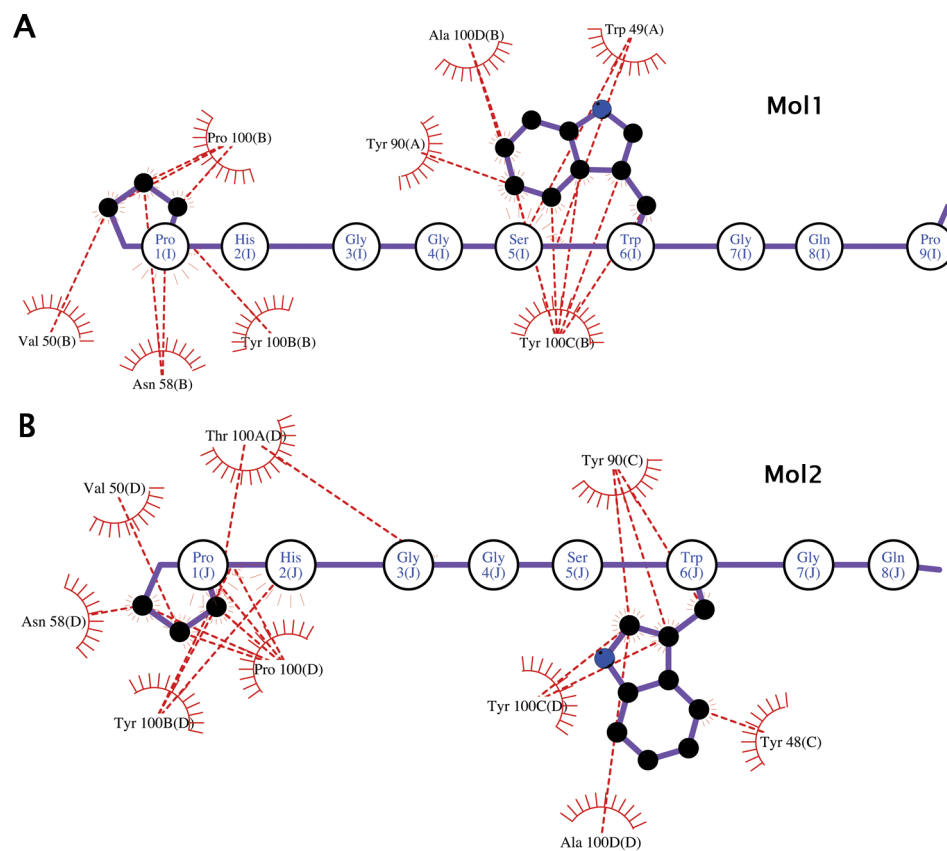


Figure 3.6: A schematic representation of the LIGPLOTs of the OR2 peptide with POM2 Fab depicting only the hydrophobic interactions between the two molecules. (A) Mol1 and (B) Mol2 . The OR2 peptide bonds are shown in purple.

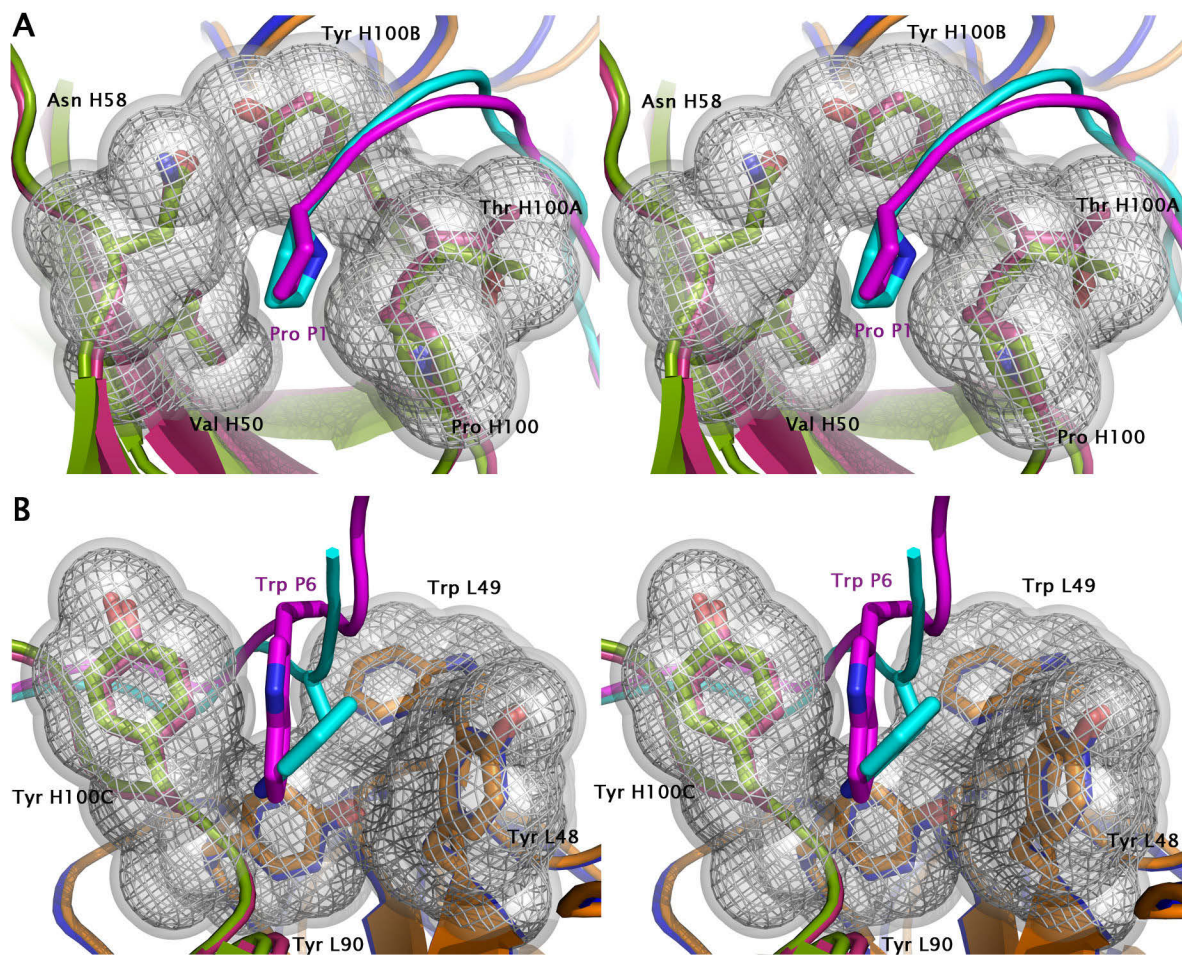


Figure 3.7: Stereo representation of the hydrophobic binding pockets around the Pro P1 and the Trp P6 residues of the OR2 peptides with the Mol1 and Mol2 molecules superimposed. (A) The hydrophobic binding pocket around the Pro P1 residue in Mol1 and Mol2; (B) The hydrophobic binding pocket around the Trp P6 residue in Mol1 and Mol2. All the residues involved in hydrophobic binding (calculated using LIGPLOT) are shown as sticks. In addition, the residues of POM2 Fab are shown with a mesh around a sphere (gray) representation. The colour scheme is similar to the one shown in Figure 3.2.

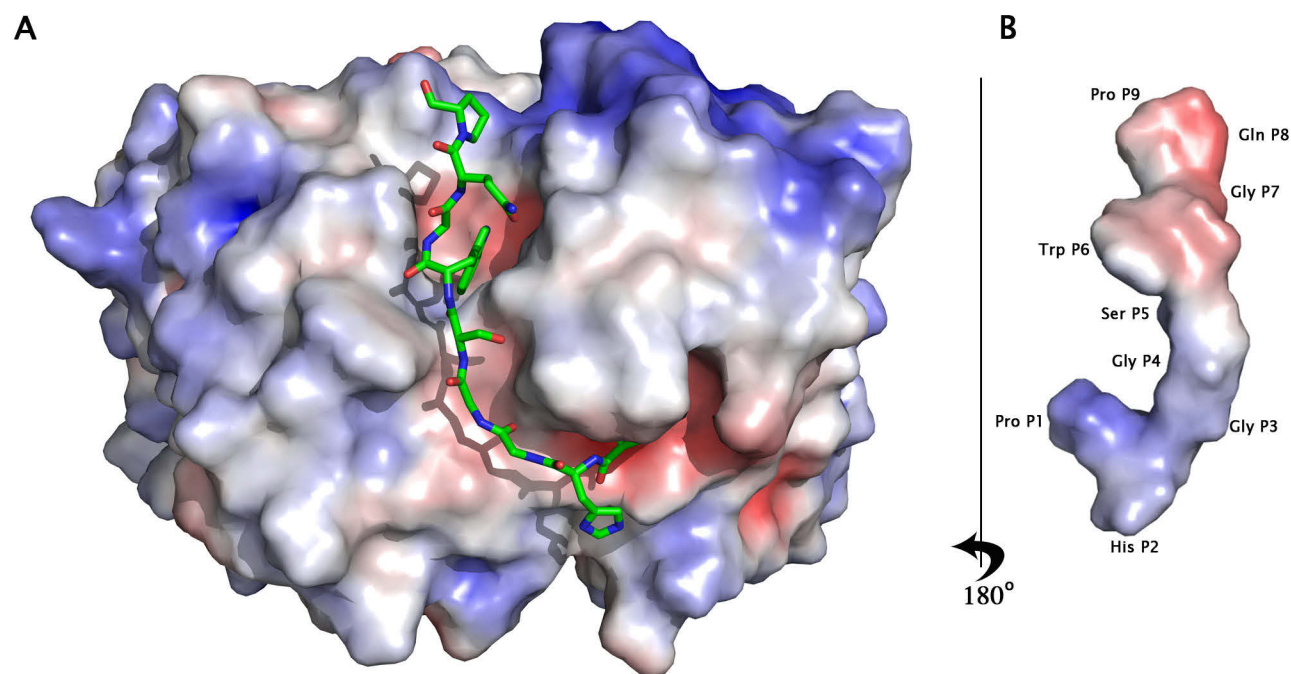


Figure 3.8: An electrostatic potential based surface representation of the POM2 Fab and the OR2 peptide. The electrostatic potential was calculated using the programs PDB2PQR<sup>49</sup> and APBS<sup>16</sup>. The color range extends from  $-5kT/e$  (red) to  $+5kT/e$  (blue). (A) The OR2 peptide (stick representation) bound to the POM2 Fab in Mol1 (surface representation) (B) The electrostatic potential surface representation of the OR2 peptide removed from the binding site by a  $180^\circ$  rotation about the vertical axis shown.

administered intra-cerebrally in prion infected animal models and has now progressed to human clinical trials showing encouraging results by extending the survival of some patients<sup>189</sup>. However, the capacity of PPS to cross the blood-brain-barrier (BBB) has not been very encouraging. Despite the availability of numerous functional studies on these polyanionic compounds, there is a definite lack of molecular level, structural studies of their interactions with the ORs. Currently, the NMR structure of PPS bound to the OR domain is the only high resolution structure available in the literature for a potentially therapeutic compound binding to the OR domain of PrP<sup>C</sup><sup>188</sup>.

The past decade has also seen considerable advances made in the field of Prion Immunotherapy using monoclonal antibodies (mAbs) with epitopes in specific regions of the PrP<sup>C</sup><sup>134</sup>. In 2003, seminal work by White et al.<sup>202</sup>, has shown the efficacy of passive immunization in protecting wild type mice from peripheral prion inoculations. Considerable work has been reported on the mAbs with epitopes in the OR domain of PrP<sup>C</sup> (anti-OR antibody) as they showed very encouraging results with their neuroprotective action in the face of peripheral prion challenge<sup>98,147,174</sup>. As the Fab fragments of these mAbs failed to cross the BBB, they were found ineffective against intra-cerebral infection. Anti-OR antibodies such as mAb110, SAF34 were found to inhibit PrP<sup>Sc</sup> formation in prion infected neuroblastoma cells. It was suggested that mAb 110 acts by promoting cell surface retention of PrP<sup>C</sup> thereby preventing PrP<sup>Sc</sup> accumulation inside the cells and SAF34 acts by preventing the formation of the molecular complexes between PrP<sup>C</sup> and PrP<sup>Sc</sup><sup>147</sup>. In a completely different study<sup>174</sup>, spinal cord lesions and other morphological abnormalities observed in the peripheral nervous system of rats caused by increased PrP<sup>C</sup> levels induced by cobalamin (Vitamin B<sub>12</sub>) deficiency were treated successfully with anti-OR antibodies. More recently, Sonati et al showed that upon binding to the OR domain, the POM2 antibody prevents the neurotoxicity induced by the POM1 antibody in cerebellar mice slices in the COCS assay<sup>54,180</sup>. These functional studies greatly increase the importance of the structural study of an anti-OR antibody fragment such as the POM2 Fab and its potential in the development of antibody based therapy for prion diseases and the recently discovered cobalamine-deficiency induced pathologies.

### 3.5 Conclusions

Our structure of the OR2 peptide complexed with the POM2 Fab is the first reported crystal structure of a complete octapeptide repeat in complex with a potentially ther-

apeutic antibody. The mode of binding of the octapeptide repeats to the antibody is very different from the solution structure of the OR domain in complex with the small molecule binding partner, PPS<sup>188</sup>. We observe critical hydrophobic and backbone interactions between the residues of the octapeptide repeat and POM2 Fab that result in the disruption of the reported  $\beta$ -turn conformation of the unbound OR domain. The POM2 Fab-OR domain peptide system has the potential to be a very useful framework for carrying out further structural studies on the OR domain and its numerous ligands. With more encouraging reports on the therapeutic uses of anti-OR antibodies<sup>98,147,174</sup>, our structure could prove to be important in designing smaller, tighter binding and BBB permeable recombinant anti-OR antibody fragments.

# Chapter 4

## The crystal structure of mouse PrP125-225 in complex with POM6 Fab

### 4.1 Introduction

The POM family of monoclonal anti-PrP antibodies can recognize epitopes within the amino and the carboxy-terminal domains of the prion protein. Our first research goal was to study the structure and binding of the POM2 antibody with its epitope in the octapeptide repeat domain of the amino terminal domain of PrP. Upon the successful completion of our first goal, we were interested in studying the binding characteristics of the other members of the POM family of antibodies with the prion protein. A comprehensive structural<sup>17,19</sup> and functional characterization<sup>180</sup> of the POM1 monoclonal antibody has already been published. The POM1 antibody binds to the carboxy-terminal domain of PrP with epitopes in the  $\beta$ 1- $\alpha$ 1 loop, and the  $\alpha$ 1 and  $\alpha$ 3 helices. Upon the functional characterization of the POM1 antibody, it was found to cause rapid toxicity in COCS assays (Section 1.4.4) leading to cell death. Extensive structural studies, however, showed that the binding of POM1 does not cause any significant conformational distortions in the globular domain of PrP. The POM2 antibody prevents the POM1 induced toxicity in COCS. It was proposed that the binding of certain antibodies to the globular domain of PrP triggers toxicity that is mediated by the octapeptide repeat domain of PrP. However, the structural basis of the POM1 induced toxicity remains to be understood.

Another interesting member of the POM family of monoclonal antibodies is the

POM6 IgG. Epitope mapping studies have shown that in a similar way to the POM1 antibody, POM6 also recognizes and binds to the  $\alpha 1$  helix of PrP<sup>154</sup>. Both POM6 and POM1 have neighbouring but non-overlapping epitopes. POM6 binds to both the glycosylated and unglycosylated versions of the prion protein. The most interesting functionality of POM6 is that despite having neighbouring epitopes with POM1, the POM6 antibody is innocuous to the cerebellar slices in a COCS assay. A comparative structural characterization of the binding of POM6 Fab and POM1 Fab with the prion protein could give insights into the toxicity inducing motifs within the globular, folded domain of the prion protein.

In this chapter, we describe the crystal and molecular structure of the complex of the POM6 Fab antibody fragment with the globular folded domain of the mouse prion protein. We reveal that POM6 binding facilitates the formation of new salt-bridges and hydrogen bonds within the prion protein that could result in an arguably stronger globular domain with a more protected hydrophobic core. We also compare the structures of the complexes of POM6 and POM1 Fab bound prion molecules that revealed differences in the stabilizing inter-domain salt bridges and hydrogen bonds.

## 4.2 Materials and Methods

### 4.2.1 Production of IgG and Fabs

The POM6 Fab production and purification protocol is similar to that followed for POM2 Fab production. Refer to section 3.2.1 for details.

### 4.2.2 Construction of the PrP clones

The plasmid for mouse PrP23-231 was obtained from the lab of Prof. Adriano Aguzzi whereas the construct for PrP117-231 was prepared by Dr. P. K. Baral. These genes were present within restriction sites BamHI and EcoRI in the PRSETA vector (Invitrogen) engineered with a Thrombin cleavage site at the amino-terminal histidine tail. The PrP125-225 clone was constructed using the two primers shown in Table 2.1 within restriction sites BamHI and EcoRI with mouse PrP23-231 as the template DNA. The PCR reaction mixture (25  $\mu$ l) contained 10 ng plasmid DNA, 0.1 mM dNTP, 0.5 mM of each primer and Go Taq polymerase reaction mix (Promega). The PCR was carried out in a Perkin-Elmer thermal cycler with an initial denaturation at 94°C for 5 min; 30 cycles of 94°C for 30sec, 60°C for 30sec, and 72°C for 1 min; and a final extension at 72°C for 10 min. The PCR product was purified on a 1% agarose

gel and extracted for restriction endonuclease digestion at 37 °C for 2h with BamHI and EcoRI. The same conditions were also used to digest the PRSETA vector with BamHI and EcoRI. The digested products were gel purified and ligated to obtain PrP125-225 in the PRSETA vector. Competent DH5 $\alpha$  cells were transformed with the ligation product and plated on Agar-LB medium with Ampicillin (100  $\mu$ g/ml). A colony PCR was performed for randomly picked colonies to identify clones with the desired construct. Plasmids were extracted from the positive clones and their sequences were verified.

### 4.2.3 Expression and purification of PrP constructs

Overnight cultures of freshly transformed colonies of BL21(DE3) cells (Stratagene) with PrP125-225 were added to LB media with 100 $\mu$ g/ml of Ampicillin at 37°C with constant shaking at 250 r.p.m. At an OD<sub>600</sub>  $\sim$  0.5, the expression of the prion protein was induced with 1mM of IPTG. The induction was allowed to proceed overnight at 30°C after which the cultures were harvested. The cells were resuspended in 1xTBS pH 8.0 and sonicated. The IB wash and solubilization protocols were described previously in Section 2.2.1. The solubilized IB of PrP125-225 was loaded onto a Ni-IMAC column. The bound PrP125-225 was refolded on-column with a 200ml gradient of Buffer U to Buffer B (10mM Tris, 100mM Na<sub>2</sub>HPO<sub>4</sub> pH 8.0). The refolded protein was washed on column with Buffer B containing 50mM Imidazole. Pure PrP125-225 was eluted with 10mM Tris, 100mM Na<sub>2</sub>HPO<sub>4</sub>, 500mM Imidazole pH 5.8 and dialyzed into water. For the cleavage of the amino-terminal histidine tag, cleavage buffer (final concentration - 50mM Tris, 10mM CaCl<sub>2</sub> pH 8.0 ) was added to the protein. 1 unit of Thrombin enzyme was added to every 1mg of protein to be cleaved and the cleavage reaction was allowed to proceed overnight at room temperature. Mouse PrP sequence numbering is used throughout the paper.

### 4.2.4 Crystallization of POM6-PrP complex

Purified POM6 Fab was mixed with 2-fold molar excess of His-tag cleaved PrP125-225 and concentrated to 15mg/ml in the buffer 50 mM Tris, 25 mM NaCl, 1mM NaN<sub>3</sub> pH 7.0. The concentrated solution of the complex was loaded onto a Hiload 16/60 Sephadex 75 (Amersham Biosciences) gel filtration column to separate the complex POM6 Fab-PrP125-225 (POM6-PrP) from unbound PrP125-225 (Figure 4.1A). After pooling the fractions containing the POM6-PrP, it was again concentrated to 15mg/ml with a 10kDa cut-off centrifugal filtration unit. The final pure POM6 Fab-



PrP125-225 (POM6-PrP) complex was stored in 50 mM Tris, 25 mM NaCl, 1mM  $\text{NaN}_3$  pH 7.0 buffer at 4°C. The procedures used for screening crystallization conditions were described previously in section 3.2.2. A crystallization hit was initially obtained with condition # 87 of the Index screen - 0.2 M Sodium malonate pH 7.0, 20% w/v Polyethylene glycol 3,350 as the reservoir solution at room temperature. The sitting drop was prepared by mixing 1 $\mu$ l of the protein solution with 1 $\mu$ l of the reservoir solution and the crystals grew within a day. However, the crystals were irregular in shape and grew in clusters (Figure 4.1B). Upon reducing the PEG concentration to 12%, we obtained larger sized, irregular shaped clusters of crystals (Figure 4.1C). Seeds were made out of these initial crystals. Upon using cat whiskers for streak seeding we obtained a shower of individual and thin but very small crystals (Figure 4.1D). The combined use of 0.1M Praseodymium acetate and TCEP as additives gave more regular shaped crystals. After further optimization of the precipitant and additives, we obtained thin, plate shaped diffraction quality crystals with 0.2M Sodium malonate pH 7.0, 12% PEG8000 along with 5mM TCEP, 5mM Praseodymium acetate and ethanol as additives (Figure 4.1E). The crystals were flash-cooled in liquid  $\text{N}_2$  after adding 30% glycerol as a cryoprotectant.

#### 4.2.5 Data collection and structure determination

Intensity data (Figure 4.1F) were collected from a single crystal at the bending magnet beamline of the Canadian Light Source (CLS), Saskatoon. The resolution of the data was 1.83 Å with an overall completeness of 99.8%. The AUTOPROCESS script which uses XDS<sup>70,93</sup> was developed at CLS and used for data processing, scaling and integration. The crystals were indexed in the orthorhombic space group  $\text{P}22_12_1$  with one molecule of the 1:1 POM6-PrP complex in the asymmetric unit. The structure of POM6-PrP was solved by molecular replacement using the program PHASER<sup>124</sup> of the PHENIX suite<sup>2</sup> with the constant domain and variable domains (without loops) of the POM2 Fab protein as the search model (PDB ID 4J8R)<sup>187</sup>. 87% of the model was built using AUTOBUILD of the PHENIX suite that uses RESOLVE, while the remaining 13% of the model was built manually to fit the electron density in the  $2|F_o| - |F_c|$  map. The data processing and refinement statistics are summarized in Table 4.1.

## 4.2.6 Structure refinement

The PHENIX suite was used to perform crystallographic refinement<sup>3</sup> on the molecular model of the POM6-PrP complex. 5% of the reflections from the data collected were randomly selected and set aside to calculate the  $R_{free}$  factor for monitoring the progress of refinement. Translation/Libration/Screw (TLS) and the individual Atomic Displacement Parameter (ADP) refinements were applied to the model. The positions of water molecules were initially identified using PHENIX and their positions were subsequently confirmed by manually checking for positive peaks in both the  $2|F_o| - |F_c|$  and the  $|F_o| - |F_c|$  electron density maps. Water molecules with B-factors greater than  $60 \text{ \AA}^2$  were removed from the coordinate list. The program COOT was used for manual model building<sup>52</sup>. Structure validation was performed with the program MOLPROBITY<sup>43</sup>. Potential hydrogen bonds and van der Waals contacts were analyzed using the program LIGPLOT<sup>196</sup>. PyMOL<sup>175</sup> was used to calculate the RMSDs and to create all the figures.

## 4.3 Results

### 4.3.1 Overall structure of the POM6-PrP complex

Our initial attempts to co-crystallize POM6 Fab with PrP117-231 (mouse PrP sequence numbering) were unsuccessful. Although we had obtained thin, plate shaped crystals of POM6-PrP117-231, none of them diffracted beyond  $4 \text{ \AA}$  resolution. In order to enable better crystal packing, we constructed mouse PrP125-225 in which the flexible regions of PrP117-231 consisting of residues 117-124 and 225-231 were removed in the hopes that it would enable better crystal packing. With that slight modification in the PrP construct, we successfully co-crystallized POM6-PrP in the space group  $P22_12_1$ . The crystals diffracted to  $1.83 \text{ \AA}$  resolution and the asymmetric unit contained one molecule of the POM6-PrP complex (Figure 4.2A). The final model was refined to a crystallographic  $R_{work}$  factor of 18.8% and  $R_{free}$  of 22.8% with 527 protein residues and 460 water molecules. The data processing and refinement statistics are summarized in Table 4.1. A MOLPROBITY validation report shows that only 4 residues (0.76%) are in the disallowed region of the Ramachandran plot. For convenience, the residue numbers of the PrP125-225, POM6 Fab heavy and light chains will be preceded by the letters P, H and L respectively.

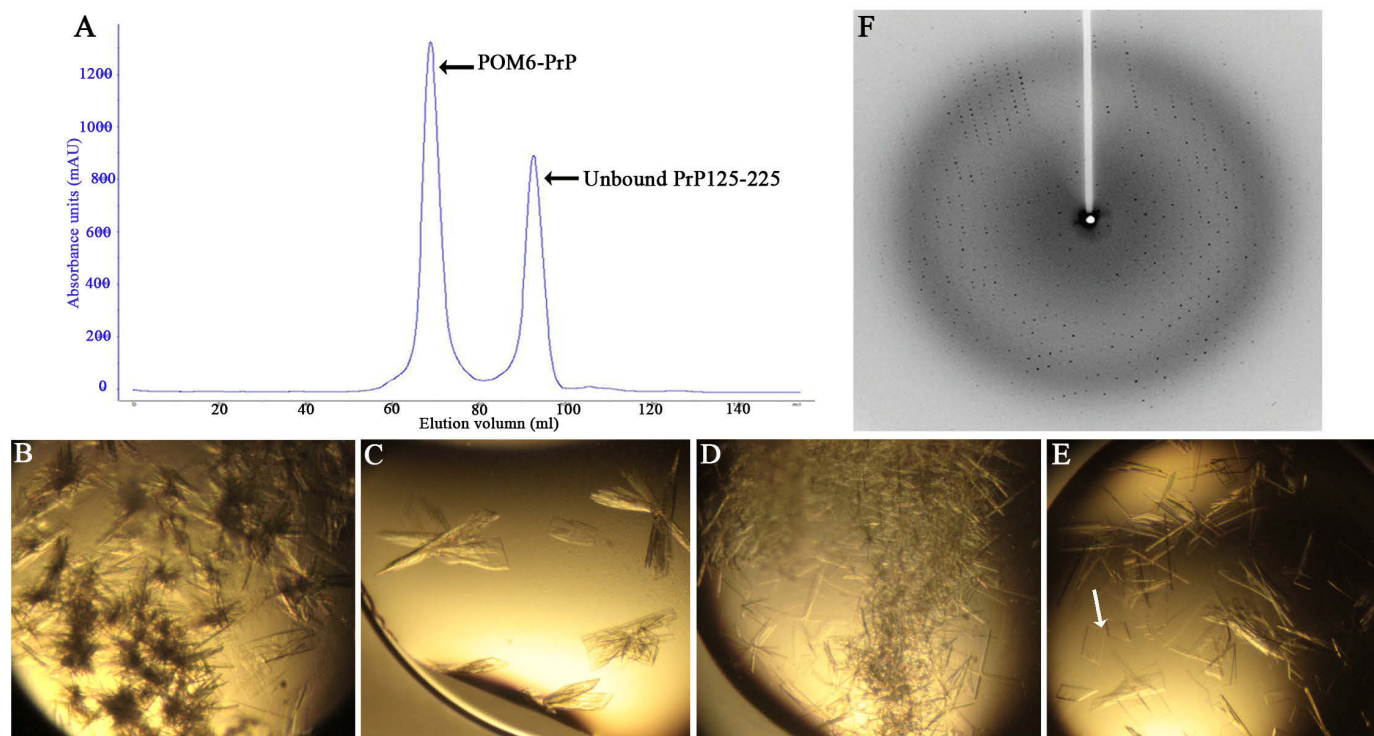


Figure 4.1: The process of obtaining diffraction quality crystals of POM6-PrP complex (counter-clockwise). (A) A size exclusion chromatogram showing the separation of the POM6-PrP complex from the unbound PrP125-225; (B) Initial crystallization hit showing a cluster of irregularly shaped crystals obtained with 0.2 M Sodium malonate pH 7.0, 20% w/v Polyethylene glycol 3,350; (C) Irregular shaped, clusters of larger crystals obtained on optimizing the concentration of the precipitant PEG from 20% to 12% (D) small, plate shaped individual crystals obtained on streak seeding using a cat whisker along with additives; (E) Regular shaped, thin flat crystals of POM6-PrP obtained on using 0.2M Sodium malonate pH 7.0, 12% PEG8000 along with 5mM TCEP, 5mM Praseodymium acetate and ethanol as additives. The white pointer shows the type of crystals selected that diffracted to 1.83Å. (F) A frame displaying the diffraction pattern obtained from one of the POM6-PrP crystals.

Table 4.1: Data-collection and refinement statistics of POM6-PrP125-225

Wavelength(Å )	0.97949
Matthew's co-efficient(Å <sup>3</sup> /Da)	2.55 (one complex in the asymmetric unit)
Space group	P22 <sub>1</sub> 2 <sub>1</sub>
Unit-cell parameters (Å)	
a, b, c	71.99, 82.39, 103.66
Resolution range (Å) <sup>a</sup>	39.6-1.83 (2.01-1.83)
Total no. of reflections	508,440 (95,752)
Unique reflections	54,956 (12,821)
$R_{meas}$ (%) <sup>b</sup>	21.6(271.7)
Average I/ $\sigma$ (I)	9.29(0.94)
$CC_{1/2}$ (%) <sup>c</sup>	99.7 (31.0)
no.of pairs of reflections <sup>d</sup>	54706 (12778)
Completeness(%)	99.8 (99.2)
Multiplicity	9.3 (7.47)
<b>Refinement</b>	
$R_{work}$ (%) <sup>e</sup>	18.8
$R_{free}$ (%) <sup>e</sup>	22.8
Number of refined atoms	
Total	4628
Protein	4139
Water	460
TCEP, Glycerol	17, 12
Mean B-factor (Å <sup>2</sup> )	
Overall	35.84
Solvent	43.06
POM6 H chain	35.37
POM6 L chain	31.55
PrP125-225	40.69
<i>Ramachandran plot</i>	
Favored(%)	97.14
Allowed(%)	2.1
Disallowed(%)	0.76
r.m.s.d. bonds (Å)	0.007
r.m.s.d. angles (°)	1.058

<sup>a</sup> Values in the parentheses are for the highest resolution shell.

<sup>b</sup>  $R_{meas} = \frac{\sum_{hkl} \sqrt{\frac{n}{n-1}} \sum_{j=1}^n |I_{hkl,j} - \langle I_{hkl} \rangle|}{\sum_{hkl} \sum_j I_{hkl,j}}$  is the redundancy independent indicator of data quality.

<sup>c</sup>  $CC_{1/2}$  = percentage of correlation between intensities from random half-datasets.

<sup>d</sup> The pairs of reflections are used in calculating  $CC_{1/2}$ .

<sup>e</sup>  $R_{work}$  and  $R_{free} = \frac{\sum_{hkl} ||F_{obs}| - |F_{calc}||}{\sum_{hkl} |F_{obs}|}$  for reflections in the working and test (5% of the data) sets, respectively.

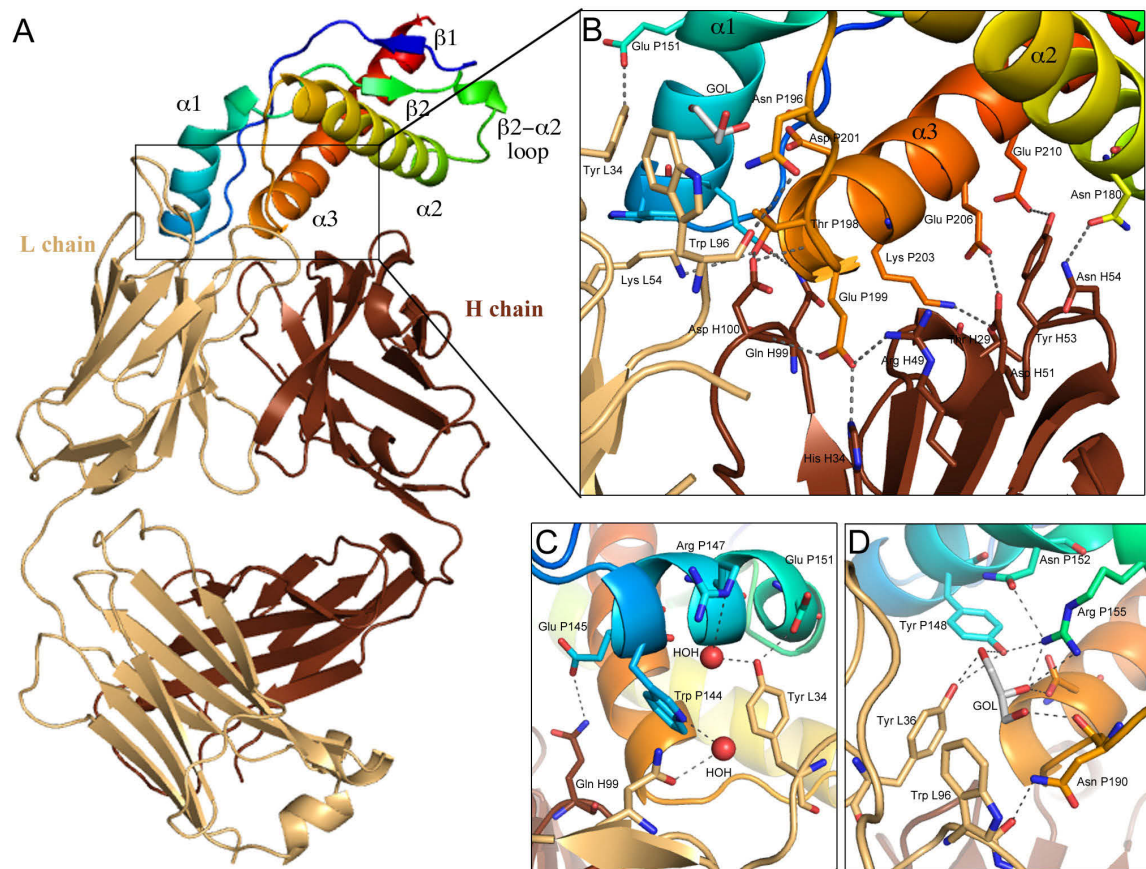


Figure 4.2: The crystal structure of the complex of recombinant mouse PrP125-225 and POM6 Fab. (A) The mouse PrP125-225 is shown in a spectral colour scheme with amino terminal domain coloured in blue to the carboxy terminal domain coloured in red. The heavy (H) and light (L) chains of POM6 Fab are colored in chocolate brown and light orange, respectively; (B) A close up of the intermolecular contacts between PrP125-225 and the POM6 Fab. All the important hydrogen bonding interactions have been depicted using dashed lines (dark gray) and the intermolecular distances have been summarized in Table 4.2; (C) A close up of the interactions between  $\alpha 1$  helix of PrP125-225 and the POM6 Fab. The structural water molecules have been shown as red spheres. (D) A close-up view of the ‘binding pocket’ present at the carboxyl terminus of  $\alpha 1$  helix. It is bounded by the  $\alpha 1$  (blue) and  $\alpha 3$  helices (orange), the  $\alpha 2$ - $\alpha 3$  loop (orange) and the CDRs L1, L3 (light orange) of POM6. A glycerol (GOL) molecule also present in this binding pocket has been shown in sticks (gray).

### 4.3.2 Overall structure of the POM6 Fab

In the POM6-PrP structure, all 6 of the CDRs of the POM6 Fab molecule have well-defined electron densities in the  $2|F_o| - |F_c|$  map. The elbow angle of POM6 Fab was calculated to be  $136.7^\circ$ . Out of the 18 standard canonical conformations described for the CDR loops, POM6 Fab CDR loops L1, L2, L3, H1 and H2 fall into canonical classes  $\kappa 4$ , 1, 1, 1 and 1, respectively<sup>13</sup>. Although, all the 6 CDRs of POM6 Fab participate in interactions with PrP125-225, the heavy (H) chain CDRs (CDR H1, residues 25-34; CDR H2, residues 49-60; CDR H3, residues 98-104) make more hydrogen bonds and electrostatic interactions with PrP125-225 than do the light (L) chain CDRs (CDR L1, residues 24-38; CDR L2, residues 54-60; CDR L3, residues 93-101). The shape complementarity scores between POM6 Fab and PrP125-225 calculated by the Sc program<sup>112</sup> of the CCP4 suite<sup>206</sup> are 0.772 and 0.652 for the H and L chains, respectively indicating good complementarity. It is very interesting to note that POM6 Fab binds to all three of the helices of PrP125-225.

### 4.3.3 Overall structure of PrP125-225

All of the residues of PrP125-225 in the POM6-PrP complex except Tyr P225 could be traced in the  $2|F_o| - |F_c|$  electron density map. The average B-factor (or temperature factor) of the POM6-PrP complex was  $35.84 \text{ \AA}^2$  whereas that of the bound PrP125-225 was slightly higher at  $40.7 \text{ \AA}^2$ . In agreement with the previously published NMR and crystallographic structures of the globular portion of the prion protein (e.g., PDB ID-1AG2), the POM6 Fab bound PrP125-225 molecule has 2  $\beta$ -strands (residues 128-130 in  $\beta 1$  and 160-162 in  $\beta 2$ ) and 3  $\alpha$ -helices (residues 143-155 in  $\alpha 1$ , 171-193 in  $\alpha 2$  and 199-223 in  $\alpha 3$ ).

### 4.3.4 Interactions between PrP125-225 and POM6 Fab

The crystal structure of the POM6-PrP complex reveals that the POM6 Fab has a conformation-dependent, discontinuous epitope in PrP125-225. POM6 Fab binding makes  $805.4 \text{ \AA}^2$  (12.54%) surface area of PrP125-225 solvent inaccessible<sup>85</sup>. The amino terminal region of helix  $\alpha 3$  and the  $\alpha 2$ - $\alpha 3$  loop are the primary occupants of the cleft between the variable domains of the L and H chains of the POM6 Fab (Figure 4.2A) and make up a major part of the epitope of the POM6 antibody. Additional epitopes are also found on the  $\alpha 1$  and  $\alpha 2$  helices of PrP125-225. The  $\alpha 3$  helix of the PrP125-225 binds predominantly to the H chain of POM6 Fab. Interestingly, residue

Glu P199 at the amino terminus of the helix  $\alpha 3$  of PrP125-225 makes interactions with all three of the H chain CDRs of POM6 (Figure 4.2B). Due to very good geometry, Glu P199 forms a hydrogen bond with N $\epsilon$ 2 of His H34 (CDR H1), the backbone amide of Asp H100 (CDR H3) as well as a salt bridge with NH1 of Arg H49 (CDR H2). In the carboxy terminal region of the  $\alpha 2$ - $\alpha 3$  loop, the backbone amides of Glu P199, Thr P200 and the side chains of Thr P198 and Thr P200 make critical hydrogen bonds with residues Gln H99 and Asp H100 (CDR H3) of POM6. Thr P200 is the only residue on helix  $\alpha 3$  that also makes hydrogen bonds with the light chain of POM6 through Lys L54 (CDR L2). Further strengthening the interactions between POM6 and PrP125-225 are the residues Lys P203 and Glu P206 on the helix  $\alpha 3$  that make a network of salt bridges and hydrogen bonds with Asp H51 (CDR H2) and the backbone carbonyl oxygen of Thr H29 (CDR H1). Glu P210 on helix  $\alpha 3$  also contributes to the interactions with POM6 by forming a hydrogen bond with Tyr H53 of the CDR H2.

The L chain of POM6 Fab predominantly binds to the  $\alpha 1$  helix of the PrP (Figure 4.2C). Previous studies have shown the importance of water molecules in mediating interactions between a protein and its ligand through a network of hydrogen bonds<sup>155</sup>. We find two well placed water molecules facilitating interactions between N $\epsilon$ 1 of Trp P144 - Asn L57 (CDR L2) and between Arg P147 - Tyr L34 (CDR L1). It confirms previous epitope binding studies that show that POM6 Fab competes with POM1 Fab (epitope residues 139-144) for PrP binding<sup>154</sup>. Glu P145 is the only residue in helix  $\alpha 1$  that interacts with a residue in the heavy chain of POM6 - Gln H99 (CDR H3) through a hydrogen bond. The residue Glu P151 on the helix  $\alpha 1$  also makes a strong hydrogen bond with Tyr L34.

The rest of the interactions between helix  $\alpha 1$  and POM6 take place in a ‘binding pocket’ that is bounded by helices  $\alpha 1$ ,  $\alpha 3$ , the  $\alpha 2$ - $\alpha 3$  loop and the CDRs L1 and L3 of POM6 (Figure 4.2D). As glycerol was used as a cryoprotectant for the POM6-PrP crystals, we found the electron density for one glycerol molecule in the  $|F_o| - |F_c|$  map in the centre of the above-described binding pocket. Within this pocket we see that Tyr P148 of helix  $\alpha 1$  forms a hydrogen bond with Tyr L36 (CDR L1) and the glycerol molecule additionally strengthens this interaction by hydrogen bonding with both of these tyrosine residues. Glycerol also forms stable hydrogen bonds with Tyr P148, Asn P152, Arg P155 (helix  $\alpha 1$ ), Asn P196 ( $\alpha 2$ - $\alpha 3$  loop) and Asp P201 (helix  $\alpha 3$ ). This network of salt bridges and hydrogen bonds orients the helix  $\alpha 1$  towards helix  $\alpha 3$  and keeps the hydrophobic core intact<sup>168</sup>. As this intricate network of residues already exists in previously published structures of PrP, we can safely

conclude that the presence of the glycerol molecule in the binding pocket does not induce the formation of any new bonds but merely serves to consolidate the existing ones. Table 4.2 summarizes all the significant interactions (less than 4.0Å in distance) between POM6 Fab and PrP125-225.

POM6 Fab also binds to Asn P180 in helix  $\alpha 2$  and to Asn P196 in the  $\alpha 2$  - $\alpha 3$  loop. Asn P180 forms a hydrogen bond with Asn H54 (CDR H2) and Asn P196 forms a hydrogen bond with the backbone carbonyl oxygen of Trp L96 (CDR L3). Interestingly, both Asn P180 and Asn P196 are the two glycosylation sites in mouse PrP. Previous studies have shown that the POM6 interacts with all three - un-, mono- and di- glycosylated versions of the prion protein<sup>154</sup>. Therefore, the crystal structure of POM6-PrP is only a true representation of the binding of the POM6 Fab to the unglycosylated version of the mouse prion protein. The prion molecule might rotate slightly away from POM6 Fab in order to accommodate the bulky glycans when they are present. But we can only speculate that despite this rotation, the binding of POM6 Fab to its epitopes in helices  $\alpha 3$  and  $\alpha 1$  remains unaffected.

The analysis of the electrostatic potential surface map of the POM6-PrP<sup>16,49</sup> shows that the interactions between POM6 Fab and PrP125-225 are predominantly electrostatic in nature. The nature of the surface presented by PrP for Fab binding is mostly basic (positively charged) whereas that presented by the POM6 Fab CDRs is mostly acidic (negatively charged) (Figure 4.3). Analysis upon using LIGPLOT<sup>196</sup> showed that the majority of the hydrophobic interactions that promote the stability of the POM6-PrP complex are contributed by Glu P199, Lys P203 and Glu P206 on helix  $\alpha 3$  and by Trp P144 and Tyr P148 on helix  $\alpha 1$  (Figure 4.4).

### 4.3.5 Crystal contacts

The POM6-PrP complex has only one molecule in the asymmetric unit (Figure 4.5A). The PrP125-225 molecule makes 11 crystal contacts with neighbouring symmetry related molecules. With the exception of Tyr P154 in helix  $\alpha 1$ , the remaining 10 residues involved in the crystal contacts are far away from the POM6 binding regions of the PrP125-225. The majority of the crystal contacts are in the carboxy-terminal region of the helix  $\alpha 3$  and one crystal contact each in helix  $\alpha 2$ , strand  $\beta 2$  and in the  $\beta 1$  - $\alpha 1$  loop (Figure 4.5B).



PrP	POM6 Fab	Distance
<b>Helix <math>\alpha 3</math></b>		
Thr P198 O $\gamma$ 1	Asp H100 O $\delta$ 2	2.60
Glu P199 N	Asp H100 O $\delta$ 2	3.52
Glu P199 O $\epsilon$ 2	His H34 N $\epsilon$ 2	2.83
Glu P199 O $\epsilon$ 2	Arg H49 NH1	2.78
Glu P199 O $\epsilon$ 1	Asp H100 N	2.88
GLU P199 O $\epsilon$ 1	SER H98 O $\gamma$	2.53
Thr P200 O $\gamma$ 1	Lys L54 N	3.82
Thr P200 N	Asp 100 O $\delta$ 2	2.98
Thr P200 O $\gamma$ 1	Asp 100 O $\delta$ 2	2.70
Lys P203 NZ	Asp H51 O $\delta$ 1	2.82
LYS P203 NZ	THR H29 O	2.76
Glu P206 O $\epsilon$ 2	Asp H51 O $\delta$ 2	2.84
Glu P210 O $\epsilon$ 1	Tyr H53 OH	3.03
<b><math>\alpha 2</math>-<math>\alpha 3</math> loop</b>		
Asn P196 O $\delta$ 1	Trp L96 C	3.50
<b>Helix <math>\alpha 2</math></b>		
Asn P180 O $\delta$ 1	Asn H54 N $\delta$ 2	3.11
<b>Helix <math>\alpha 1</math></b>		
Glu P145 O $\epsilon$ 2	Gln H99 N $\epsilon$ 2	3.75
Glu P151 O $\epsilon$ 1	Tyr L34 OH	2.70
ARG P155 NH2	GOL 1 O2	2.60
ARG P155 NH1	GOL 1 O2	3.22

Table 4.2: Summary of interactions of PrP125-225 with POM6 Fab

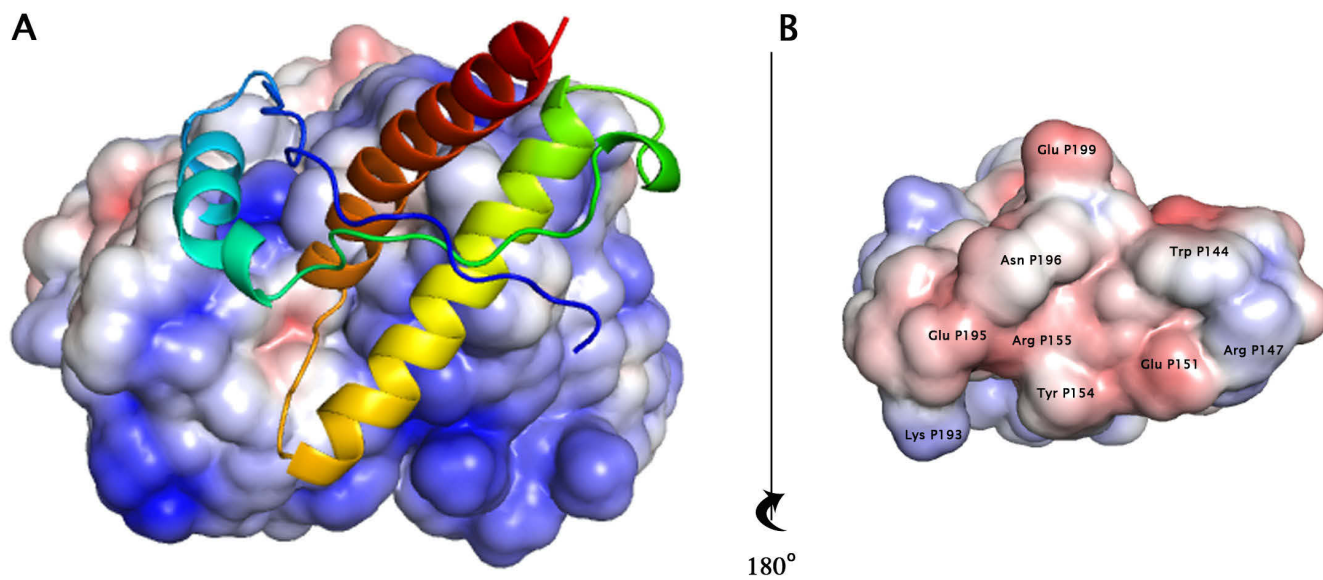


Figure 4.3: An electrostatic potential based surface representation of the POM6 Fab and PrP125-225. The electrostatic potential was calculated using the programs PDB2PQR<sup>49</sup> and APBS<sup>16</sup>. The color range extends from  $-4kT/e$  (red) to  $+4kT/e$  (blue). (A) PrP125-225 (cartoon representation) bound to the POM6 Fab (surface representation) (B) The electrostatic potential surface representation of the POM6 Fab binding surface of PrP125-225 removed from the binding site by a 180° rotation about the vertical axis shown.

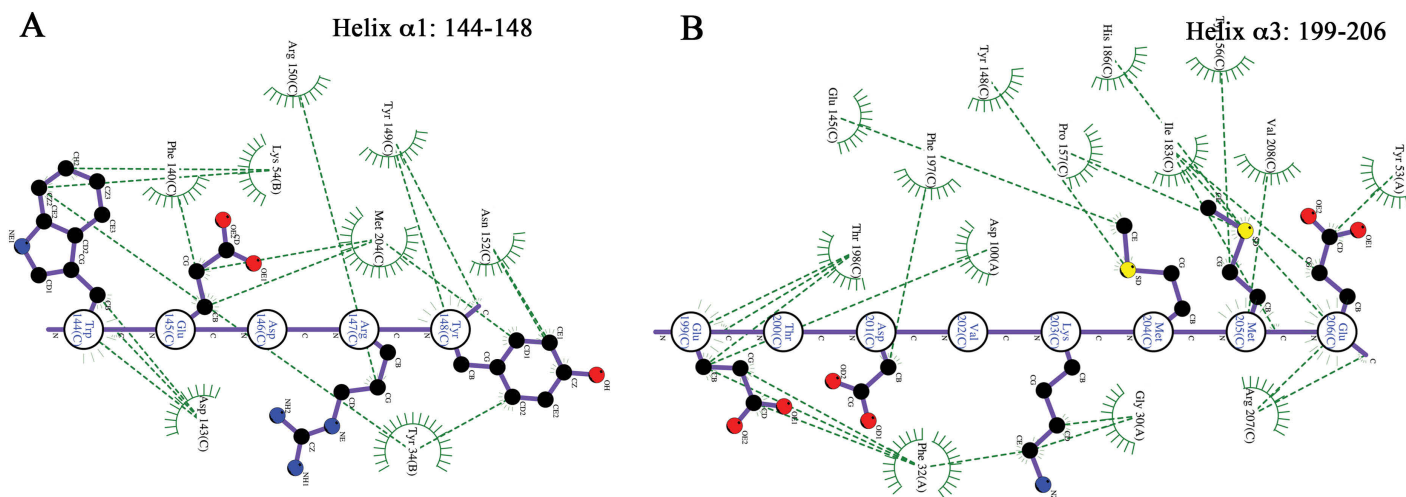


Figure 4.4: A schematic LIGPLOT depicting the hydrophobic interactions between the residues in POM6 Fab (chain A and B) and PrP125-225 (chain C). The carbon-carbon bonds are shown in purple and the hydrophobic interactions between the atoms are shown in olive green colored dashes. (A) Depicts the interactions between residues 144-148 on helix  $\alpha 1$  of PrP125-225 and POM6 Fab and (B) Depicts the interactions between residues 199-206 on helix  $\alpha 3$  of PrP125-225 and POM6 Fab

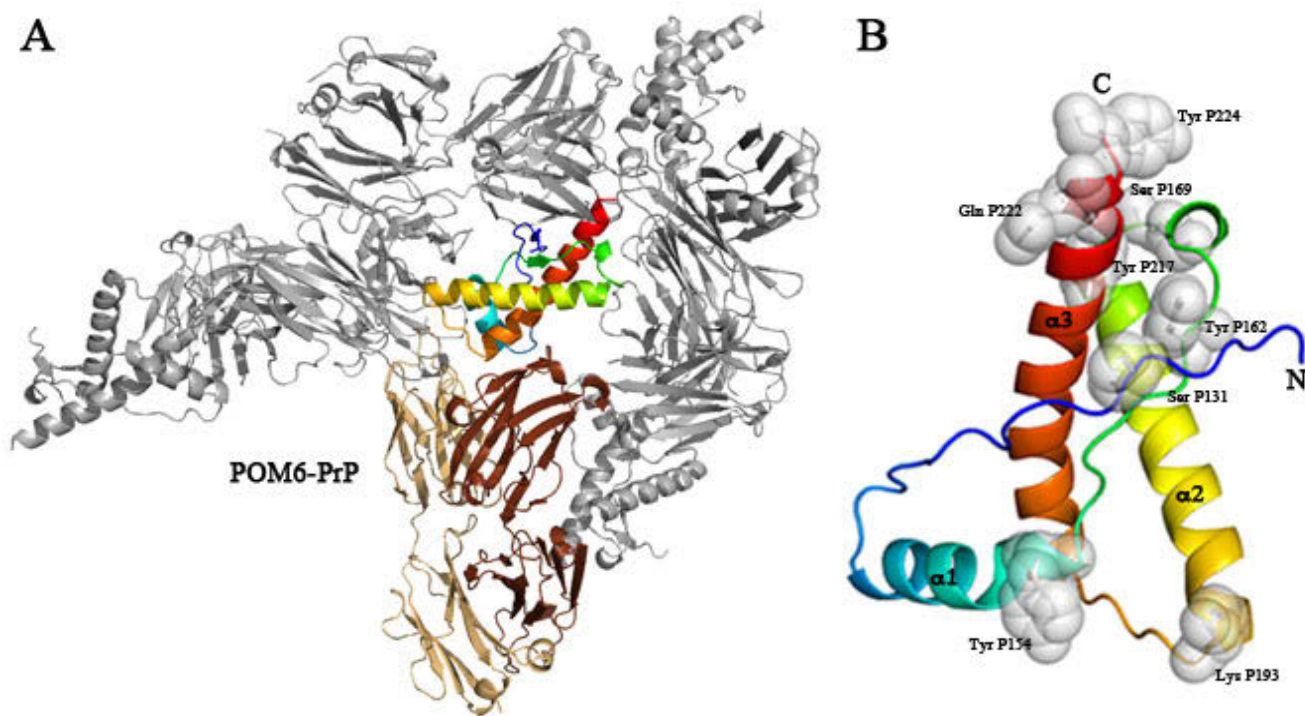


Figure 4.5: Crystal contacts in the POM6 bound PrP125-225 molecule. The POM6-PrP complex was crystallized in the orthorhombic spacegroup  $P22_12_1$ . In the POM6-PrP crystal, (A) depicts the symmetry related POM6-PrP molecules (in gray) neighbouring only the PrP125-225 molecule present in the highlighted POM6-PrP molecule. The colour scheme of the highlighted molecule is described in Figure 4.2A. In this crystal, we do not observe any crystal contacts between two symmetry related adjacent molecules of PrP125-225. (B) The residues of POM6 bound PrP125-225 that are participating in crystal contacts are shown as spheres (light gray) on a cartoon representation of a molecule of PrP125-225 (spectral color scheme). N and C represent the amino- and carboxy- termini of PrP125-225, respectively.

## 4.4 Discussion

### 4.4.1 Stabilizing salt bridges in POM6-PrP

Salt bridges within a protein molecule are formed due to the proximity of oppositely charged groups that are in spatial proximity (usually less than  $4\text{\AA}$ )<sup>21</sup>. Buried salt bridges are energetically very strong and contribute tremendously to a protein's stability. The salt bridges on the solvent accessible surface of a protein however, may not be as strong as hydrophobic interactions, but they do make slight contributions to the stability of a protein molecule<sup>21</sup>. Salt bridges may be broadly classified into local and non-local interactions depending on the sequence proximity of the residues involved. Using molecular dynamic simulations (MDS), it has been observed that three commonly populated 'local' or intradomain salt bridges in an unbound PrP molecule are - (i)Arg147 - Glu151 on helix  $\alpha 1$ , (ii)Arg207 - Glu210 on helix  $\alpha 3$  and (iii) Arg163 - Asp166 in the  $\beta 2$ -  $\alpha 2$  loop (mouse PrP numbering)<sup>75,133,214</sup>. These interactions serve to self-stabilize the secondary structures of the PrP domains involved. Also through MDS, it was determined that the highly populated 'non-local' or interdomain salt bridges in unbound PrP are Glu145 - Lys 203, Arg155 - Glu195 and Arg163 - Asp177. These three interactions serve to stabilize the overall tertiary fold of PrP by linking its secondary structure domains to one another<sup>75,76</sup>.

The first of the three stabilizing local salt bridges- Arg P147 - Glu P152 is absent in POM6-PrP (Figure 4.6A). Previous cell free conversion experiments have shown that this salt bridge stabilizes the PrP<sup>sen</sup> molecule (see Table 1.3 for its definition) from converting into PrP<sup>res</sup><sup>181</sup>. However, despite the disruption of the salt bridge, POM6 Fab interacts with both Arg P147 and Glu P152 residues via Tyr L34 (CDR L1) as described in section 4.3.4 (Figure 4.6A). In an MDS simulation<sup>214</sup>, the percentage occupancy of this salt bridge Arg P147 - Glu P152 in an unbound PrP molecule was found to be 68.5%. It is highly likely that the formation of the Arg P147 - Glu P152 -Tyr L34 network in POM6-PrP complex, potentially increases the occupancy of this salt bridge and improves the maintenance of the structural integrity of the helix  $\alpha 1$ . POM6 Fab binding also disrupts the second local salt bridge Arg P207 - Glu P210 (Figure 4.6B). In an unbound prion protein, the Arg P207-Glu P210 salt bridge functions to keep the helix  $\alpha 3$  stable<sup>75,133</sup>. In POM6-PrP, Glu P210 forms a hydrogen bond with Tyr H53 whereas Arg P207 forms potential cation-pi interactions with Phe P140 of helix  $\alpha 1$  (Figure 4.6B). Surprisingly, in the vicinity of the Glu P210 - Tyr H53 bond, we found the side chain of the residue His P176 of helix  $\alpha 2$ . As the distance between the imidazole plane of His and Tyr H53 is  $3.96\text{\AA}$  it is possible that

the His and Tyr residues could interact with each other via an offset-face-stacked  $\pi$ - $\pi$  interactions<sup>26</sup>. In 2011, an MDS study on horse prion protein at low pH showed the salt bridge Glu P210 - His P176 that connects helices  $\alpha$ 3 and  $\alpha$ 2, contributed to the stability of the horse prion protein<sup>212</sup>. As horses are one of the few mammals that are resistant to TSEs, the formation of this salt bridge could be one of the contributing factors to the stability of the cellular form of Horse PrP<sup>C</sup>. Therefore, we speculate that the Glu P210 - Tyr H53 - His P176 network contributes to interdomain stabilization forces between the helices  $\alpha$ 2 and  $\alpha$ 3 .

POM6 Fab also causes a disruption in the non-local Glu P145-Lys P203 salt bridge connecting helices  $\alpha$ 1 and  $\alpha$ 3 (Figure 4.6C). In the POM6-PrP complex, Glu P145 forms a hydrogen bond with Gln H99 (CDR H3) and the side chain of Lys P203 forms a salt bridge with Asp H51 (CDR H2) and a hydrogen bond with the carboxyl oxygen of Thr H29. The Lys P203- Asp H51 salt bridge is a buried salt bridge and therefore, is energetically very strong and will contribute to the stability of the POM6-PrP complex. Studies have shown that residues with long side chains such as Lys and Glu that contain hydrophobic methylene groups can also participate in hydrophobic interactions if their polar groups participate in a salt bridge<sup>51</sup>. Despite the disruption of the Glu P145-Lys P203 salt bridge, the formation of the Lys P203-Asp H51 salt bridge enables Lys P203 to make hydrophobic contacts with Phe H32 and Gly H30 of CDR H1 of POM6 Fab to further stabilize the POM6-PrP complex. The Glu P145 residue also participates in hydrophobic interactions with the residue Met P204 which is part of the hydrophobic core of PrP between helices  $\alpha$ 1 and  $\alpha$ 3. The rest of the two populated non-local salt bridges, ArgP155 -GluP195 and Arg P163- Asp P177 were found intact in POM6-PrP.

#### 4.4.2 Structural comparisons of POM6-PrP and POM1-PrP

The POM6 Fab bound PrP is innocuous to cerebellar slices whereas POM1 bound PrP is severely toxic<sup>180</sup>. A comparative structural analysis of the complexes of POM6 and POM1 Fab with PrP may give clues towards the existence of the functional differences between the two antibodies. The binding of POM6 Fab buries a surface area of 803  $\text{\AA}^2$  on the PrP molecule while binding all of the three  $\alpha$ -helices whereas the binding of POM1 buries only an area of 580  $\text{\AA}^2$  binding predominantly to the  $\beta$ 1- $\alpha$ 1 loop, helices  $\alpha$ 1 and  $\alpha$ 3. A backbone carbon atom ( $C_\alpha$ ) alignment of the structures of POM6 Fab bound PrP125-225 and POM1 Fab bound mouse PrP120-231 (PDB ID 4H88)<sup>19</sup> using Pymol<sup>175</sup> resulted in an r.m.s.d. of 0.621  $\text{\AA}^2$  (100  $C_\alpha$  pairs) (Figure

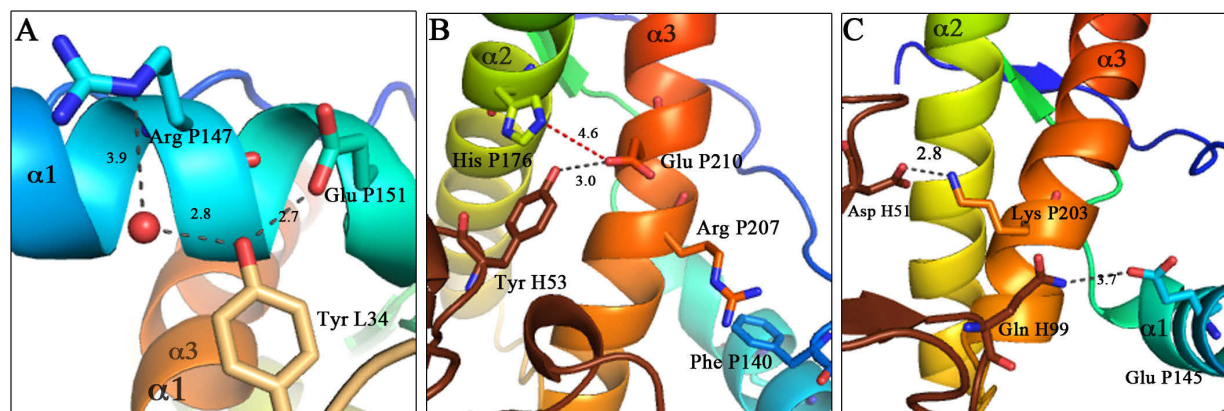


Figure 4.6: The salt bridges affected by the binding of POM6 Fab to PrP125-225. PrP125-225 is shown as a cartoon and the residues of interest are shown as sticks. The distance (in Å) between the residues is depicted using black dashes. The interactions that are improbable to form are shown in red dashes. The color scheme is similar to that in Figure 4.2A. (A) The local salt bridge between Arg P147-Glu P151 on helix  $\alpha 1$ ; (B) The local salt bridge between Arg P207-Glu P210 on helix  $\alpha 3$ ; (C) The non-local salt bridge between Glu P145 on helix  $\alpha 1$  and Lys P203 on helix  $\alpha 3$ .

4.7), which shows that neither of the Fabs significantly altered the global structure of the globular domain of PrP. The comparison of the local structures of the Fab bound PrP molecules however, revealed interesting changes in the intra- and interdomain interactions within the globular domain of the PrP molecule.

Several experimental studies have implicated the  $\beta 2$ - $\alpha 2$  loop of PrP in playing a role in prion transmission across species<sup>109,176</sup>. The non-local salt bridge between residues Arg P163 and Asp P177 has been shown by MDS studies to be highly populated with a 90.4% occupancy<sup>214</sup>. This salt bridge anchors the  $\beta 2$  strand of PrP to the helix  $\alpha 2$ <sup>75</sup>. The Arg P163 - Asp P177 salt bridge is formed in POM6-PrP but not in POM1-PrP (Figure 4.8A, B). In POM6-PrP, we also see that the buried Tyr P168 of the  $\beta 2$ - $\alpha 2$  loop forms hydrogen bonds with both of the residues of the salt bridge Arg P163 - Asp P177. In POM1-PrP however, Tyr P168 forms a hydrogen bond with only the residue Asp P177. A second Tyrosine residue, Tyr P127 of the amino terminus of PrP125-225 forms cation-pi interactions with Arg P163 in POM6 bound PrP (4.1 Å) but a much weaker interaction in POM1 (5.2 Å) bound PrP. In POM6-PrP, Tyr P127 forms an additional critical hydrogen bond with Asp P177 on the helix  $\alpha 2$ . The Asp177Asn mutation (mouse numbering) is associated with FFI and familial CJD depending on the amino acid in position 128<sup>168</sup>. In the Asp177Asn mutation, the hydrogen bond between residues Tyr P127 to Asp 177 is abolished. The Tyr P127 to Asp 177 serves to anchor the flexible amino terminus of the globular domain of PrP125-225 to the helix  $\alpha 2$ <sup>168</sup>. MDS studies have shown that the Asp177Asn mutation increases the flexibility of amino terminal end of globular domain of PrP<sup>74</sup> and may also lead to the breaking of the  $\beta$  sheet<sup>20</sup> resulting in the destabilization of the hydrophobic core. In POM1-PrP, Tyr P127 is too far (6.5 Å) to form the hydrogen bond with Asp P177. Interestingly, with the exception of the salt bridge between Arg P163 - Asp P177, the above described network of interactions amongst residues Arg P163, Tyr P168, Asp P177 and Tyr P127 in the  $\beta 2$ - $\alpha 2$  loop is also seen in the Promazine bound structure of the POM1-PrP complex (PDB ID 4MA7)<sup>17</sup>. This network of interactions was suggested to make the  $\beta 2$ - $\alpha 2$  loop more stable<sup>17</sup>. Judging by the additional interactions, the  $\beta 2$ - $\alpha 2$  loop in POM6-PrP appears more stable than the one in POM1-PrP. It must be noted, however, that in POM1-PrP, Arg P163 participates in a crystal contact. Hence the biological relevance of the absence of this network of interactions in the POM1-PrP crystal structure remains to be determined.

The non-local salt bridge between residues Arg-P155 - Glu-P195 orients the carboxy terminus of the helix  $\alpha 1$  closer to the  $\alpha 2$ - $\alpha 3$  loop<sup>168</sup> (Figure 4.8C). The salt



bridge has also been proposed to play a role in protecting the residue Phe P197, which is part of the hydrophobic core<sup>168</sup> of PrP from solvent exposure<sup>91</sup>. A recent MDS study showed that the pathogenic mutant Glu195Lys (mouse numbering) disrupted the salt bridge Arg155-Glu195 which destabilized the Phe197 hydrophobic pocket and resulted in the detachment of the  $\alpha 1$  helix from the hydrophobic core<sup>91</sup>. In POM6-PrP, the salt bridge Arg P155- Glu P195 remains intact (Figure 4.8C) whereas in POM1-PrP, the residues Glu P195 and Arg P155 are too far to interact with each other (5.1 Å) (Figure 4.8D). It is probable that the missing critical salt bridge in the POM1 Fab bound PrP weakens the inter-domain interactions between the helix  $\alpha 1$  and the  $\alpha 2$ - $\alpha 3$ .

In POM6-PrP, POM6 Fab disrupts the local salt bridge Arg P207 - Glu P210 in PrP. Upon disruption, the residue Arg P207 forms aromatic  $\pi$ - $\pi$  interactions with Phe P140 in the helix  $\alpha 1$  and POM6 Fab potentially facilitates the formation of the His P176 -Tyr H53 and Glu P210 network as described in Section 4.4.1(Figure 4.8E). Therefore, POM6 Fab facilitates the conversion of an intradomain salt bridge serving to stabilize only the  $\alpha 3$  helix into two potential interdomain bonds stabilizing helices  $\alpha 3$  and  $\alpha 1$  as well as helices  $\alpha 3$  and  $\alpha 2$ . In the case of POM1-PrP however, the residues Glu P210 and His P176 are too far apart to interact with each other (Figure 4.8F) and therefore, are unable to create an inter-domain interaction. In POM1-PrP, Arg P207 forms  $\pi$ - $\pi$  interactions with Phe P140 and with a Tyr in POM1 Fab.

Finally, we observe that the non-local salt bridge Glu P145 and Lys P203 is disrupted by the POM6 Fab but remains intact in POM1-PrP (Figure 4.8G, H). Glu P145 forms a hydrogen bond with Gln H99 of POM6 Fab and Lys P203 forms a salt bridge and a hydrogen bond with Asp H51 and Thr H29 of POM6 Fab, respectively. As the Lys P203-Asp H51 salt bridge is buried between the surfaces of POM6 Fab and PrP125-225, it is highly likely to be energetically very strong. In addition, Lys P203 also forms hydrophobic contacts with residues Gly H30, Phe H32 and Tyr H53 of POM6 Fab and Glu P145 forms hydrophobic contacts with Met P204 on helix  $\alpha 3$  of PrP125-225 which is part of the hydrophobic core of the PrP molecule. Hence, despite the disruption of the Glu P145-Lys P203 salt bridge, the stability of the PrP molecule in POM6-PrP is most likely not compromised.

## 4.5 Conclusions

The crystal and molecular structures of the complex of POM6 Fab with mouse PrP125-225 were successfully solved at a resolution of 1.83 Å. POM6 Fab has a unique

epitope on the globular domain of PrP making it one of the first anti-PrP antibodies (with a crystal structure) to be shown to bind to all three helices of PrP. POM6 Fab forms hydrogen bonds and salt bridges with residues 145\151\180\196\198-200\203\206 and 210 in recombinant mouse PrP. Most of the interactions of POM6 Fab are formed with the residues on the helix  $\alpha 3$  of PrP125-225. Although the nature of the interactions between PrP125-225 and POM6 Fab are predominantly electrostatic, the residues on helices  $\alpha 3$  and  $\alpha 1$  also participate in hydrophobic interactions with POM6 Fab. The binding of POM6 Fab to PrP125-225 buries over 800  $\text{\AA}^2$  (12.5%) surface area of the PrP molecule. The PrP125-225 molecule does not show any significant global structural changes upon binding to POM6 Fab. One of the major local structural changes that takes place in the PrP125-225 molecule upon POM6 Fab binding is in the  $\beta 2$ - $\alpha 2$  loop where a network of hydrogen bonds and salt bridges between residues Tyr P127, Arg P163, Tyr P168 and the Asp P177 creates a multitude of stabilizing forces. The POM6 Fab bound PrP is also seemingly stabilized by the presence of the important wild-type salt bridge Arg P155 - Glu P195 that protects the hydrophobic residue Phe P197 from solvent exposure. POM6 Fab binding also facilitates the creation of a potentially new network of interdomain interactions between the residues His P176 and Glu P210 in helices  $\alpha 2$  and  $\alpha 3$ , respectively. The results of the biological functional effects of the POM6 antibody on prion conversion in cerebellar slices remains to be determined. However, it is conceivable that the cumulative effect of the presence of the additional network of salt bridges and hydrogen bonds in POM6 bound PrP and the stability imparted by the burial of a large surface area of PrP by the POM6 Fab molecule could make the POM6 Fab bound prion protein resistant to prion conversion. Upon comparison of the structures of the toxicity inducing POM1-PrP complex with that of the innocuous POM6-PrP complex, we observed more stabilization forces within the POM6 bound PrP. The stabilizing forces within the  $\beta 2$ - $\alpha 2$  loop that contribute to anchoring the  $\beta$  sheet to the helix  $\alpha 2$  had a larger network of hydrogen bonds and salt bridges in POM6-PrP than in POM1-PrP. The pathologically important Tyr P127- Asp P177 hydrogen bond was also missing in POM1-PrP. Similarly, the important wild-type salt bridge Arg P155-Glu P195 was absent in POM1-PrP. As the details of the energetics of the salt bridges and hydrogen bonds mentioned above are not known, the implications of the presence or absence of these interactions must be taken with caution. However, the structural vulnerabilities within the PrP molecule highlighted by the differences in the structures of POM1 and POM6 bound PrPs may point the way for future anti-PrP therapeutics.

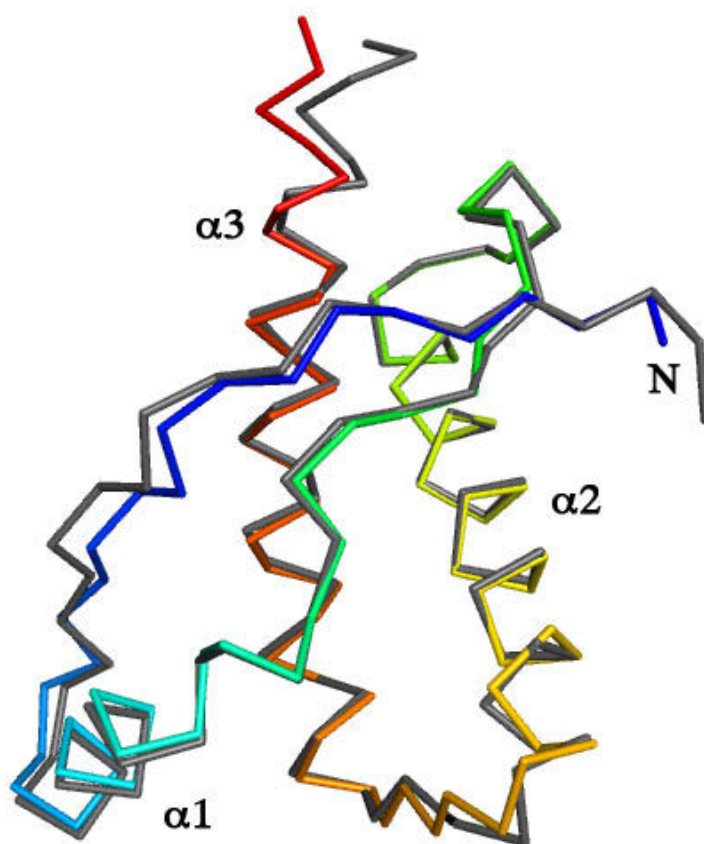


Figure 4.7: A backbone carbon alignment of POM6 and POM1 Fab bound globular domain of the PrP molecules. The figure shows a ribbon representation of the alignment of PrP125-225 molecule (spectral colours) in the crystal structure of POM6-PrP with the PrP120-230 molecule (dark gray) in the crystal structure of POM1-PrP (PDB ID 4H88). Pymol was used for the alignment<sup>175</sup>

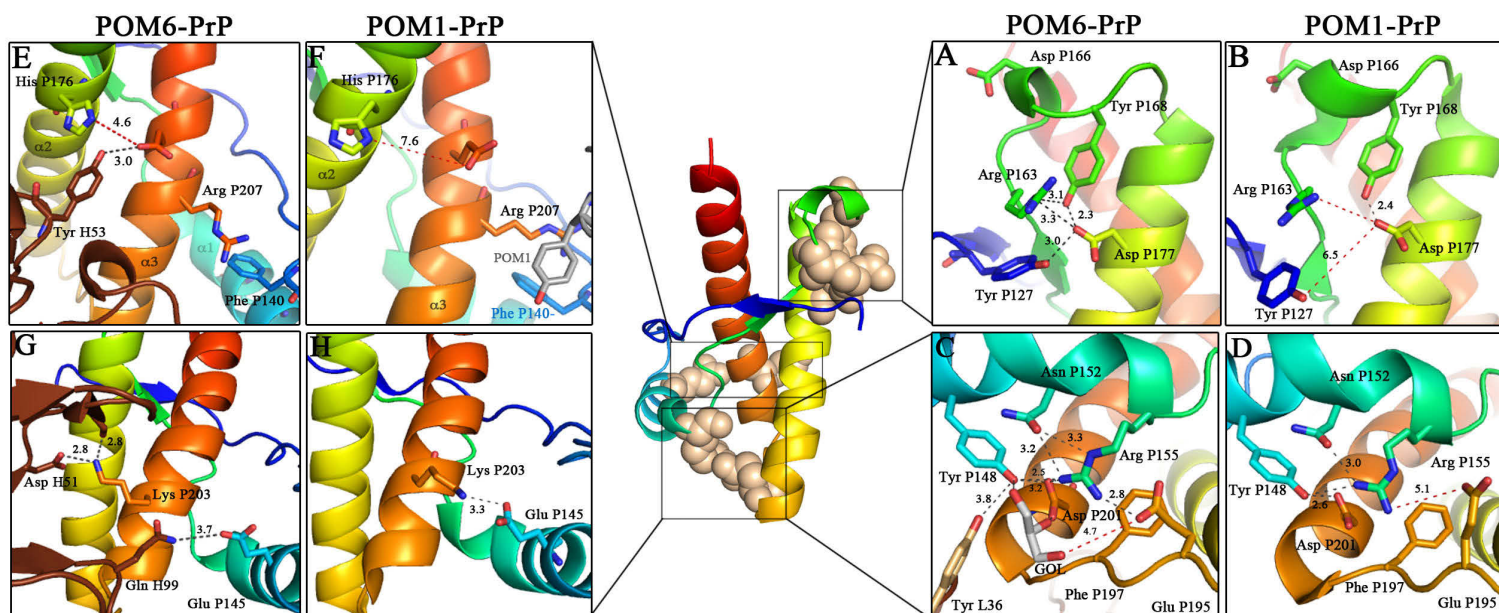


Figure 4.8: The local structural differences between the crystal structures of the complexes of POM6 Fab and mouse PrP125-225 and POM1 Fab and mouse PrP120-231 (PDB ID 4H88). PrP125-225 is shown as a cartoon and the residues of interest are shown as sticks. The distances (in Å) between the residues is depicted using black dashes. The interactions that are improbable to form are shown in red dashes. The color scheme is similar to that in Figure 4.2A. The stabilizing interactions in the  $\beta$ 2- $\alpha$ 2 loop around the salt bridge Arg P163-Asp P177 in (A) POM6-PrP (B) POM1-PrP; the salt bridge between Arg P155 in the helix  $\alpha$ 1 and Glu P195 in the  $\alpha$ 2- $\alpha$ 3 loop in (C) POM6-PrP (D) POM1-PrP; the salt bridge Arg P207-Glu P210 on helix  $\alpha$ 3 in (E) POM6-PrP (F) POM1-PrP; the salt bridge between Glu P145 on helix  $\alpha$ 1 and Lys P203 on helix  $\alpha$ 3 in (G) POM6-PrP and (H) POM1-PrP.

# Chapter 5

## Conclusions

### 5.1 Introduction

Infectious and fatal neurodegenerative disorders such as Mad-Cow disease in cattle, Scrapie in sheep, Chronic Wasting Disease in cervids and Creutzfeldt-Jacob Disease in humans belong to a class of protein misfolding diseases known as the Transmissible Spongiform Encephalopathies (TSEs). In the mid- 1990s , the Bovine Spongiform Encephalopathy epidemic in the UK which also eventually spread to humans exemplified the havoc that a TSE outbreak could have on the financial, political and agricultural machinery of a country. Due to the unusually long incubation periods of TSEs in humans, the overall impact of the epidemic in the UK is still unknown. Governments of the affected countries such as Japan, Canada and the USA have initiated stringent surveillance programs to check for TSEs in cattle and in humans<sup>4,105,139,164</sup>. TSEs are also transmissible in humans through grafts transplants and blood transfusions which have resulted the implementation of new stringent donor criteria amongst humans. As there is also a dramatic rise in the CWD cases in the US and in Canada<sup>200</sup>, the fear of spread to humans through consumption of contaminated venison is very real. There is as yet, no cure for TSEs. Once the clinical symptoms of TSEs manifest, the progression to death in the affected individual is relatively rapid. There is a need to design better diagnostic and therapeutic solutions for the TSEs.

Decades of research has proved that the central event in the TSEs is the self-catalytic misfolding and aggregation of the native, cellular prion protein ( $\text{PrP}^C$ ) into an infectious, neurotoxic isoform, termed  $\text{PrP}^{Sc}$  (Table 1.3). The mature, full length  $\text{PrP}^C$  is a GPI anchored glycoprotein. The amino terminal portion of  $\text{PrP}^C$  from residues 23-124 is intrinsically disordered and its carboxyl terminal portion from residues 125-231 is globular and folded consisting of three  $\alpha$ -helices and two short

$\beta$ -strands (Figure 1.5)<sup>102,167</sup>. Over the last decade, several research groups have endeavoured to develop passive immunity towards TSEs by developing monoclonal antibodies to target the prevention of the structural conversion of the PrP<sup>C</sup> into PrP<sup>Sc</sup> (Figure 1.7A). Polymenidou et al., developed a unique panel of monoclonal antibodies named POM1 through POM19 that have epitopes ranging throughout the mature prion protein<sup>154</sup>. Of these antibodies, the POM2 antibody recognizes an epitope in the octapeptide repeat (OR) domain and POM1 and POM6 antibodies recognize neighbouring but non-overlapping epitopes in the globular folded domain<sup>154</sup>. In the COCS assay, the POM1 antibody was found to induce severe toxicity akin to that seen in prion infections<sup>180</sup> whereas the POM2 antibody was found to prevent the POM1 induced toxicity. Interestingly, the POM6 antibody was completely innocuous in the COCS assay. The effect of the POM6 antibody on prion replication is not known as yet. The structural characterization of the binding of POM1 to the prion protein has been extensively studied using X-ray crystallography<sup>17,19</sup>. However, the structural characterization of the binding of the POM2 and the POM6 antibodies to the prion protein has never been attempted. The determination of POM2 binding to PrP specifically the OR repeats might provide clues to the mechanism of action of preventing POM1- induced toxicity. The structure of POM6 Fab with PrP and its comparison with the POM1 Fab antibody might provide insights into structural differences induced within the prion protein that could make the POM1 bound PrP molecule toxic and prone to aggregation.

Due to the potential shown by the POM2 antibody as a therapeutic antibody that can successfully prevent POM1- induced toxicity, our primary research goal was to determine the mode of binding of the POM2 antibody fragment to its epitope in the prion protein using X-ray crystallography. Due to its smaller size and more efficient blood brain barrier permeability, the single chain variable fragment (scFv) of the POM2 antibody was chosen initially as our preferred antibody fragment of choice. The construct for POM2 scFv was previously generated by the phage display method by Polymenidou et al<sup>154</sup>. Our first objective was to produce large quantities of purified POM2 scFv for the purposes of crystallization. Although we eventually purified POM2 scFv by bacterial periplasmic expression, we were unable to concentrate POM2 scFv to the levels that were amenable for protein crystallization due to excessive protein aggregation. In order to improve the solubility of POM2 scFv, we designed a construct with a modified linker. However, we were still unable to produce crystals with the resulting linker modified POM2 scFv. In order to reduce the segmental flexibility within the scFv molecule and to improve its crystallizability,

we introduced one cysteine mutation each in the heavy and light variable chains of POM2 scFv to enable the formation of a disulfide linked Fv (dsFv). However, due to the low expression levels of the light variable chain, it was not possible to generate the dsFv molecules. Finally, to circumvent the low expression of the light chain, we tried to express a dsFv molecule with both its heavy and light variable domains joined by a linker. However, this construct resulted in copious protein aggregation. Therefore, despite numerous attempts at improving the solubility of POM2 scFv to make it amenable to crystallization, we were unable to produce large quantities of high concentrations of POM2 scFv. In order to achieve our overall goal of understanding the binding between POM2 and PrP, we next selected the more stable and less flexible antibody fragment - Fab to be used for crystallization purposes.

Our second research goal was to characterize the binding of the POM2 Fab with the octapeptide repeat domain of the mouse prion protein using X-ray crystallography. We were successful in co-crystallizing the complex of the POM2 Fab with the peptide containing the tandem repeats (OR2) of the octapeptide repeat of the prion protein in the orthorhombic space group  $P2_122_1$ <sup>187</sup>. We collected the data from a single crystal which diffracted to a resolution of 2.3 Å and refined the final model to a crystallographic  $R_{work}$  factor of 24.7% and  $R_{free}$  of 25.8%. The crystal structure shows that the POM2 Fab has a continuous epitope in the OR domain comprising of residues PHGGSW and that a single OR adopts an extended conformation when in complex with POM2 Fab. The OR2 peptide binds to the POM2 Fab by embedding the Pro P1 residue in a hydrophobic binding pocket while the residues HGGS are firmly anchored to the heavy chain CDR loop of POM2 Fab by main chain-main chain hydrogen bonds. The tryptophan residue of OR2 also contributes to the binding through hydrophobic contacts. The POM2 Fab-OR2 is the first reported crystal structure of an amino terminal domain binding anti-PrP antibody in complex with its epitope. There are several differences observed in the structure of the ORs in the POM2 Fab-OR2 complex and in the NMR structure of the OR domain in complex with the small therapeutic molecule, Pentosan Polysulphate (PPS)<sup>188</sup>. While the ORs retained their reported  $\beta$ -turn conformation when in complex with PPS, critical hydrophobic and backbone interactions between OR2 and POM2 Fab disrupted the  $\beta$ -turn conformation of the OR. In addition to the POM2 Fab and PPS, there are several other OR binding anti-PrP antibodies<sup>98,147,174</sup> and small molecule ligands<sup>48,95,189,199</sup> that have shown promising therapeutic activity in peripherally infected mice. The crystal structure of the POM2-OR2 would be very beneficial to enable the design of smaller, tighter binding anti-PrP antibodies or small molecule ligands.

Our third research goal was to characterize the binding of POM6 Fab with mouse PrP125-225 using X-ray crystallography. We successfully co-crystallized the complex of POM6 Fab with the mouse PrP125-225 in the spacegroup  $P2_12_1$ . A complete dataset was collected from a single crystal of POM6-PrP to a resolution of 1.83 Å and the final model was refined to a crystallographic  $R_{work}$  factor of 18.8% and  $R_{Free}$  of 22.8%. The crystal structure revealed that the POM6 Fab has a unique, discontinuous, conformation based epitope on the globular domain of PrP. POM6 Fab buries 803 Å<sup>2</sup> (12.5%) of solvent accessible area on the surface of the PrP molecule and has epitopes on all three helices of the PrP molecule. In the crystal structure of POM6-PrP, most of the interactions of POM6 Fab are formed with the residues on the helix  $\alpha3$  of PrP125-225. The majority of the interactions between PrP125-225 and POM6 Fab are electrostatic with the residues on helices  $\alpha3$  and  $\alpha1$  also participating in hydrophobic interactions with POM6 Fab. Although POM6 Fab binding does not induce any significant global structural changes within the PrP125-225, it either creates or facilitates the creation of a local network of hydrogen bonding and electrostatic interactions that have the potential for stabilizing the PrP molecule. One such major network of interactions is formed in the important  $\beta2$ - $\alpha2$  loop amongst the residues Arg P163, Tyr P168 and the Asp P177 and the residue Tyr P128 of the amino terminal strand. This network of interactions serves to anchor the  $\beta$  strand to the helix  $\alpha2$ . POM6 Fab also facilitates the creation of a second network of newly discovered inter-domain interactions between the residues His P177 and Glu P210 in helices  $\alpha2$  and  $\alpha3$ , respectively. The critical wild type salt bridge Arg P155 - Glu P195 is maintained in the POM6 Fab PrP molecule; it helps maintain the stability of the hydrophobic core. Due to the new networks of interactions formed and the integrity of critical salt bridges seen in wild type PrP maintained in POM6-PrP complex, it is conceivable that the POM6 Fab binding to PrP helps in stabilizing the PrP molecule against protein aggregation. The results of the functional assays that test the effect of POM6 Fab on prion replication are eagerly awaited from our collaborators in Zurich. The comparison of the POM1<sup>19</sup> and POM6 Fab complexes with the PrP molecule show that the lack of inter-domain salt bridges and hydrogen bonds in POM1 bound Fab between  $\beta1$  to the  $\beta2$ - $\alpha2$  loop (Tyr P128-Arg P163- Tyr P168-Asp P177) and between the helix  $\alpha1$  and the  $\alpha2$ - $\alpha3$  loop and (Arg P155 - Glu P195) have the potential to compromise the overall stability of the PrP molecule. However, as the energetics of the missing network of bonds have not been calculated yet, their impact on the overall stability of the PrP molecule must be taken with caution.

Our two major goals of structurally characterizing the binding of POM2 and



POM6 Fab molecules to the prion protein using protein X-ray crystallography have been successfully achieved. The POM2 Fab molecule binds to the octapeptide repeats of PrP and disrupts their native  $\beta$ -turn conformation using backbone and hydrophobic interactions. Deducing the mode of prevention of POM1 induced toxicity by POM2 using only the crystal structure of POM2-OR2 is not feasible. However, as numerous studies have shown the potential of many OR ligands as promising therapeutic molecules<sup>98,147,174</sup>, the details of OR2 binding obtained from the structure of POM2 Fab with OR2 could contribute to designing better ligands for the octapeptide repeats. The crystal structure of the POM6 Fab with the PrP molecule revealed that the stability against protein aggregation may be imparted to the prion molecule through the creation of new networks of interdomain interactions as well as the maintenance of the critical inter-domain salt bridges within the prion molecule. A comparison of the structures of the two complexes of POM6 and POM1 Fab to the PrP molecule revealed the absence of critical hydrogen bonds and salt bridges that might compromise the stability of the POM1-PrP molecule. However, a definitive conclusions can only be made upon the calculation of the energetics of these bonds and their contributions to the overall stability of the prion molecule.

Therefore, by utilizing the POM2 Fab antibody, we have made contributions towards designing better octapeptide repeat ligands and from the crystal structure of POM6, we have made inroads into identifying potential networks of interactions that might protect the prion molecule from aggregation. Future work may include the making of humanized POM2 scFv with modified CDR regions to enable tighter binding to the OR domain and the designing of blood brain barrier permeable, small molecule OR ligands. The POM2-OR2 complex may also be used as a tool to study the binding of potential OR ligands using X-ray crystallography. MDS may be used to determine the energetics of the critical salt bridges and hydrogen bonds within the PrP molecule that were recognized using the crystal structure of POM6-PrP. Crystallization of POM6 Fab with the disease mutants (human numbering)- D178N, E196K PrP may also be attempted to determine the affect of the missing hydrogen bonds and salt bridges on the structure of PrP. Crystallization of POM6 Fab with a glycosylated molecule of PrP may also be attempted to determine the affect of the glycans on the Fab-PrP complex.

# Bibliography

- [1] K. Abhinandan and A. C. Martin. Analysis and improvements to kabat and structurally correct numbering of antibody variable domains. *Molecular Immunology*, 45(14):3832 – 3839, 2008.
- [2] P. D. Adams, P. V. Afonine, G. Bunkoczi, V. B. Chen, I. W. Davis, N. Echols, J. J. Headd, L.-W. Hung, G. J. Kapral, R. W. Grosse-Kunstleve, A. J. McCoy, N. W. Moriarty, R. Oeffner, R. J. Read, D. C. Richardson, J. S. Richardson, T. C. Terwilliger, and P. H. Zwart. Phenix: a comprehensive python-based system for macromolecular structure solution. *Acta Crystallographica Section D*, 66(Pt 2):213–221, 2010.
- [3] P. V. Afonine, R. W. Grosse-Kunstleve, N. Echols, J. J. Headd, N. W. Moriarty, M. Mustyakimov, T. C. Terwilliger, A. Urzhumtsev, P. H. Zwart, and P. D. Adams. Towards automated crystallographic structure refinement with *phenix.refine*. *Acta Crystallographica Section D*, 68(4):352–367, 2012.
- [4] C. F. I. Agency. BSE enhanced surveillance program. <http://www.inspection.gc.ca/animals/terrestrial-animals/diseases/reportable/bse/enhanced-surveillance/eng/1323992647051/1323992718670>.
- [5] C. F. I. Agency. Chronic wasting disease (CWD) of deer and elk. <http://www.inspection.gc.ca/eng/1297964599443/1297965645317>.
- [6] A. Aguzzi, F. Baumann, and J. Bremer. The prion’s elusive reason for being. *Annual Review of Neuroscience*, 31(1):439–477, 2008.
- [7] A. Aguzzi and A. M. Calella. Prions: Protein aggregation and infectious diseases. *Physiological Reviews*, 89(4):1105–1152, 2009.
- [8] A. Aguzzi and A. M. Calella. Prions: protein aggregation and infectious diseases. *Physiological Reviews*, 89(4):1105–1152, 2009.

- [9] A. Aguzzi, M. Nuvolone, and C. Zhu. The immunobiology of prion diseases. *Nature Reviews Immunology*, 13(12):888–902, 12 2013.
- [10] A. Aguzzi and C. J. Sigurdson. Antiprion immunotherapy: to suppress or to stimulate? *Nature Reviews Immunology*, 4(9):725–736, 09 2004.
- [11] A. Aguzzi and C. Weissmann. Prion research: the next frontiers. *Nature*, 389(6653):795–798, 1997.
- [12] Z. A. Ahmad, S. K. Yeap, A. M. Ali, W. Y. Ho, N. B. M. Alitheen, and M. Hamid. scfv antibody: principles and clinical application. *Clinical and Developmental Immunology*, 2012:980250, 2012.
- [13] B. Al-Lazikani, A. M. Lesk, and C. Chothia. Standard conformations for the canonical structures of immunoglobulins. *Journal of Molecular Biology*, 273(4):927–948, 1997.
- [14] S. M. Andrew and J. A. Titus. Fragmentation of immunoglobulin G. *Current Protocols in Immunology*, 2001.
- [15] E. Aronoff-Spencer, C. S. Burns, N. I. Avdievich, G. J. Gerfen, J. Peisach, W. E. Antholine, H. L. Ball, F. E. Cohen, S. B. Prusiner, and G. L. Millhauser. Identification of the Cu<sup>2+</sup> binding sites in the N-terminal domain of the prion protein by EPR and CD spectroscopy. *Biochemistry*, 39(45):13760–13771, 2000.
- [16] N. A. Baker, D. Sept, S. Joseph, M. J. Holst, and J. A. McCammon. Electrostatics of nanosystems: Application to microtubules and the ribosome. *Proceedings of the National Academy of Sciences of the United States of America*, 98(18):10037–10041, 2001.
- [17] P. K. Baral, M. Swayampakula, M. K. Rout, N. N. V. Kav, L. Spyropoulos, A. Aguzzi, and M. N. G. James. Structural basis of prion inhibition by phenothiazine compounds. *Structure*, 22(2):291–303, 2014.
- [18] P. K. Baral, B. Wieland, M. Swayampakula, M. Polymenidou, A. Aguzzi, N. N. V. Kav, and M. N. G. James. Crystallization and preliminary X-ray diffraction analysis of prion protein bound to the Fab fragment of the POM1 antibody. *Acta Crystallographica Section F*, 67(10):1211–1213, 2011.
- [19] P. K. Baral, B. Wieland, M. Swayampakula, M. Polymenidou, M. H. Rahman, N. N. V. Kav, A. Aguzzi, and M. N. G. James. Structural studies on the folded

- domain of the human prion protein bound to the fab fragment of the antibody pom1. *Acta Crystallographica Section D*, 68(Pt 11):1501–1512, 2012.
- [20] A. Barducci, R. Chelli, P. Procacci, and V. Schettino. Misfolding pathways of the prion protein probed by molecular dynamics simulations. *Biophysical Journal*, 88(2):1334–1343, 2005.
- [21] D. Barlow and J. Thornton. Ion-pairs in proteins. *Journal of Molecular Biology*, 168(4):867 – 885, 1983.
- [22] J. C. Bartz, A. E. Kincaid, and R. A. Bessen. Retrograde transport of transmissible mink encephalopathy within descending motor tracts. *Journal of Virology*, 76(11):5759–5768, 2002.
- [23] K. Basler, B. Oesch, M. Scott, D. Westaway, M. Walchli, D. F. Groth, M. P. McKinley, S. B. Prusiner, and C. Weissmann. Scrapie and cellular PrP isoforms are encoded by the same chromosomal gene. *Cell*, 46(3):417–428, 1986.
- [24] C. Bate, M. Salmona, L. Diomedea, and A. Williams. Squalastatin cures prion-infected neurons and protects against prion neurotoxicity. *J Biological Chemistry*, 279(15):14983–14990, 2004.
- [25] E. D. Belay, R. A. Maddox, E. S. Williams, M. W. Miller, P. Gambetti, and L. B. Schonberger. Chronic wasting disease and potential transmission to humans. *Emerging Infectious Diseases*, 10(6):977–984, 2004.
- [26] R. Bhattacharyya, R. P. Saha, U. Samanta, and P. Chakrabarti. Geometry of interaction of the histidine ring with other planar and basic residues. *Journal of Proteome Research*, 2(3):255–263, 2003.
- [27] R. E. Bird, K. D. Hardman, J. W. Jacobson, S. Johnson, B. M. Kaufman, S.-M. Lee, T. Lee, S. H. Pope, G. S. Riordan, and M. Whitlow. Single-chain antigen-binding proteins. *Science*, 242(4877):423–426, 10 1988.
- [28] D. C. Bolton, M. P. McKinley, and S. B. Prusiner. Identification of a protein that purifies with the scrapie prion. *Science*, 218(4579):1309–1311, 1982.
- [29] J. Bremer, F. Baumann, C. Tiberi, C. Wessig, H. Fischer, P. Schwarz, A. D. Steele, K. V. Toyka, K.-A. Nave, J. Weis, and A. Aguzzi. Axonal prion protein is required for peripheral myelin maintenance. *Nature Neuroscience*, 13(3):310–318, 03 2010.

- [30] D. R. Brown, K. Qin, J. W. Herms, A. Madlung, J. Manson, R. Strome, P. E. Fraser, T. Kruck, A. von Bohlen, W. Schulz-Schaeffer, A. Giese, D. Westaway, and H. Kretzschmar. The cellular prion protein binds copper in vivo. *Nature*, 390(6661):684–687, 12 1997.
- [31] H. Budka. Histopathology and immunohistochemistry of human transmissible spongiform encephalopathies (tses). *Archives of Virology. Supplementa*, (16):135–142, 2000.
- [32] H. Budka, A. Aguzzi, P. Brown, J. M. Brucher, O. Bugiani, F. Gullotta, M. Haltia, J. J. Hauw, J. W. Ironside, and K. Jellinger. Neuropathological diagnostic criteria for creutzfeldt-jakob disease (cjd) and other human spongiform encephalopathies (prion diseases). *Brain Pathology*, 5(4):459–466, 1995.
- [33] H. Bueler, A. Aguzzi, A. Sailer, R. A. Greiner, P. Autenried, M. Aguet, and C. Weissmann. Mice devoid of PrP are resistant to scrapie. *Cell*, 73(7):1339–1347, 1993.
- [34] H. Bueler, M. Fischer, Y. Lang, H. Bluethmann, H.-P. Lipp, S. J. DeArmond, S. B. Prusiner, M. Aguet, and C. Weissmann. Normal development and behaviour of mice lacking the neuronal cell-surface PrP protein. *Nature*, 356(6370):577–582, 04 1992.
- [35] C. S. Burns, E. Aronoff-Spencer, C. M. Dunham, P. Lario, N. I. Avdievich, W. E. Antholine, M. M. Olmstead, A. Vrieling, G. J. Gerfen, J. Peisach, W. G. Scott, and G. L. Millhauser. Molecular features of the copper binding sites in the octarepeat domain of the prion protein. *Biochemistry*, 41(12):3991–4001, 2002.
- [36] D. C. Gajdusek, C. J. Gibbs, and M. Alpers. Experimental transmission of a kuru-like syndrome to chimpanzees. *Nature*, 209(5025):794–796, 02 1966.
- [37] T. A. Campbell, M. S. Palmer, R. G. Will, W. R. Gibb, P. J. Luthert, and J. Collinge. A prion disease with a novel 96-base pair insertional mutation in the prion protein gene. *Neurology*, 46(3):761–766, 1996.
- [38] B. Caughey. Formation of protease-resistant prion protein in cell-free systems. *Current Issues in Molecular Biology*, 2(3):95–101, 2000.
- [39] B. Caughey and G. S. Baron. Prions and their partners in crime. *Nature*, 443(7113):803–810, 10 2006.

- [40] B. Caughey, D. A. Kocisko, G. J. Raymond, and P. T. J. Lansbury. Aggregates of scrapie-associated prion protein induce the cell-free conversion of protease-sensitive prion protein to the protease-resistant state. *Chemistry and Biology*, 2(12):807–817, 1995.
- [41] M. Charveriat, M. Reboul, Q. Wang, C. Picoli, N. Lenuzza, A. Montagnac, N. Nhiri, E. Jacquet, F. Gueritte, J.-Y. Lallemand, J.-P. Deslys, and F. Mouthon. New inhibitors of prion replication that target the amyloid precursor. *Journal of General Virology*, 90(Pt 5):1294–1301, 2009.
- [42] M. Chattopadhyay, E. D. Walter, D. J. Newell, P. J. Jackson, E. Aronoff-Spencer, J. Peisach, G. J. Gerfen, B. Bennett, W. E. Antholine, and G. L. Millhauser. The octarepeat domain of the prion protein binds Cu(II) with three distinct coordination modes at pH 7.4. *Journal of the American Chemical Society*, 127(36):12647–12656, 2005.
- [43] V. B. Chen, W. B. Arendall, III, J. J. Headd, D. A. Keedy, R. M. Immormino, G. J. Kapral, L. W. Murray, J. S. Richardson, and D. C. Richardson. *MolProbity*: all-atom structure validation for macromolecular crystallography. *Acta Crystallographica Section D*, 66(1):12–21, 2010.
- [44] B. Chesebro. Introduction to the transmissible spongiform encephalopathies or prion diseases. *British Medical Bulletin*, 66:1–20, 2003.
- [45] B. Chesebro, R. Race, K. Wehrly, J. Nishio, M. Bloom, D. Lechner, S. Bergstrom, K. Robbins, L. Mayer, J. M. Keith, C. Garon, and A. Haase. Identification of scrapie prion protein-specific mRNA in scrapie-infected and uninfected brain. *Nature*, 315(6017):331–333, 05 1985.
- [46] J. H. Come, P. E. Fraser, and P. T. J. Lansbury. A kinetic model for amyloid formation in the prion diseases: importance of seeding. *Proceedings of the National Academy of Sciences of the United States of America*, 90(13):5959–5963, 1993.
- [47] D. R. Davies, E. A. Padlan, and D. M. Segal. Three-dimensional structure of immunoglobulins. *Annual Review of Biochemistry*, 44(1):639–667, 1975.
- [48] S. Dealler and N. G. Rainov. Pentosan polysulfate as a prophylactic and therapeutic agent against prion disease. *IDrugs*, 6(5):470–478, 2003.

- [49] T. J. Dolinsky, P. Czodrowski, H. Li, J. E. Nielsen, J. H. Jensen, G. Klebe, and N. A. Baker. Pdb2pqr: expanding and upgrading automated preparation of biomolecular structures for molecular simulations. *Nucleic Acids Research*, 35(suppl 2):W522–W525, 2007.
- [50] R. S. Doody, R. G. Thomas, M. Farlow, T. Iwatsubo, B. Vellas, S. Joffe, K. Kieburtz, R. Raman, X. Sun, P. S. Aisen, E. Siemers, H. Liu-Seifert, and R. Mohs. Phase 3 trials of solanezumab for mild-to-moderate alzheimer’s disease. *New England Journal of Medicine*, 370(4):311–321, 2014.
- [51] H. J. Dyson, P. E. Wright, and H. A. Scheraga. The role of hydrophobic interactions in initiation and propagation of protein folding. *Proceedings of the National Academy of Sciences of the United States of America*, 103(35):13057–13061, 2006.
- [52] P. Emsley, B. Lohkamp, W. G. Scott, and K. Cowtan. Features and development of *Coot*. *Acta Crystallographica Section D*, 66(4):486–501, 2010.
- [53] J. Falsig and A. Aguzzi. The prion organotypic slice culture assay[mdash]posca. *Nature Protocols*, 3(4):555–562, 04 2008.
- [54] J. Falsig, T. Sonati, U. S. Herrmann, D. Saban, B. Li, K. Arroyo, B. Ballmer, P. P. Liberski, and A. Aguzzi. Prion pathogenesis is faithfully reproduced in cerebellar organotypic slice cultures. *PLoS Pathogens*, 8(11):e1002985, 11 2012.
- [55] H. J. Federoff. Development of vaccination approaches for the treatment of neurological diseases. *Journal of Comparative Neurology*, 515(1):4–14, 2009.
- [56] F. A. Fellouse, P. A. Barthelemy, R. F. Kelley, and S. S. Sidhu. Tyrosine plays a dominant functional role in the paratope of a synthetic antibody derived from a four amino acid code. *Journal of Molecular Biology*, 357(1):100 – 114, 2006.
- [57] M. Fischer, T. Rulicke, A. Raeber, A. Sailer, M. Moser, B. Oesch, S. Brandner, A. Aguzzi, and C. Weissmann. Prion protein (PrP) with amino-proximal deletions restoring susceptibility of PrP knockout mice to scrapie. *EMBO Journal*, 15(6):1255–1264, 1996.
- [58] E. Flechsig, D. Shmerling, I. Hegyi, A. J. Raeber, M. Fischer, A. Cozzio, C. von Mering, A. Aguzzi, and C. Weissmann. Prion protein devoid of the octapeptide repeat region restores susceptibility to scrapie in PrP knockout mice. *Neuron*, 27(2):399–408, 2000.

- [59] E. C. Food and feed safety. TSE/BSE - Introduction. [http://ec.europa.eu/food/food/biosafety/tse\\_bse/index\\_en.htm](http://ec.europa.eu/food/food/biosafety/tse_bse/index_en.htm).
- [60] C. for Disease Control. BSE (Bovine Spongiform Encephalopathy, or Mad Cow Disease). <http://www.cdc.gov/ncidod/dvrd/bse/>.
- [61] G. Forloni, N. Angeretti, R. Chiesa, E. Monzani, M. Salmona, O. Bugiani, and F. Tagliavini. Neurotoxicity of a prion protein fragment. *Nature*, 362(6420):543–546, 1993.
- [62] K. N. Frankenfield, E. T. Powers, and J. W. Kelly. Influence of the N-terminal domain on the aggregation properties of the prion protein. *Protein Science*, 14(8):2154–2166, 2005.
- [63] C. Freund, A. Ross, B. Guth, A. Plückthun, and T. A. Holak. Characterization of the linker peptide of the single-chain fv fragment of an antibody by nmr spectroscopy. *FEBS Letters*, 320(2):97 – 100, 1993.
- [64] C. Freund, A. Ross, A. Pluckthun, and T. A. Holak. Structural and dynamic properties of the fv fragment and the single-chain fv fragment of an antibody in solution investigated by heteronuclear three-dimensional nmr spectroscopy. *Biochemistry*, 33(11):3296–3303, 1994.
- [65] R. Gabizon, M. P. McKinley, D. Groth, and S. B. Prusiner. Immunoaffinity purification and neutralization of scrapie prion infectivity. *Proceedings of the National Academy of Sciences of the United States of America*, 85(18):6617–6621, 1988.
- [66] D. C. Gajdusek. Transmissible and non-transmissible amyloidoses: autocatalytic post-translational conversion of host precursor proteins to beta-pleated sheet configurations. *Journal of Neuroimmunology*, 20(2-3):95–110, 1988.
- [67] M. Gasset, M. A. Baldwin, D. H. Lloyd, J. M. Gabriel, D. M. Holtzman, F. Cohen, R. Fletterick, and S. B. Prusiner. Predicted alpha-helical regions of the prion protein when synthesized as peptides form amyloid. *Proceedings of the National Academy of Sciences of the United States of America*, 89(22):10940–10944, 1992.
- [68] M. Glatzel, F. L. Heppner, K. M. Albers, and A. Aguzzi. Sympathetic innervation of lymphoreticular organs is rate limiting for prion neuroinvasion. *Neuron*, 31(1):25–34, 2001.



- [69] A. P. Golovanov, G. M. Hautbergue, S. A. Wilson, and L.-Y. Lian. A simple method for improving protein solubility and long-term stability. *Journal of the American Chemical Society*, 126(29):8933–8939, 2004.
- [70] A. Gonzalez and Y. Tsai. autoxds, 2010. [http://smb.slac.stanford.edu/facilities/software/xds/#autoxds\\_script](http://smb.slac.stanford.edu/facilities/software/xds/#autoxds_script).
- [71] H. Gram, L. A. Marconi, C. F. Barbas, T. A. Collet, R. A. Lerner, and A. S. Kang. In vitro selection and affinity maturation of antibodies from a naive combinatorial immunoglobulin library. *Proceedings of the National Academy of Sciences of the United States of America*, 89(8):3576–3580, 1992.
- [72] J. K. Griffin and N. R. Cashman. Progress in prion vaccines and immunotherapies. *Expert Opinion on Biological Therapy*, 5(1):97–110, 2005.
- [73] J. S. GRIFFITH. Nature of the scrapie agent: Self-replication and scrapie. *Nature*, 215(5105):1043–1044, 09 1967.
- [74] J. Gsponer, P. Ferrara, and A. Caffisch. Flexibility of the murine prion protein and its asp178asn mutant investigated by molecular dynamics simulations. *Journal of Molecular Graphics and Modelling*, 20(2):169–182, 2001.
- [75] W. C. Guest, N. R. Cashman, and S. S. Plotkin. Electrostatics in the stability and misfolding of the prion protein: salt bridges, self energy, and solvation. *Biochemistry and Cell Biology*, 88(2):371–381, 2010.
- [76] W. C. Guest, N. R. Cashman, and S. S. Plotkin. Electrostatics in the stability and misfolding of the prion protein: salt bridges, self energy, and solvation. *Biochemistry and Cell Biology*, 88(2):371–381, 2010.
- [77] W. J. Hadlow. Reflections on the transmissible spongiform encephalopathies. *Veterinary Pathology*, 36(6):523–529, 1999.
- [78] W. J. Hadlow. Kuru likened to scrapie: the story remembered. *Philosophical transactions of the royal society B*, 363:3644, 2008.
- [79] T. Haraguchi, S. Fisher, S. Olofsson, T. Endo, D. Groth, A. Tarentino, D. R. Borchelt, D. Teplow, L. Hood, A. Burlingame, E. Lycke, A. Kobata, and S. B. Prusiner. Asparagine-linked glycosylation of the scrapie and cellular prion proteins. *Archives of Biochemistry and Biophysics*, 274(1):1–13, 1989.

- [80] F. L. Heppner, C. Musahl, I. Arrighi, M. A. Klein, T. Rüllicke, B. Oesch, R. M. Zinkernagel, U. Kalinke, and A. Aguzzi. Prevention of scrapie pathogenesis by transgenic expression of anti-prion protein antibodies. *Science*, 294(5540):178–182, 2001.
- [81] F. L. Heppner, M. Prinz, and A. Aguzzi. Pathogenesis of prion diseases: possible implications of microglial cells. *Progress in Brain Research*, 132:737–750, 2001.
- [82] A. Honegger, S. Spinelli, C. Cambillau, and A. Plückthun. A mutation designed to alter crystal packing permits structural analysis of a tight-binding fluorescein–scfv complex. *Protein Science*, 14(10):2537–2549, 2005.
- [83] S. Hornemann, C. Schorn, and K. Wuthrich. Nmr structure of the bovine prion protein isolated from healthy calf brains. *EMBO Reports*, 5(12):1159–1164, 2004.
- [84] R. M. Horton, H. D. Hunt, S. N. Ho, J. K. Pullen, and L. R. Pease. Engineering hybrid genes without the use of restriction enzymes: gene splicing by overlap extension. *Gene*, 77(1):61 – 68, 1989.
- [85] S. Hubbard and J. Thornton. ‘naccess’. Department of Biochemistry and Molecular Biology, University College London. *Computer Program*, 1993.
- [86] R. Huber, J. Deisenhofer, P. M. Colman, M. Matsushima, and W. Palm. Crystallographic structure studies of an igg molecule and an fc fragment. *Nature*, 264(5585):415–420, 12 1976.
- [87] C. A. Hunter and J. K. M. Sanders. The nature of .pi.-.pi. interactions. *Journal of the American Chemical Society*, 112(14):5525–5534, 1990.
- [88] J. S. Huston, D. Levinson, M. Mudgett-Hunter, M. S. Tai, J. Novotn, M. N. Margolies, R. J. Ridge, R. E. Brucoleri, E. Haber, and R. Crea. Protein engineering of antibody binding sites: recovery of specific activity in an anti-digoxin single-chain fv analogue produced in escherichia coli. *Proceedings of the National Academy of Sciences of the United States of America*, 85(16):5879–5883, 1988.
- [89] C. J and C. P. L. Pathologie animale: la maladie dite tremblante du mouton est-elle inoculable? *C R Acad Sci*, 203(1552–1554.), 1936.

- [90] C. J and C. PL. Experimental transmission of trembling to the goat. *Comptes Rendus des Séances Acad Sci*, 208(1058-160), 1939.
- [91] C. Jung Cheng and V. Daggett. Different misfolding mechanisms converge on common conformational changes: Human prion protein pathogenic mutants y218n and e196k. *Prion*, 8(1), 2014.
- [92] E. Kabat, T. Wu, H. Perry, K. Gottesman, and C. Foeller. *Sequences of proteins of immunological interest (1991)*. U.S. Dept. of Health and Human Services, Public Health Service, NIH, Bethesda, MD, 5 edition, 1991.
- [93] W. Kabsch. Xds. *Acta Crystallographica Section D*, 66(Pt 2):125–132, 2010.
- [94] H. Kadokura and J. Beckwith. Mechanisms of oxidative protein folding in the bacterial cell envelope. *Antioxid Redox Signal*, 13(8):1231–1246, 2010.
- [95] Y. O. Kamatari, Y. Hayano, K.-i. Yamaguchi, J. Hosokawa-Muto, and K. Kuwata. Characterizing anti-prion compounds based on their binding properties to prion proteins: Implications as medical chaperones. *Protein Science*, pages 22–34, 2012.
- [96] P. A. Karplus and K. Diederichs. Linking crystallographic model and data quality. *Science*, 336(6084):1030–1033, 2012.
- [97] A. E. Karu, C. W. Bell, and T. E. Chin. Recombinant antibody technology. *Institute for Laboratory Animal Research Journal*, 37(3):132–141, 1995.
- [98] C.-L. Kim, A. Karino, N. Ishiguro, M. Shinagawa, M. Sato, and M. Horiuchi. Cell-surface retention of PrP<sup>C</sup> by anti-PrP antibody prevents protease-resistant prp formation. *Journal of General Virology*, 85(11):3473–3482, 2004.
- [99] R. H. Kimberlin and C. A. Walker. Pathogenesis of scrapie in mice after intragastric infection. *Virus Research*, 12(3):213–220, 1989.
- [100] S. M. Kipriyanov. High-level periplasmic expression and purification of scfvs. *Methods in Molecular Biology*, 562:205–214, 2009.
- [101] S. M. Kipriyanov and M. Little. Generation of recombinant antibodies. *Molecular Biotechnology*, 12(2):173–201, 1999.

- [102] K. J. Knaus, M. Morillas, W. Swietnicki, M. Malone, W. K. Surewicz, and V. C. Yee. Crystal structure of the human prion protein reveals a mechanism for oligomerization. *Nature Structural & Molecular Biology*, 8(9):770–774, 09 2001.
- [103] D. A. Kocisko, J. H. Come, S. A. Priola, B. Chesebro, G. J. Raymond, P. T. Lansbury, and B. Caughey. Cell-free formation of protease-resistant prion protein. *Nature*, 370(6489):471–474, 1994.
- [104] S. Koide and S. S. Sidhu. The importance of being tyrosine: Lessons in molecular recognition from minimalist synthetic binding proteins. *ACS Chemical Biology*, 4(5):325–334, 2009.
- [105] N. Koizumi, H. Iguchi, and T. E. Smith. Comparison and verification of bse surveillance in usa and japan. *Environmental Health and Preventive Medicine*, 10(3):130–137, 2005.
- [106] C. Krammer, I. Vorberg, H. M. Schatzl, and S. Gilch. Therapy in prion diseases: from molecular and cellular biology to therapeutic targets. *Infectious Disorders - Drug Targets*, 9(1):3–14, 2009.
- [107] J. Kranich, N. J. Krautler, J. Falsig, B. Ballmer, S. Li, G. Hutter, P. Schwarz, R. Moos, C. Julius, G. Miele, and A. Aguzzi. Engulfment of cerebral apoptotic bodies controls the course of prion disease in a mouse strain-dependent manner. *The Journal of Experimental Medicine*, 207(10):2271–2281, 2010.
- [108] H. A. Kretzschmar, T. Tings, A. Madlung, A. Giese, and J. Herms. Function of PrP<sup>C</sup> as a copper-binding protein at the synapse. *Archives of Virology, Supplement*, 16:239–249, 2000.
- [109] T. D. Kurt, C. Bett, N. Fernandez-Borges, S. Joshi-Barr, S. Hornemann, T. Rulicke, J. Castilla, K. Wuthrich, A. Aguzzi, and C. J. Sigurdson. Prion transmission prevented by modifying the  $\beta 2$ - $\alpha 2$  loop structure of host PrP<sup>C</sup>. *The Journal of Neuroscience*, 34(3):1022–1027, 2014.
- [110] P. LANTOS. From slow virus to prion: a review of transmissible spongiform encephalopathies. *Histopathology*, 20(1):1–11, 1992.
- [111] M. A. Larkin, G. Blackshields, N. P. Brown, R. Chenna, P. A. McGettigan, H. McWilliam, F. Valentin, I. M. Wallace, A. Wilm, R. Lopez, J. D. Thomp-

- son, T. J. Gibson, and D. G. Higgins. Clustal w and clustal x version 2.0. *Bioinformatics*, 23(21):2947–2948, 2007.
- [112] M. C. Lawrence and P. M. Colman. Shape complementarity at protein/protein interfaces. *Journal of Molecular Biology*, 234(4):946 – 950, 1993.
- [113] J. Lee, S. Y. Kim, K. J. Hwang, Y. R. Ju, and H.-J. Woo. Prion diseases as transmissible zoonotic diseases. *Osong Public Health and Research Perspectives*, 4(1):57 – 66, 2013.
- [114] G. Legname, I. V. Baskakov, H.-O. B. Nguyen, D. Riesner, F. E. Cohen, S. J. DeArmond, and S. B. Prusiner. Synthetic mammalian prions. *Science*, 305(5684):673–676, 2004.
- [115] P. P. Liberski. Historical overview of prion diseases: a view from afar. *Folia Neuropathologica*, 50(1):1–12, 2012.
- [116] P. P. Liberski and J. W. Ironside. An outline of the neuropathology of transmissible spongiform encephalopathies (prion diseases). *Folia Neuropathologica*, 42 Suppl B:39–58, 2004.
- [117] C. Locht, B. Chesebro, R. Race, and J. M. Keith. Molecular cloning and complete sequence of prion protein cDNA from mouse brain infected with the scrapie agent. *Proceedings of the National Academy of Sciences of the United States of America*, 83(17):6372–6376, 1986.
- [118] D. A. Lysek, C. Schorn, L. G. Nivon, V. Esteve-Moya, B. Christen, L. Calzolari, C. von Schroetter, F. Fiorito, T. Herrmann, P. Güntert, and K. Wüthrich. Prion protein nmr structures of cats, dogs, pigs, and sheep. *Proceedings of the National Academy of Sciences of the United States of America*, 102(3):640–645, 2005.
- [119] N. A. Mabbott, J. Young, I. McConnell, and M. E. Bruce. Follicular dendritic cell dedifferentiation by treatment with an inhibitor of the lymphotoxin pathway dramatically reduces scrapie susceptibility. *Journal of Virology*, 77(12):6845–6854, 2003.
- [120] C. Mangels, R. Kellner, J. Einsiedel, P. R. Weiglmeier, P. Rosch, P. Gmeiner, and S. Schwarzinger. The therapeutically anti-prion active antibody-fragment scfv-w226: paramagnetic relaxation-enhanced nmr spectroscopy aided structure

- elucidation of the paratope-epitope interface. *J Biomolecular Structure and Dynamics*, 28(1):13–22, 2010.
- [121] M. Marquart, J. Deisenhofer, R. Huber, and W. Palm. Crystallographic refinement and atomic models of the intact immunoglobulin molecule kol and its antigen-binding fragment at 3.0 Å and 1.9 Å resolution. *Journal of Molecular Biology*, 141(4):369 – 391, 1980.
- [122] J. A. Mastrianni. NIH- Genetic Testing Registry. <http://www.ncbi.nlm.nih.gov/gtr/conditions/C0022336/>.
- [123] D. Matthews. Bovine spongiform encephalopathy. *Journal of the Royal Society of Health*, 111(1):3–5, 1991.
- [124] A. J. McCoy, R. W. Grosse-Kunstleve, P. D. Adams, M. D. Winn, L. C. Storoni, and R. J. Read. Phaser crystallographic software. *Journal of Applied Crystallography*, 40(Pt 4):658–674, 2007.
- [125] P. A. Merz, R. A. Somerville, H. M. Wisniewski, L. Manuelidis, and E. E. Manuelidis. Scrapie-associated fibrils in Creutzfeldt-Jakob Disease. *Nature*, 306(5942):474–476, 1983.
- [126] R. K. Meyer, M. P. McKinley, K. A. Bowman, M. B. Braunfeld, R. A. Barry, and S. B. Prusiner. Separation and properties of cellular and scrapie prion proteins. *Proceedings of the National Academy of Sciences of the United States of America*, 83(8):2310–2314, 1986.
- [127] I. S. Mian, A. R. Bradwell, and A. J. Olson. Structure, function and properties of antibody binding sites. *Journal of Molecular Biology*, 217(1):133–151, 1991.
- [128] K. Midelfort, H. Hernandez, S. Lippow, B. Tidor, C. Drennan, and K. Wittrup. Substantial energetic improvement with minimal structural perturbation in a high affinity mutant antibody. *Journal of Molecular Biology*, 343(3):685 – 701, 2004.
- [129] T. Miura, A. Hori-i, H. Mototani, and H. Takeuchi. Raman spectroscopic study on the copper(II) binding mode of prion octapeptide and its pH dependence. *Biochemistry*, 38(35):11560–11569, 1999.
- [130] S. Mohri, S. Handa, and J. Tateishi. Lack of effect of thymus and spleen on the incubation period of creutzfeldt-jakob disease in mice. *Journal of General Virology*, 68 ( Pt 4):1187–1189, 1987.

- [131] V. Morea, A. Tramontano, M. Rustici, C. Chothia, and A. M. Lesk. Conformations of the third hypervariable region in the vh domain of immunoglobulins. *Journal of Molecular Biology*, 275(2):269 – 294, 1998.
- [132] J. A. Morris and G. D. Carleton. Encephalopathy in mice following inoculation of scrapie sheep brain. *Nature*, 197(4872):1084–1086, 03 1963.
- [133] M. P. Morrissey and E. I. Shakhnovich. Evidence for the role of PrP<sup>C</sup> helix 1 in the hydrophilic seeding of prion aggregates. *Proceedings of the National Academy of Sciences of the United States of America*, 96(20):11293–11298, 1999.
- [134] A. Muller-Schiffmann and C. Korth. Vaccine approaches to prevent and treat prion infection : progress and challenges. *BioDrugs*, 22(1):45–52, 2008.
- [135] K. Nazor Friberg, G. Hung, E. Wancewicz, K. Giles, C. Black, S. Freier, F. Bennett, S. J. DeArmond, Y. Freyman, P. Lessard, S. Ghaemmaghami, and S. B. Prusiner. Intracerebral infusion of antisense oligonucleotides into prion-infected mice. *Molecular Therapy - Nucleic Acids*, 1:e9–, 02 2012.
- [136] A. L. Nelson. Antibody fragments: hope and hype. *MAbs*, 2(1):77–83, 2010.
- [137] S. D. Nuttall, M. L. Wilkins, V. A. Streltsov, L. Pontes-Braz, O. Dolezal, H. Tran, and C.-Q. Liu. Isolation, kinetic analysis, and structural characterization of an antibody targeting the bacillus anthracis major spore surface protein bcla. *Proteins: Structure, Function, and Bioinformatics*, 79(4):1306–1317, 2011.
- [138] B. Oesch, D. Westaway, M. Walchli, M. P. McKinley, S. B. Kent, R. Aebersold, R. A. Barry, P. Tempst, D. B. Teplow, and L. E. Hood. A cellular gene encodes scrapie prp 27-30 protein. *Cell*, 40(4):735–746, 1985.
- [139] P. H. A. of Canada. CJD-Surveillance System. <http://www.phac-aspc.gc.ca/hcai-iamss/cjd-mcj/cjdss-ssmcj/stats-eng.php>
- [140] N. I. of Neurological Disorders and Stroke. Gerstmann-Straussler-Sheinker disease information page. <http://www.ninds.nih.gov/disorders/gss/gss.htm>.
- [141] N. Ohsawa, C.-H. Song, A. Suzuki, H. Furuoka, R. Hasebe, and M. Horiuchi. Therapeutic effect of peripheral administration of an anti-prion protein antibody on mice infected with prions. *Microbiology and Immunology*, 57(4):288–297, 2013.

- [142] T. Olafsen, D. Betting, V. E. Kenanova, F. B. Salazar, P. Clarke, J. Said, A. A. Raubitschek, J. M. Timmerman, and A. M. Wu. Recombinant anti-cd20 antibody fragments for small-animal pet imaging of b-cell lymphomas. *Journal of Nuclear Medicine*, 50(9):1500–1508, 2009.
- [143] W. organisation for animal health. BSE situation in the world and annual incidence rate. <http://www.oie.int/animal-health-in-the-world/bse-specific-data/number-of-cases-in-the-united-kingdom/>.
- [144] K. M. Pan, M. Baldwin, J. Nguyen, M. Gasset, A. Serban, D. Groth, I. Mehlhorn, Z. Huang, R. J. Fletterick, and F. E. Cohen. Conversion of alpha-helices into beta-sheets features in the formation of the scrapie prion proteins. *Proceedings of the National Academy of Sciences of the United States of America*, 90(23):10962–10966, 1993.
- [145] P. K. Panegyres and E. Armari. Therapies for human prion diseases. *American Journal of Neurodegenerative Disease*, 2(3):176–186, 2013.
- [146] C. Papworth, J. Bauer, B. J., and W. D.A. Site-directed mutagenesis in one day with >80% efficiency. *Strategies*, 9(3):3–14, 1996.
- [147] V. Perrier, J. Solassol, C. Crozet, Y. Frobert, C. Mourton-Gilles, J. Grassi, and S. Lehmann. Anti-PrP antibodies block PrP<sup>Sc</sup> replication in prion-infected cell cultures by accelerating PrP<sup>C</sup> degradation. *Journal of Neurochemistry*, 89(2):454–463, 2004.
- [148] D. Peschen, H.-P. Li, R. Fischer, F. Kreuzaler, and Y.-C. Liao. Fusion proteins comprising a fusarium-specific antibody linked to antifungal peptides protect plants against a fungal pathogen. *Nature Biotechnology*, 22(6):732–738, 06 2004.
- [149] D. Peschen, H.-P. Li, R. Fischer, F. Kreuzaler, and Y.-C. Liao. Fusion proteins comprising a fusarium-specific antibody linked to antifungal peptides protect plants against a fungal pathogen. *Nature Biotechnology*, 22(6):732–738, 06 2004.
- [150] A. Pfeifer, S. Eigenbrod, S. Al-Khadra, A. Hofmann, G. Mitteregger, M. Moser, U. Bertsch, and H. Kretzschmar. Lentivector-mediated RNAi efficiently suppresses prion protein and prolongs survival of scrapie-infected mice. *Journal of Clinical Investigation*, 116(12):3204–3210, 2006.
- [151] H. Pflanz, K. Vana, G. Mitteregger, C. Pace, D. Messow, C. Sedlaczek, D. Nikles, H. A. Kretzschmar, and S. F. T. Weiss. Microinjection of lentiviral



- vectors expressing small interfering RNAs directed against laminin receptor precursor mRNA prolongs the pre-clinical phase in scrapie-infected mice. *Journal of General Virology*, 90(Pt 1):269–274, 2009.
- [152] V. Pietrini, G. Puoti, L. Limido, G. Rossi, G. Di Fede, G. Giaccone, M. Mangieri, F. Tedeschi, A. Bondavalli, D. Mancina, O. Bugiani, and F. Tagliavini. Creutzfeldt-jakob disease with a novel extra-repeat insertional mutation in the prnp gene. *Neurology*, 61(9):1288–1291, 2003.
- [153] V. M. Pietrini, G. M. Puoti, L. P. Limido, G. P. Rossi, G. Di Fede, G. M. Giaccone, M. V. Mangieri, F. M. Tedeschi, A. D. Bondavalli, D. M. Mancina, O. M. Bugiani, and F. M. Tagliavini. Creutzfeldt-jakob disease with a novel extra-repeat insertional mutation in the PRNP gene. *Neurology*, 61(9):1288–1291, 2003.
- [154] M. Polymenidou, R. Moos, M. Scott, C. Sigurdson, Y. Z. Shi, B. Yajima, I. Hafner-Bratkovič, R. Jerala, S. Hornemann, K. Wuthrich, A. Bellon, M. Vey, G. Garen, M. N. G. James, N. Kav, and A. Aguzzi. The POM monoclonals: A comprehensive set of antibodies to non-overlapping prion protein epitopes. *PLoS ONE*, 3(12):e3872, 12 2008.
- [155] C. S. Poornima and P. M. Dean. Hydration in drug design. 1. multiple hydrogen-bonding features of water molecules in mediating protein-ligand interactions. *Journal of Computer- Aided Molecular Design*, 9(6):500–512, 1995.
- [156] M. Prinz, M. Heikenwalder, T. Junt, P. Schwarz, M. Glatzel, F. L. Heppner, Y.-X. Fu, M. Lipp, and A. Aguzzi. Positioning of follicular dendritic cells within the spleen controls prion neuroinvasion. *Nature*, 425(6961):957–962, 2003.
- [157] M. Prior, S. Lehmann, M.-S. Sy, B. Molloy, and H. E. M. McMahon. Cyclodextrins inhibit replication of scrapie prion protein in cell culture. *Journal of Virology*, 81(20):11195–11207, 2007.
- [158] S. B. Prusiner. Novel proteinaceous infectious particles cause scrapie. *Science*, 216(4542):136–144, 1982.
- [159] S. B. Prusiner, D. F. Groth, D. C. Bolton, S. B. Kent, and L. E. Hood. Purification and structural studies of a major scrapie prion protein. *Cell*, 38(1):127–134, 1984.

- [160] S. B. Prusiner, M. P. McKinley, K. A. Bowman, D. C. Bolton, P. E. Bendheim, D. F. Groth, and G. G. Glenner. Scrapie prions aggregate to form amyloid-like birefringent rods. *Cell*, 35(2 Pt 1):349–358, 1983.
- [161] T. Ramaraj, T. Angel, E. A. Dratz, A. J. Jesaitis, and B. Mumey. Antigen–antibody interface properties: Composition, residue interactions, and features of 53 non-redundant structures. *Biochimica et Biophysica Acta (BBA) - Proteins and Proteomics*, 1824(3):520 – 532, 2012.
- [162] Y. Reiter, U. Brinkmann, B. Lee, and I. Pastan. Engineering antibody fv fragments for cancer detection and therapy: Bisulfide-stabilized fv fragments. *Nature Biotechnology*, 14(10):1239–1245, 10 1996.
- [163] J. R. Requena and H. Wille. The structure of the infectious prion protein: Experimental data and molecular models. *Prion*, 8(1), 2014.
- [164] T. N. C. Research and S. Unit. Cjd figures. <http://www.cjd.ed.ac.uk/>
- [165] J. S. Richardson, E. D. Getzoff, and D. C. Richardson. The beta bulge: a common small unit of nonrepetitive protein structure. *Proceedings of the National Academy of Sciences of the United States of America*, 75(6):2574–2578, 1978.
- [166] R. Riek, S. Hornemann, G. Wider, M. Billeter, R. Glockshuber, and K. Wuthrich. NMR structure of the mouse prion protein domain PrP(121-231). *Nature*, 382(6587):180–182, 1996.
- [167] R. Riek, S. Hornemann, G. Wider, R. Glockshuber, and K. Wuthrich. NMR characterization of the full-length recombinant murine prion protein, mPrP(23-231). *FEBS Letters*, 413(2):282 – 288, 1997.
- [168] R. Riek, G. Wider, M. Billeter, S. Hornemann, R. Glockshuber, and K. Wuthrich. Prion protein NMR structure and familial human spongiform encephalopathies. *Proceedings of the National Academy of Sciences of the United States of America*, 95(20):11667–11672, 1998.
- [169] X. Robert and P. Gouet. Deciphering key features in protein structures with the new endscript server. *Nucleic Acids Research*, 42(W1):W320–W324, 2014.
- [170] J. D. Rodwell and F. Karush. A general method for the isolation of the V<sub>H</sub> domain from IgM and other immunoglobulins. *The Journal of Immunology*, 121(4):1528–1531, 1978.

- [171] Y. Roettger, Y. Du, M. Bacher, I. Zerr, R. Dodel, and J.-P. Bach. Immunotherapy in prion disease. *Nature Reviews Neurology*, 9(2):98–105, 2013.
- [172] G. P. Saborio, B. Permanne, and C. Soto. Sensitive detection of pathological prion protein by cyclic amplification of protein misfolding. *Nature*, 411(6839):810–813, 06 2001.
- [173] M. J. Sadowski, J. Pankiewicz, F. Prelli, H. Scholtzova, D. S. Spinner, R. B. Kasczak, R. J. Kasczak, and T. Wisniewski. Anti-PrP mAb 6d11 suppresses PrP<sup>Sc</sup> replication in prion infected myeloid precursor line FDC-p1/22l and in the lymphoreticular system in vivo. *Neurobiology of Disease*, 34(2):267–278, 2009.
- [174] G. Scalabrino, E. Mutti, D. Veber, V. Rodriguez Menendez, C. Novembrino, A. Calligaro, and G. Tredici. The octapeptide repeat PrP<sup>C</sup> region and cobalamin-deficient polyneuropathy of the rat. *Muscle Nerve*, 44(6):957–967, 2011.
- [175] Schrodinger, LLC. The PyMOL molecular graphics system, version 1.3r1, 2010. <http://www.pymol.org/>.
- [176] C. J. Sigurdson, K. P. R. Nilsson, S. Hornemann, G. Manco, N. Fernandez-Borges, P. Schwarz, J. Castilla, K. Wuthrich, and A. Aguzzi. A molecular switch controls interspecies prion disease transmission in mice. *Journal of Clinical Investigation*, 120(7):2590–2599, 2010.
- [177] S. Sisó, L. González, and M. Jeffrey. Neuroinvasion in prion diseases: The roles of ascending neural infection and blood dissemination. *Interdisciplinary Perspectives on Infectious Diseases*, 2010:16, 2010.
- [178] P. Smith, R. Krohn, G. Hermanson, A. Mallia, F. Gartner, M. Provenzano, E. Fujimoto, N. Goeke, B. Olson, and D. Klenk. Measurement of protein using bicinchoninic acid. *Analytical Biochemistry*, 150(1):76 – 85, 1985.
- [179] S. M. Soltis, A. E. Cohen, A. Deacon, T. Eriksson, A. Gonzalez, S. McPhillips, H. Chui, P. Dunten, M. Hollenbeck, I. Mathews, M. Miller, P. Moorhead, R. P. Phizackerley, C. Smith, J. Song, H. van dem Bedem, P. Ellis, P. Kuhn, T. McPhillips, N. Sauter, K. Sharp, I. Tsyba, and G. Wolf. New paradigm for macromolecular crystallography experiments at ssl: automated crystal

- screening and remote data collection. *Acta Crystallographica Section D*, 64(Pt 12):1210–1221, 2008.
- [180] T. Sonati, R. R. Reimann, J. Falsig, P. K. Baral, T. O’Connor, S. Horne-  
mann, S. Yaganoglu, B. Li, U. S. Herrmann, B. Wieland, M. Swayampakula,  
M. H. Rahman, D. Das, N. Kav, R. Riek, P. P. Liberski, M. N. G. James, and  
A. Aguzzi. The toxicity of antiprion antibodies is mediated by the flexible tail  
of the prion protein. *Nature*, 501(7465):102–106, 09 2013.
- [181] J. O. Speare, T. S. r. Rush, M. E. Bloom, and B. Caughey. The role of helix  
1 aspartates and salt bridges in the stability and conversion of prion protein.  
*Journal of Biological Chemistry*, 278(14):12522–12529, 2003.
- [182] D. S. Spinner, R. B. Kascsak, G. Lafauci, H. C. Meeker, X. Ye, M. J. Flory,  
J. I. Kim, G. B. Schuller-Levis, W. R. Levis, T. Wisniewski, R. I. Carp, and  
R. J. Kascsak. Cpg oligodeoxynucleotide-enhanced humoral immune response  
and production of antibodies to prion protein PrP<sup>Sc</sup> in mice immunized with  
139a scrapie-associated fibrils. *Journal of Leukocyte Biology*, 81(6):1374–1385,  
2007.
- [183] N. Stahl, M. A. Baldwin, D. B. Teplow, L. Hood, B. W. Gibson, A. L.  
Burlingame, and S. B. Prusiner. Structural studies of the scrapie prion protein  
using mass spectrometry and amino acid sequencing. *Biochemistry*, 32(8):1991–  
2002, 1993.
- [184] N. Stahl, D. R. Borchelt, K. Hsiao, and S. B. Prusiner. Scrapie prion protein  
contains a phosphatidylinositol glycolipid. *Cell*, 51(2):229 – 240, 1987.
- [185] R. L. Stanfield, A. Zemla, I. A. Wilson, and B. Rupp. Antibody elbow angles are  
influenced by their light chain class. *Journal of Molecular Biology*, 357(5):1566–  
1574, 2006.
- [186] J. Stockel, J. Safar, A. C. Wallace, F. E. Cohen, and S. B. Prusiner. Prion  
protein selectively binds copper(II) ions. *Biochemistry*, 37(20):7185–7193, 1998.
- [187] M. Swayampakula, P. K. Baral, A. Aguzzi, N. N. V. Kav, and M. N. G. James.  
The crystal structure of an octapeptide repeat of the prion protein in complex  
with a fab fragment of the pom2 antibody. *Protein Science*, 22(7):893–903,  
2013.

- [188] L. M. Taubner, E. A. Bienkiewicz, V. Copié, and B. Caughey. Structure of the flexible amino-terminal domain of prion protein bound to a sulfated glycan. *Journal of Molecular Biology*, 395(3):475 – 490, 2010.
- [189] Y. Tsuboi, K. Doh-ura, and T. Yamada. Continuous intraventricular infusion of pentosan polysulfate: Clinical trial against prion diseases. *Neuropathology*, 29(5):632–636, 2009.
- [190] D. J. Turner, M. A. Ritter, and A. J. George. Importance of the linker in expression of single-chain fv antibody fragments: optimisation of peptide sequence using phage display technology. *Journal of Immunological Methods*, 205(1):43 – 54, 1997.
- [191] V. Vagenende, M. G. S. Yap, and B. L. Trout. Mechanisms of protein stabilization and prevention of protein aggregation by glycerol. *Biochemistry*, 48(46):11084–11096, 2009.
- [192] K. Vana, C. Zuber, H. Pflanz, D. Kolodziejczak, G. Zemora, A.-K. Bergmann, and S. Weiss. Lrp/lr as an alternative promising target in therapy of prion diseases, alzheimer’s disease and cancer. *Infectious Disorders - Drug Targets*, 9(1):69–80, 2009.
- [193] J. H. Viles, F. E. Cohen, S. B. Prusiner, D. B. Goodin, P. E. Wright, and H. J. Dyson. Copper binding to the prion protein: Structural implications of four identical cooperative binding sites. *Proceedings of the National Academy of Sciences of the United States of America*, 96(5):2042–2047, 1999.
- [194] A. Vital, J.-L. Laplanche, J.-R. Bastard, X. Xiao, W.-Q. Zou, and C. Vital. A case of Gerstmann-Straussler-Scheinker disease with a novel six octapeptide repeat insertion. *Neuropathology and Applied Neurobiology*, 37(5):554–559, 2011.
- [195] C. Vital, F. Gray, A. Vital, P. Parchi, S. Capellari, R. B. Petersen, X. Ferrer, D. Jarnier, J. Julien, and P. Gambetti. Prion encephalopathy with insertion of octapeptide repeats: the number of repeats determines the type of cerebellar deposits. *Neuropathology and Applied Neurobiology*, 24(2):125–130, 1998.
- [196] A. C. Wallace, R. A. Laskowski, and J. M. Thornton. Ligplot: a program to generate schematic diagrams of protein-ligand interactions. *Protein Engineering*, 8(2):127–134, 1995.

- [197] F. Wang, S. Yin, X. Wang, L. Zha, M.-S. Sy, and J. Ma. Role of the highly conserved middle region of prion protein (PrP) in PrP-lipid interaction. *Biochemistry*, 49(37):8169–8176, 2010.
- [198] F. Wang, Z. Zhang, X. Wang, J. Li, L. Zha, C.-G. Yuan, C. Weissmann, and J. Ma. Genetic informational rna is not required for recombinant prion infectivity. *Journal of Virology*, 86(3):1874–1876, 2012.
- [199] R. G. Warner, C. Hundt, S. Weiss, and J. E. Turnbull. Identification of the heparan sulfate binding sites in the cellular prion protein. *Journal of Biological Chemistry*, 277(21):18421–18430, 2002.
- [200] J. C. Watts, A. Balachandran, and D. Westaway. The expanding universe of prion diseases. *PLoS Pathogens*, 2(3):e26, 03 2006.
- [201] A. R. White, P. Enever, M. Tayebi, R. Mushens, J. Linehan, S. Brandner, D. Anstee, J. Collinge, and S. Hawke. Monoclonal antibodies inhibit prion replication and delay the development of prion disease. *Nature*, 422(6927):80–83, 03 2003.
- [202] A. R. White, P. Enever, M. Tayebi, R. Mushens, J. Linehan, S. Brandner, D. Anstee, J. Collinge, and S. Hawke. Monoclonal antibodies inhibit prion replication and delay the development of prion disease. *Nature*, 422(6927):80–83, 03 2003.
- [203] M. Whitlow, B. A. Bell, S.-L. Feng, D. Filpula, K. D. Hardman, S. L. Hubert, M. L. Rollence, J. F. Wood, M. E. Schott, D. E. Milenic, T. Yokota, and J. Schlom. An improved linker for single-chain fv with reduced aggregation and enhanced proteolytic stability. *Protein Engineering*, 6(8):989–995, 1993.
- [204] E. S. Williams and S. Young. Chronic wasting disease of captive mule deer: a spongiform encephalopathy. *J Wildl Dis*, 16(1):89–98, 1980.
- [205] M. Wink, editor. *An Introduction to Molecular Biotechnology: Fundamentals, Methods and Applications*. Wiley-Blackwell, 2 edition, 2011.
- [206] M. D. Winn, C. C. Ballard, K. D. Cowtan, E. J. Dodson, P. Emsley, P. R. Evans, R. M. Keegan, E. B. Krissinel, A. G. W. Leslie, A. McCoy, S. J. McNicholas, G. N. Murshudov, N. S. Pannu, E. A. Potterton, H. R. Powell, R. J. Read, A. Vagin, and K. S. Wilson. Overview of the ccp4 suite and current developments. *Acta Crystallographica Section D*, 67(Pt 4):235–242, 2011.

- [207] F. Wopfner, G. Weidenhofer, R. Schneider, A. von Brunn, S. Gilch, T. F. Schwarz, T. Werner, and H. M. Schatzl. Analysis of 27 mammalian and 9 avian PrPs reveals high conservation of flexible regions of the prion protein. *J Molecular Biology*, 289(5):1163–1178, 1999.
- [208] A. Y. Yam, C. M. Gao, X. Wang, P. Wu, and D. Peretz. The octarepeat region of the prion protein is conformationally altered in PrP<sup>Sc</sup>. *PLoS ONE*, 5(2):e9316, 02 2010.
- [209] R. Zahn. The octapeptide repeats in mammalian prion protein constitute a pH-dependent folding and aggregation site. *Journal of Molecular Biology*, 334(3):477 – 488, 2003.
- [210] C. Zahnd, S. Spinelli, B. Luginbühl, P. Amstutz, C. Cambillau, and A. Plückthun. Directed in vitro evolution and crystallographic analysis of a peptide-binding single chain antibody fragment (scfv) with low picomolar affinity. *Journal of Biological Chemistry*, 279(18):18870–18877, 2004.
- [211] A. Zdanov, Y. Li, D. R. Bundle, S. J. Deng, C. R. MacKenzie, S. A. Narang, N. M. Young, and M. Cygler. Structure of a single-chain antibody variable domain (fv) fragment complexed with a carbohydrate antigen at 1.7-Å resolution. *Proceedings of the National Academy of Sciences of the United States of America*, 91(14):6423–6427, 1994.
- [212] J. Zhang. The structural stability of wild-type horse prion protein. *Journal of Biomolecular Structure and Dynamics*, 29(2):369–377, 2011.
- [213] Zomosa-Signoret, Viviana, Arnaud, Jacques-Damien, Fontes, Pascaline, Alvarez-Martinez, Maria-Teresa, and Liautard, Jean-Pierre. Physiological role of the cellular prion protein. *Veterinary Research*, 39(4):09, 2008.
- [214] J. Zuegg and J. E. Gready. Molecular dynamics simulation of human prion protein including both n-linked oligosaccharides and the gpi anchor. *Glycobiology*, 10(10):959–974, 2000.